Strongly Interacting Fermions in Optical Lattices and Superlattices

by
Timothy S. Goodman

A dissertation submitted in partial fulfillment
of the requirements for the degree of
Doctor of Philosophy
(Physics)
in The University of Michigan
2009

Doctoral Committee:

Associate Professor Luming Duan, Chair
Professor James W. Allen
Professor Paul R. Berman
Professor Georg A. Raithel
Professor Duncan G. Steel

To my wife, Elizabeth. I promise I won't make you read it.

ACKNOWLEDGEMENTS

Firstly, I would like to thank my research advisor Luming Duan for all his help and support over the course of my Ph.D. studies. He has been an always-patient teacher, and I have benefitted tremendously from his knowledge and the guidance he provided. I could not ask for more in a mentor.

I would like to thank the members of my thesis committee, Jim Allen, Paul Berman, Georg Raithel, and Duncan Steel for the time they have devoted to reading my thesis and judging my defense, and for the helpful feedback they have provided. Having been fortunate enough to take courses taught by Professors Berman and Raithel, I thank them also for their dedication as teachers, and for the great many things I learned in their classes.

I would also like to thank all the members of Professor Duan's reasearch group, both past and present, for the many enlightening discussions we have had. To them I can ask the questions I would be too embarrassed to ask a professor – which often enough turn out to be the most important ones. My graduate education would not have been the same without them.

I wish also to acknowledge and thank all my many teachers over the years, both at the University of Michigan and at my undergraduate institution, the University of Virginia. In particular, I would like to acknowledge my undergraduate research advisor, the late Julian Noble. His passing leaves me as perhaps the last person on Earth who appreciates a good pun. I also would like to thank my first physics teacher,

Deborah Waldron of Yorktown High School in Arlington, VA. She was perhaps the most enthusiastic teacher I ever had. It is certainly no coincidence that after a year in her A.P. Physics class several of her students intended to pursue higher education in physics. I am pleased to say at least one of them did.

I am grateful to my family for over 27 years of supporting and encouraging me in everything I do. In particular, I would like to thank my parents for nurturing my interest in physics as a child by providing me with so many wonderful books. I also would like to thank my grandparents for the many physics-related questions and newspaper clippings.

I wish to thank my infant daughter, Charlotte. Her birth has provided me with a strong financial incentive to finish my degree and go get a "real job".

Lastly, I wish to thank my wonderful wife, Elizabeth. In this way I bookend these acknowledgements with the two people without whom this work would simply not have been possible: my research advisor for his intellectual support, and my wife for her emotional support. Elizabeth, I wish I could express in print how much you mean to me, but I fear there is no way to do so adequately while maintaining even the slightest semblance of professionalism. My experience as a graduate student has made me a more knowledgeable man, and for that I am grateful, but you make me a better man, and for that gratitude is insufficient. Physics explains how the universe works. You give it a reason to exist.

To those I have forgotten to thank, I thank you for your forgiveness.

TABLE OF CONTENTS

LIST OF FIGURES

Figure

ABSTRACT

This dissertation summarizes my recent work regarding systems of strongly interacting fermionic atoms in optical lattices. This work addresses the combination of two experimental techniques that have been the subject of much recent research in ultracold atom physics. One is the use of optical lattices, which provide a means to realize diverse interaction configurations within a clean, controllable system. The other is the use of magnetically tunable Feshbach resonances to control the strength of the interatomic interaction. Together, these techniques offer the possibility of an experimental realization of many important model Hamiltonians of condensed matter physics, and may also lead to the discovery of new physics.

Recent study of this system has shown that strong interactions near Feshbach resonance will lead to the population of multiple lattice bands, and that collisions between atoms on neighboring sites cannot be neglected. These effects lead to a complicated Hamiltonian, but one which can be simplified to an effective single-band model equivalent to the generalized Hubbard model (GHM), which is an extension of the Hubbard model that includes correlated hopping terms. My main results concern the study of this model.

The strong correlations between the particles make it difficult to definitively determine the many body physics of the GHM. As a first approach to understanding the GHM in optical lattices, I focus mainly on cases where the problem is greatly simplified by allowing interactions among only small groups of lattice sites. This

restriction can be implemented in experiments using an optical superlattice potential. Our results include a proposed scheme (based on double-well superlattices) to empirically verify that the GHM describes this system and to directly measure the various parameters of this model. Other results include exact solutions on four-site square plaquettes, which demonstrate that d-wave excitations can occur in the low-energy states. By using a superlattice to give an array of weakly coupled plaquettes, one can thus produce a d-wave superfluid state. This is of relevance to the study of high-T_c superconductors, although I note certain key differences between the sort of d-wave superfluid described here and that of the superconductors.

CHAPTER I

Introduction

Nature is replete with examples of lattices. These structures are characterized by a discrete translational symmetry, such that if the position of the lattice is translated by a fixed amount, then (defects and boundaries aside) the original lattice is recovered. Lattice Hamiltonians have long been used in describing many important systems in condensed matter physics.[4–6] More recently, the use of optical lattices has played an important role in experiments with ultracold atoms.[7–10] An optical lattice potential is formed by a standing wave produced by counter-propagating laser beams. These lattices have been utilized in the trapping, cooling, and manipulation of ultracold atoms. As we will see, the physics of such systems can be described by lattice Hamiltonians which are much the same as those used in condensed matter physics. Thus, optical lattices provide a clean, highly controllable testbed for many important condensed matter Hamiltonians, as well as offering the possibility of new physics.

In addition to optical lattices, the use of Feshbach resonance provides another experimental technique which has been the subject of significant recent research in ultracold atomic physics.[11–15] A Feshbach resonance is a resonance between a scattering state and a (quasi)bound state. Such resonances can be exploited to allow the strength of inter-atomic interactions to be tuned over a wide range through

control of the external magnetic field. The use of optical lattices and Feshbach resonances are thus somewhat complementary, with optical lattices making it possible to engineer diverse Hamiltonians, with tunneling between lattice sites controlled by the lattice depth, and with on-site interactions controlled by the external magnetic field via Feshbach resonance. Naturally, there has been significant investigation into the combination of these two techniques.[16–23]

In this dissertation, we focus on the case of ultracold fermionic atoms in an optical lattice. It is arguable that the fermionic case provides richer physics than that of bosons, as bosonic physics can also be achieved with fermions in the limit where the atoms bind tightly to form diatomic molecules. Additionally, the fermionic atoms we study here can serve as an analog to fermionic charge carriers (e.g., electrons) in comparisons between optical lattices and condensed matter systems. As we will see, the physics of ultracold fermions in optical lattices and near Feshbach resonance is somewhat more complicated than the simplified picture given in the previous paragraph. It has been shown that, even for atoms which occupy a single lattice band far from resonance, as resonance is approached multiple lattice bands become occupied due to the strong collisional interactions between atoms on the same site.[16] Furthermore, our group has shown that for a wide Feshbach resonance (as is typical for experiments with potassium-40 and lithium-6), the direct collisional interaction between atoms and molecules on neighboring sites can be significantly larger than the kinetic tunneling between sites, and thus cannot be ignored in consideration of the multi-site physics.[3] This leads to a complicated Hamiltonian which includes on-site and nearest-neighbor interactions between atoms and Feshbach molecules over many lattice bands. However, under typical experimental conditions this Hamiltonian can be greatly simplified to yield an effective single-band Hamiltonian which is equivalent

to the generalized Hubbard model.[3, 24] In that form, the Hamiltonian is:

$$H = \sum_i (\Delta/2) n_i (n_i - 1) + \sum_{\langle i,j \rangle, \sigma} \left[-t + g_1 \left(n_{i\bar{\sigma}} + n_{j\bar{\sigma}} \right) + g_2 n_{i\bar{\sigma}} n_{j\bar{\sigma}} \right] a^\dagger_{i\sigma} a_{j\sigma} + \text{H.c.} + \quad (1.1)$$

Here $a^\dagger_{i\sigma}$ creates an atom with hyperfine state $\sigma = \uparrow, \downarrow$ in the Wannier state[25] centered at site i, where $n_{i\sigma} = a^\dagger_{i\sigma} a_{i\sigma}$, and $n_i = n_{i\uparrow} + n_{i\downarrow}$ Δ represents the on-site interaction energy, and t is the tunneling matrix element for a single atom moving between two sites i and j, with g_1 and g_2 altering the effective t in cases where sites i and j are occupied by additional atoms. This Hamiltonian has been studied previously in various contexts in condensed matter physics. [26–39] (In particular, several authors have suggested that the generalized Hubbard model is relevant to the high-T_c cuprates.[33–36])

The generalized Hubbard model is an extension of the Hubbard model, originally proposed by Hubbard in 1963.[4] The key difference from the standard Hubbard model is the addition of the g_1 and g_2 terms above. These terms described correlated tunneling effects – that is, the tunneling rate for one spin species is dependent on whether an atom of the opposite spin species is present. There exist no exact solutions for the generalized Hubbard model except for a few highly specialized cases [37–39]. (Generally, these require the special condition $g_1 = t$, which prevents the single-site molecules from being able to split into two atoms on two neighboring sites. This condition is not expected to be satisfied for the system we consider in this thesis.) The full phase diagram of the generalized Hubbard model is not known. Even for the standard Hubbard model there remain disputes about its phase diagram[40], and the addition of correlated tunneling clearly adds further complications. Furthermore, as we shall see it is difficult to even make a theoretical prediction of the values of the correlated hopping parameters g_1 and g_2 for optical lattices.

The bulk of this dissertation examines the generalized Hubbard model in optical lattices, and in superlattices which limit the interactions to groups of a few sites so as to make the physics more tractable. In the remainder of this chapter, we will first review the origins of the standard Hubbard model, along the way reviewing the important formalism of Bloch and Wannier states. We give particular attention to the various assumptions and approximations made by Hubbard in deriving this model, so as to contrast them to the derivation of the generalized Hubbard model presented in the next chapter. We then discuss the theory of Feshbach resonance as it pertains to ultracold fermionic atoms. The experimental implementation of optical lattices and superlattices is also reviewed. At the end of the chapter, we outline the remainder of this dissertation.

1.1 From Bloch States to the Hubbard Model

The Hubbard model was originally proposed by John Hubbard in 1963 in order to describe properties of the transition and rare earth metals which are not accurately described by band theory.[4] In particular, many transition metal oxides which the theory predicts to be conductors were in fact found to be insulators.[41] This was explained by Nevill Mott and Rudolph Peierls as arising due to the Coulomb interactions between electrons, which were neglected in deriving the band theory.[42, 43] This lead to a theory in which a conductor can become insulating as the bandwidth is decreased.[44–46] Such metal-insulator transitions cannot be understood in the context of band theory. The Hubbard model is the simplest model Hamiltonian which includes the competition between kinetic energy and Coulomb repulsion necessary to understand the metal-insulator transitions. In spite of the simple form of the model, it gives rise to a wide range of interesting physics.

Before discussing the Hubbard model further, we first present a few key results from band theory, in particular the Bloch state and Wannier state formalism. We do this in part to provide some historical context for the Hubbard model, but mostly because the formalism outlined here will be of use in subsequent sections.

1.1.1 Bloch States and Wannier States

The band theory of electrons in solids is based on a set of seemingly rather drastic approximations, but which nevertheless proved sufficient for making a great deal of progress in the early history of solid state physics.[47] In particular, it treats the electrons as a gas of non-interacting particles each subject to the same effective potential $U_{eff}(\mathbf{r})$. Ideally the effective potential would approximate the effect of the Coulomb forces both between the electrons and the atomic nuclei, and among the electrons themselves. However, due to the neglect of electron correlation the electron-electron interaction can at best be included at a mean-field level. A key assumption is that this Hamiltonian is periodic, with this periodicity arising from the arrangement of nuclei on fixed lattice sites. (At this level of approximation, we neglect the effects of the nuclear motion.)

Suppose the positions of the nuclei are given by the points $\mathbf{R}$ of a Bravais lattice. The D-dimensional Bravais lattice is given by all vectors $\mathbf{R} = n_1\mathbf{a_1} + \ldots + n_D\mathbf{a_D}$ for any integers n_1, . . . , n_D and some particular set of primitive vectors $\mathbf{a_1}$, $\mathbf{a_2}$, . . . , $\mathbf{a_D}$. The effective potential then has the property that it is unchanged by translation by any of the lattice vectors $\mathbf{R}$: $U_{eff}(\mathbf{r}) = U_{eff}(\mathbf{r} + \mathbf{R})$.

In 1928 it was shown by Felix Bloch that for such a periodic potential the solutions to the one-particle time-independent Schrödinger equation can be expressed as the product of a plane wave and a periodic function: $\psi_{n\mathbf{k}}(\mathbf{r}) = \mathrm{e}^{\mathbf{i}\mathbf{k}\cdot\mathbf{r}}u_{n\mathbf{k}}(\mathbf{r})$ where $u_{n\mathbf{k}}(\mathbf{r} + \mathbf{R}) = u_{n\mathbf{k}}(\mathbf{r})$ for every lattice vector $\mathbf{R}$.[6] This result is known as Bloch's theorem.

The wavefunctions $\psi_{n\mathbf{k}}(\mathbf{r})$ we call Bloch states. We see that under translation by a lattice vector $\mathbf{R}$ the Bloch states change only by a phase factor: $\psi_{n\mathbf{k}}(\mathbf{r}+\mathbf{R}) = e^{i\mathbf{k}\cdot\mathbf{R}}\psi_{n\mathbf{k}}(\mathbf{r})$. This is an equivalent statement of Bloch's theorem. It follows that the Bloch state $\psi_{n\mathbf{k}}$ is unchanged by shifting $\mathbf{k}$ by a vector $\mathbf{K}$ in the reciprocal lattice (defined by the condition $e^{i\mathbf{K}\cdot\mathbf{R}} = 1$). Therefore without loss of generality $\mathbf{k}$ may be restricted to the first Brillouin zone (that is, the Wigner-Seitz primitive cell of the reciprocal lattice), since any other vector $\mathbf{k}$ may be translated into the first Brillouin zone by the addition of a reciprocal lattice vector.

Because $\psi_{n\mathbf{k}}(\mathbf{r}) = e^{i\mathbf{k}\cdot\mathbf{r}}u_{n\mathbf{k}}(\mathbf{r})$ is an eigenstate of the Hamiltonian, we have for any fixed $\mathbf{k}$ a corresponding eigenvalue problem to determine the periodic functions $u_{n\mathbf{k}}$. Moreover, the periodic nature of $u_{n\mathbf{k}}$ means we can treat the problem as restricted to a single primitive cell of the lattice, which results in discretely spaced eigenvalues (enumerated by the band index n). The full eigenenergy then depends discretely on n but continuously on $\mathbf{k}$, giving rise to the energy bands with energies given by some $\epsilon_n(\mathbf{k})$. Note that $\mathbf{k}$ is allowed to vary continuously if the lattice is infinite in extent. Of course this cannot be true of any physical lattice structures, but is an acceptable approximation when the lattice size is much larger than the spacing between sites.

Thus for a system of many non-interacting electrons in a periodic potential, the eigenstates can be written as Slater determinants (that is, antisymmetrized products) of the Bloch wavefunctions. This is most conveniently represented in the language of creation and annihilation operators, where we define $a^\dagger_{n\mathbf{k}\sigma}$ ($a_{n\mathbf{k}\sigma}$)as the operator that creates (annihilates) an electron in the Bloch state $|\psi_{n\mathbf{k}\sigma}\rangle$ with the single-particle wavefunction $\psi_{n\mathbf{k}}(\mathbf{r})$ and a spin state specified by the index σ. In other words, $a^\dagger_{n\mathbf{k}\sigma}|0\rangle = |\psi_{n\mathbf{k}\sigma}\rangle$, where $|0\rangle$ is the vacuum state. The operators satisfy the standard fermion anticommutation relations: $\left\{a_{n\mathbf{k}\sigma}, a^\dagger_{n'\mathbf{k}'\sigma'}\right\} = \delta_{n,n'}\delta_{\mathbf{k},\mathbf{k}'}\delta_{\sigma,\sigma'}$, $\left\{a_{n\mathbf{k}\sigma}, a_{n'\mathbf{k}'\sigma'}\right\} =$

$\left\{a^\dagger_{n\mathbf{k}\sigma}, a^\dagger_{n'\mathbf{k}'\sigma'}\right\} = 0$. From this it follows that a product of the Bloch state creation operators automatically creates an antisymmetrized state.

Of course, if we include the Coulomb interactions between electrons then we can no longer expect the many-body eigenstates to be antisymmetrized products of Bloch states, as we no longer have a separate eigenvalue equation for the state of each particle. Even including inter-electron interactions at a mean field level leads to eigenstates that are Slater determinants of some more complicated states (generally determined iteratively, as in the Hartree-Fock method). In systems of correlated electrons, the many-body state can not even be expressed by a single Slater determinant, but rather is a sum of multiple such determinants. Nevertheless, antisymmetrized products of the Bloch states of non-interacting electrons provide a useful basis for describing more general many-body states of electrons in a periodic potential.

The Bloch states are entirely non-localized in terms of the position coordinate $\mathbf{r}$. At times it is useful to instead consider a set many-electron basis states which are Slater determinants of some spatially localized single-electron functions. (Here by "localized" we mean that the norm of the single-electron wave function is bounded by an envelope which peaks at some particular position and decays as we move further from this position.) This is particularly beneficial if we wish to consider local interactions, as is the case for the Hubbard model. An appropriate set of localized orthogonal single-electron basis functions is provided by the Wannier functions.[25]

The Wannier functions are defined as $\phi_n(\mathbf{r}) = \frac{1}{\sqrt{N}} \sum_{\mathbf{k}} \psi_{n\mathbf{k}}(\mathbf{r})$. Because the Bloch wavefunction $\phi_n(\mathbf{r})$ is changes only by a phase factor under displacement by any lattice vector $\mathbf{R}$, we can write: $\phi_n(\mathbf{r} - \mathbf{R}) = \frac{1}{\sqrt{N}} \sum_{\mathbf{k}} \mathrm{e}^{-\mathrm{i}\mathbf{k}\cdot\mathbf{R}} \psi_{n\mathbf{k}}(\mathbf{r})$. We can see that this is just the Fourier transform of $\psi_{n\mathbf{k}}(\mathbf{r})$ with respect to the variable $\mathbf{k}$. (In this case we keep $\mathbf{k}$ discrete and take the discrete Fourier transform.) Thus the

Bloch wave function has a Fourier expansion in terms of Wannier functions $\psi_{n\mathbf{k}}(\mathbf{r}) = \frac{1}{\sqrt{N}} \sum_i \mathrm{e}^{\mathrm{i}\mathbf{k}\cdot\mathbf{R}_i} \phi_n(\mathbf{r}-\mathbf{R}_i)$, where the sum is performed over the full set of lattice vectors R_i as indexed by i. We can also define operators that create or annihilate an electron in a Wannier state – that is, whose single-particle wave function is given by $\phi_n(\mathbf{r}-\mathbf{R}_i)$ for some i. The creation (annihilation) operator to create (annihilate) an atom in the Wannier state $\phi_n(\mathbf{r}-\mathbf{R}_i)$ and with spin σ is given by $a^\dagger_{in\sigma} = \frac{1}{\sqrt{N}} \sum_{\mathbf{k}} \mathrm{e}^{\mathrm{i}\mathbf{k}\cdot\mathbf{R}_i} a^\dagger_{n\mathbf{k}\sigma}$ $\left(a_{in\sigma} = \frac{1}{\sqrt{N}} \sum_{\mathbf{k}} \mathrm{e}^{-\mathrm{i}\mathbf{k}\cdot\mathbf{R}_i} a_{n\mathbf{k}\sigma}\right)$. As for the Bloch operators, the Wannier operators satisfy the usual fermionic anticommutation relations: $\left\{a_{in\sigma}, a^\dagger_{jn'\sigma'}\right\} = \delta_{i,j}\delta_{n,n'}\delta_{\sigma,\sigma'}$, $\left\{a_{n\mathbf{k}\sigma}, a_{jn'\sigma'}\right\} = \left\{a^\dagger_{in\sigma}, a^\dagger_{jn'\sigma'}\right\} = 0$.

Expressing the Wannier functions in terms of the periodic Bloch functions $u_{n\mathbf{k}}$, we have $\phi_n(\mathbf{r}-\mathbf{R}) = \frac{1}{\sqrt{N}} \sum_{\mathbf{k}} \mathrm{e}^{\mathrm{i}\mathbf{k}\cdot(\mathbf{r}-\mathbf{R})} u_{n\mathbf{k}}(\mathbf{r})$. Thus we see that $\phi_n(\mathbf{r}-\mathbf{R})$ oscillates in k-space at an angular frequency $\mathbf{r}-\mathbf{R}$, and for $\mathbf{r}$ far from the lattice site $\mathbf{R}$ the Wannier function is suppressed by these high frequency oscillations. In this way, the Wannier functions have the desired behavior that they are peaked near the corresponding lattice site and decay as we move further away, with the rate of decay determined by the depth of the periodic potential wells. For this reason, in the subsequent discussion we may refer to the Wannier operators as "creating or annihilating a particle at site i", when what we really mean is creating a particle in the Wannier state centered at the i-th lattice site. This does not imply that the norm of the wavefunction is precisely zero at any other lattice sites.

For a sufficiently deep potential, we can make the tight binding approximation, in which the Wannier states become simply the single-atom electron orbitals. While Hubbard himself made such an approximation in estimating the parameters of the Hubbard model and determining which terms to neglect, it is important to remember that it is possible to speak of Wannier functions for any periodic potential, even in

the case where tight binding fails. In that case, of course, the Wannier functions will not resemble atomic orbital states.

Before proceeding further it is worth reiterating that in the optical lattice systems with which this thesis is concerned, it is neutral atoms that are the mobile particles, not electrons. Moreover, the lattice is generated not by Coulomb interactions with some fixed atomic nuclei, but rather by the electric dipole interaction between the atoms and an optical standing wave. In this section we use the picture of electrons in a crystalline solid because this is the historical context in which the Hubbard model developed. In subsequent sections it should be understood that the creation and annihilation operators refer to the creation and annihilation of atoms, not electrons. We also note that the tight binding approximation is not appropriate for our subsequent calculations. In particular, as the lattice potential is not the sum of the contributions from separate sources at each lattice site, it does not make sense to speak of the states in the potential generated by a single such source. We can however consider the states of a single well by approximating that well as a harmonic potential, and in this sense one can have a sort of tight binding limit. However, such a harmonic approximation becomes increasingly inaccurate when considering atoms in higher bands, as we must when considering interatomic interactions near a broad Feshbach resonance. For our purposes it is best to determine the exact Wannier functions numerically, as can be done by variational methods.[48]

1.1.2 The Hubbard Model

As we have discussed, in band theory the many-body wavefunction of electrons in a periodic potential is given by an antisymmetrized product of the Bloch states. Due to the Pauli exclusion principle, we may have at most two electrons in each Bloch state (one spin up, one spin down). Thus in the ground state the electrons

fill the Bloch states starting from the lowest energy levels up to the Fermi level. If the Fermi level lies in the middle of a band, band theory predicts that the material will be a conductor, whereas if the Fermi level lies between bands the material is expected to be an insulator. However, as noted above these predictions were found not always to be in good agreement with experimental results. In particular, many transition metal oxides with the d-electron bands only partially filled were found to nevertheless be poor conductors or even insulators.[41]

Nevill Mott argued that if the interactions between electrons were sufficiently large relative to the width of the band, then a single band could actually be split into two separate bands.[43–46] In particular, if the band is more than half-filled (that is, if the average number of particles per site is greater than unity) then there will necessarily be sites which are doubly occupied. In that case, the close proximity of the electrons leads to a strong Coulomb repulsion which raises the overall energy of the state. In this way, we see that there is a gap between the states where the band is less than half filled and those with greater than half filling. If the fermi level lies within this gap, we have an insulating state precisely at half-filling: the Mott insulator state. Moreover this theory suggests that a transition from conductor to insulator occurs as the band-width is decreased relative to the Coulomb repulsion between electrons.

The Hubbard model is the simplest model that can describe such a transition, as it contains only the two essential terms: one representing the Coulomb repulsion between electrons, and the other representing the energy of electronic motion between lattice sites.[4] The Hubbard model is written as:

$$H_{Hub} = -t \sum_{<i,j>,\sigma} a^{\dagger}_{i\sigma} a_{j\sigma} + H.c. + U \sum_{i} n_{i\sigma} n_{i\bar{\sigma}} \tag{1.2}$$

Here $a^\dagger_{i\sigma}$ ($a_{i\sigma}$) creates (annihilates) an electron with spin σ in a Wannier state centered at lattice site i, and $n_{i\sigma} = a^\dagger_{i\sigma} a_{i\sigma}$. The sum over $< i, j >$ represents a sum over all pairs of nearest-neighbor sites i and j. U represents the interaction energy of two atoms on the same site, and t is the tunneling matrix element describing the tunneling of atoms between two neighboring sites. The interaction term is sometimes written as $U/2 \sum_i n_i(n_i - 1)$ where $n_i = n_{i\uparrow} + n_{i\downarrow}$, so as to generalize to the case of bosonic particles where more than one particle of each spin is allowed on a site. The Hubbard model, despite its minimalistic form, does indeed show the desired behavior of a transition from a conducting state to a Mott insulating state as the ratio U/t becomes sufficiently large.[49]

1.1.3 Key Approximations in Deriving the Hubbard Model

Hubbard made several simplifying approximations in deriving the model Hamiltonian that bears his name, such as taking all the electrons to be in a single band. Hubbard derived the model starting from the usual k-space Hamiltonian of non-interacting electrons in the band theory, $H = \sum_{k\sigma} \epsilon_k a^\dagger_{k\sigma} a_{k\sigma}$, and then added a Coulomb interaction proportionate to the two-particle matrix elements of $1/r$ (with r the distance between the particles) as well as adding a corresponding exchange term. The role of the exchange term is to enforce the anti-symmetry of the fermionic electrons, and avoid double counting the interactions between electrons due to their role in determining ϵ_k in Hartree-Fock calculations. Hubbard expanded the Bloch states in this Hamiltonian in terms of Wannier functions, as described above. In order to simplify the calculation, he took the Wannier functions to be s-wave atomic orbital states, even though in the transition metals Hubbard was studying the conduction band corresponds to d-wave orbitals. It is also this assumption that allows us to consider only two internal states per electron (spin up and spin down).

The expansion in Wannier functions results in a Hamiltonian which includes Coulomb interactions for particles on any two initial and two final sites. Hubbard estimated these matrix elements so as to determine which could be neglected.[4] The interaction between electrons all on the same site was 20 eV. For electrons on neighboring sites, the diagonal matrix element (diagonal in the basis of tensor products of Wannier functions) was estimated to be 3 eV. Among the off-diagonal matrix elements and diagonal matrix elements between atoms at next-nearest-neighbor or greater separations, Hubbard found no contribution greater than 1/2 eV. Hubbard took the relative magnitudes of each of these interaction matrix elements as a justification for neglecting all but the largest contribution, that of the on-site interaction. There has also been significant interest in extended Hubbard models which include the next largest contribution, that of the diagonal matrix elements for next-nearest neighbors.[50]

We put particular emphasis on the approximations made by Hubbard in deriving the Hubbard model, so as to call attention to the fact that these approximations generally *do not* apply to the case we consider in the bulk of this thesis, that of strongly interacting fermions in an optical lattice. As we discuss in more detail in the next chapter, the strong interatomic interaction ensures that multiple bands are populated whenever two atoms come to the same site, even if all atoms were initially in the lowest band. Thus, it is not sufficient to consider atoms only in a single lattice band. States in higher-bands are increasingly poorly approximated by taking the Wannier functions to be the eigenstates of a single potential well. For this reason it is more appropriate to calculate the Wannier functions numerically using variational methods, rather than to make some form of tight-binding approximation. Moreover, near a broad Feshbach resonance such as is typical in experiments with ^{40}K or ^{6}Li, the

interaction contributes off-diagonal matrix elements between nearest neighbors that are non-negligible in comparison to the single-particle tunneling matrix elements. (These are off-diagonal in reference to the basis of Wannier-state tensor products – that is, they involve an atom moving from one site to another.) This is in contrast to the case considered by Hubbard, where nearest-neighbor interactions and especially off-diagonal nearest-neighbor interactions were comparatively small.

1.2 Feshbach Resonance

Feshbach resonances were first studied in the context of nuclear physics. They describe how during neutron scattering processes it is possible to form a quasibound nucleus at an energy level close to that of the free neutrons.[51, 52] Similarly, in ultracold atomic gasses scattering processes can involve a resonance between the incoming states and a quasibound diatomic molecule state.[14] As we shall see, the hyperfine state of the atoms in the molecular bound state (known as the "closed" channel) will be different than for the initial incoming atoms (the "open" channel). With an applied magnetic field this results in different Zeeman shifts for the two channels, making it possible to adjust the energy difference between the two. There will be some magnetic field for which the closed channel bound state energy level matches the free atom threshold in the open channel, which is the condition for Feshbach resonance. At this point, the s-wave scattering length describing these collisions diverges. Furthermore, the magnetic field can be adjusted to either side of the resonance so as to tune the scattering length over a wide range of values.

1.2.1 Low Energy Scattering

At this point, it is useful to review the basics of low-energy scattering theory[53]. For a two-particle scattering process with energy $E_k = \hbar k/2m_r$ the Schrödinger

equation takes the form:

$$\left(-\frac{\hbar^2}{2m_r}\nabla^2 + V(\mathbf{r})\right)\psi_k(\mathbf{r}) = E_k\psi_k(\mathbf{r}) \tag{1.3}$$

where $\mathbf{r}$ is the relative coordinate and the reduced mass $m_r = m/2$ for particles of equal mass.

We can write the solution for large r as a plane wave plus an outgoing spherical wave. For spherically symmetric potential $V(\mathbf{r}) = V(r)$, this takes the form:

$$\psi_k \sim e^{i\mathbf{k}\cdot\mathbf{r}} + f_k(\theta)\frac{e^{ikr}}{r} \tag{1.4}$$

ψ can also be expanded in terms of partial waves $(u_{l,k}(r)/r)\,Y_l^m(\theta,\phi)$, where $Y_l^m(\theta,\phi)$ are spherical harmonics and $u_{l,k}(r)$ solves the equation:

$$\left[-\frac{d^2}{dr^2} + \frac{l(l+1)}{r^2} + \frac{2m}{\hbar^2}V(r) - k^2\right]u_{l,k}(r) = 0 \tag{1.5}$$

Thus the effective potential includes a centrifugal barrier:

$$V_c = \frac{\hbar^2 l(l+1)}{2mr^2} \tag{1.6}$$

At low temperatures the interaction energy of the particles is two small to overcome this barrier, and thus $V(r)$ can only produce scattering for the s-wave ($l = 0$) case. (For Lithium, the centrifugal barrier is $7mK \times k_B$ [54]).

Thus, instead of the usual sum over partial waves, $f(k)$ is given by the $l = 0$ case alone:

$$f_k = \frac{1}{k}e^{i\delta_0(k)}\sin(\delta_0(k)) \tag{1.7}$$

where $\delta_0(k)$ is the s-wave scattering phase shift. The cross section is:

$$\sigma = \int |f_k|^2\, d\Omega = \frac{4\pi}{k^2}\sin^2(\delta_0(k)) \tag{1.8}$$

and the s-wave scattering length is given by: $a_s = -\lim_{k\to 0}\tan(\delta_0(k))/k$

For the case of identical fermions, s-wave scattering is prevented by the Pauli exclusion principle. But as shown above, for sufficiently low energies there can be *only* s-wave scattering, due to the centrifugal barrier. Thus, in a sufficiently cold vapor of identical fermions, the particles do not interact. In order to produce a system of ultracold interacting fermions it is therefore necessary to have at least two species of particle. This can be achieved by using fermionic atoms in two different hyperfine states. (Interactions are also necessary to maintain thermal equilibrium as the atoms are cooled to low temperature, but in that case we have the alternative of placing all the fermions in a single state but allowing them to interact with a vapor of bosonic particles. This is known as "sympathetic cooling".)

1.2.2 Hyperfine states of ^{6}Li and ^{40}K

For an alkali atom in the ground state the electron angular momentum (quantum number J) corresponds to the spin of the valence electron. (Filled electron shells cannot contribute, and the groundstate has zero orbital angular momentum.) Thus, the total angular momentum is the sum of the electron spin and the nuclear spin. For a given nuclear spin quantum number I, the hyperfine energies for each of the quantum numbers F (total spin) and m_F can be determined (as a function of the magnetic field B) from the Breit-Rabi formula[55]:

$$E_{hf}(B, F = I \pm \frac{1}{2}, m_F) = -\frac{\Delta E_0}{2(2+I)} + m_F g_I \mu_B B \pm \frac{\Delta E_0}{2}\sqrt{1 + \frac{4m_F}{2I+1}x + x^2} \quad (1.9)$$

where $x = (g_I - g_J)\mu_B B/\Delta E_0$ and ΔE_0 is the separation between the hyperfine levels at $B = 0$.

^{6}Li has nuclear spin 1, giving rise to six groundstate hyperfine levels, whereas ^{40}K has nuclear spin 4, giving rise to eighteen groundstate hyperfine levels (see Fig. 1.1). m_F is a good quantum number over any magnetic field strength, whereas m_J and

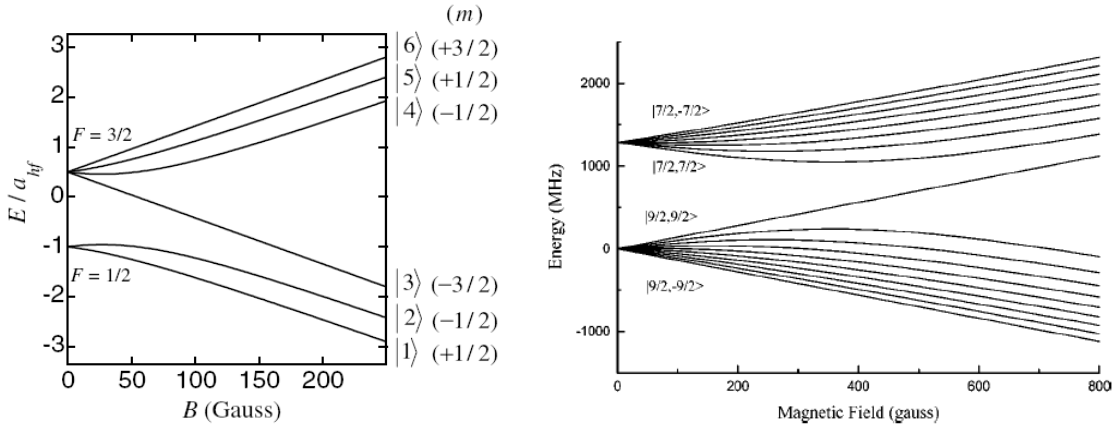

Figure 1.1: Groundstate hyperfine structure for the isotopes most commonly used in experiments with ultracold fermions. Left figure: Hyperfine Structure of ^{6}Li ($a_{hf} = 152.1MHz$) (from [1]). Right figure: Hyperfine Structure of ^{40}K (from [2])

m_I are only good quantum numbers in the limit of strong fields, where the electron spin essentially decouples from the nuclear spin.

1.2.3 s-wave Scattering Length near Feshbach Resonance

Two atom scattering processes will depend on the initial hyperfine states of the atoms. As noted above, at low temperatures fermions can only be scattered if they are in two different hyperfine states. The hyperfine interaction may couple these states to other hyperfine states, but if those states have higher total energy in the limit of large separation between the atoms, then as the atoms move apart they must ultimately end up back in the channel in which they started. In this sense we may speak of the "open channel" (with the lower potential at large separation distances) and the "closed channel" with the higher potential at large separations. Even though the closed channel is excluded as a final state, there may be bound states in the "closed channel" which are allowed as an intermediate state. Thus, the bound states contribute a correction to the final state that is second order in the hyperfine interaction (or whatever part of the Hamiltonian takes one hyperfine state to another). This contribution is greatest when the energy of the bound state is equal

to the incident scattering energy – this is the condition for a Feshbach resonance.

The importance of Feshbach resonance in atomic physics stems from the fact that, when the magnetic moment of the atoms in the closed channel differs from that in the open channel, the energy levels in the two channels experience different Zeeman shifts in response to an applied magnetic field. Thus, the energy of the closed channel bound state can be tuned relative to the open channel, going from one side of the Feshbach resonance to the other simply by changing the strength of the applied magnetic field.

The scattering length can be readily shown to depend on the energy difference between the detuning of closed channel bound state from Feshbach resonance, and thus on the applied magnetic field.[56] The bound state radial wave function $\phi(R)$ solves the equation:

$$\left(-\frac{\hbar^2}{2\mu}\frac{d^2}{dR} + U(B,R)\right)\phi(R) = \epsilon(B)\phi(R) \tag{1.10}$$

where μ is the reduced mass and $U(B,R)$ is the closed channel effective potential. If B_0 is the magnetic field where the energy of the closed channel bound state crosses the open channel threshold energy ($\epsilon(B_0) = 0$), then for B close to B_0 we can write:

$$\epsilon(B) = \mu_{co}\,(B - B_0) \tag{1.11}$$

where μ_{co} is the difference in magnetic moments between the open and closed channels.

For B far from resonance, the closed channel does not contribute to the scattering. In that case, the radial wave function $\psi(R)$ in the open channel is:

$$\left(-\frac{\hbar^2}{2\mu}\frac{d^2}{dR} + U_{bg}(R)\right)\psi(R) = \epsilon_0\psi(R) \tag{1.12}$$

where U_{bg} is the open channel effective potential and ϵ_0 is collision kinetic energy.

As $R \to \infty$, we have:

$$\psi(R) \to \sqrt{\frac{2\mu}{\pi\hbar^2 k}} \sin\left(kR + \xi_{bg}\right) \tag{1.13}$$

where $k = \sqrt{2\mu\epsilon_0/\hbar^2}$.

If we take B close to resonance so that the closed channel bound state contributes to scattering, we find that the open channel wavefunction $\psi(R, \epsilon, B)$ has the same asymptotic form but with a change in the phaseshift ξ:

$$\psi(R, \epsilon_0, B) \to \sqrt{\frac{2\mu}{\pi\hbar^2 k}} \sin\left(kR + \xi(\epsilon_0, B)\right) \tag{1.14}$$

where $\xi(\epsilon_0, B) = \xi_{bg} + \Delta\xi(\epsilon_0, B)$.

For small $\epsilon(B)$ (i.e., the closed channel bound state close to the open channel threshold), we have:

$$\tan\left(\Delta\xi(\epsilon_0, B)\right) = \frac{\Gamma(\epsilon_0)}{2\left(\epsilon_0 - \epsilon(B) - \delta\epsilon(B)\right)} \tag{1.15}$$

where $\delta\epsilon(B)$ is a shift of the bare resonance crossing point, and $\Gamma(\epsilon_0)$ is the excited state decay width, which can be determined from Fermi's golden rule: $\Gamma(\epsilon_0) = 2\pi \left|\langle\phi| V |\psi\rangle\right|^2$

The scattering length is given by:

$$a_s = -\lim_{k\to 0} \frac{\tan(\xi(\epsilon_0, B))}{k} \approx -\lim_{k\to 0} \frac{\tan(\xi_{bg})}{k} - \lim_{k\to 0} \frac{\tan(\Delta\xi(\epsilon_0, B))}{k} \tag{1.16}$$

for $ka_s \gg 1$. Thus,

$$\begin{aligned} a_s = a_{bg} - \frac{\Gamma(\epsilon_0)}{2k\left(\epsilon_0 - \epsilon(B) - \delta\epsilon(B)\right)} &= a_{bg} - \frac{\Gamma(\epsilon_0)}{2k\mu_{co}\left(B - B_0 - \delta B_0\right)} \\ &= a_{bg}\left(1 - \frac{W}{B - B_0 - \delta B_0}\right) \end{aligned} \tag{1.17}$$

where the resonance width W is given by:

$$W = \frac{\Gamma(\epsilon_0)}{2ka_{bg}\mu_{co}} = \frac{\pi\left|\langle\phi| V |\psi\rangle\right|^2}{ka_{bg}\mu_{co}} \tag{1.18}$$

(W can be positive or negative depending on the sign of $\Delta\mu a_{bg}$)

Redefining B_0 as the true resonance crossing $B_0 + \delta B_0$, this is the usual formula for the scattering length near a Feshbach resonance:

$$a_s = a_{bg}\left(1 - \frac{W}{B - B_0}\right) \tag{1.19}$$

Thus we can see that near a Feshbach resonance the scattering length can be tuned over a wide range of positive and negative values as the applied magnetic field is varied, and that it diverges at the resonance point. It is worth noting, however, that the scattering cross section remains finite:

$$\sigma = \frac{4\pi a_s^2}{1 + k^2 a_s^2} \tag{1.20}$$

Although for simplicity the case of a single closed channel bound state coupling to the open channel was treated above, in practice one may have multiple bound states in different closed channels coupling to a single open channel. Nevertheless, one finds that the above expression for the scattering length holds, albeit with a somewhat more complicated derivation of W and B_0 than given above. In practice, the location and width of the resonance are determined by experiment.

The most frequently utilized Feshbach resonance in experiments on ^{6}Li occurs for the $|1/2, 1/2\rangle$, $|1/2, -1/2\rangle$ (open) channel and is located at $B_0 = 834G$, with an extremely large width $W = 300G$. ^{40}K experiments have utilized a Feshbach resonance in the $|9/2, -9/2\rangle$, $|9/2, -7/2\rangle$ channel located at $B_0 = 202G$ and with a width of $W = 8G$.[57]

1.2.4 The Two Channel Model of Feshbach Resonance

We can write an effective Hamiltonian that describes ultracold fermions near a Feshbach resonance. Proposed Hamiltonians for this purpose fall into two general

classes: two channel models and single channel models. Two channel models include both the closed channel molecules and open channel atoms explicitly, whereas in single channel models the closed channel state is adiabatically eliminated, leaving a Hamiltonian in terms of open channel atoms with an effective interaction determined by the scattering length a_s.[58, 59] For the single-channel model to be valid, it is necessary that the closed channel population is small. Here we use the more generally valid two-channel model, such as was first proposed by Holland et al.[60–62]

$$\begin{aligned} H-\mu N = & \sum_{\mathbf{k},\sigma}\left(\epsilon_{\mathbf{k}}-\mu\right)a^{\dagger}_{\mathbf{k}\sigma}a_{\mathbf{k}\sigma}+\sum_{\mathbf{k}}\left(\epsilon_{\mathbf{k}}/2-2\mu+\nu\right)b^{\dagger}_{\mathbf{k}}b_{\mathbf{k}} \\ & +\frac{\alpha}{\sqrt{V}}\sum_{\mathbf{k},\mathbf{q}}\left(b^{\dagger}_{\mathbf{q}}a_{-\mathbf{k}+\mathbf{q}/2,\downarrow}a_{\mathbf{k}+\mathbf{q}/2,\uparrow}+H.c.\right) \\ & +\frac{U_{bg}}{V}\sum_{\mathbf{k},\mathbf{k}',\mathbf{q}}a^{\dagger}_{\mathbf{k}+\mathbf{q}/2,\uparrow}a^{\dagger}_{-\mathbf{k}+\mathbf{q}/2,\downarrow}a_{-\mathbf{k}+\mathbf{q}/2,\downarrow}a_{\mathbf{k}+\mathbf{q}/2,\uparrow} \end{aligned} \tag{1.21}$$

where $a^{\dagger}_{\mathbf{k}\sigma}$ creates an open-channel atom in hyperfine state σ and $b^{\dagger}_{\mathbf{k}}$ creates an closed-channel molecule. The total number of particles is $N=\sum_{\mathbf{k},\sigma}a^{\dagger}_{\mathbf{k}\sigma}a_{\mathbf{k}\sigma}+2\sum_{\mathbf{k},\sigma}b^{\dagger}_{\mathbf{k}}b_{\mathbf{k}\sigma}$, μ is the chemical potential, and V is the quantization volume. Here α and U_{bg} and ν represent unrenormalized values of the atom-molecule coupling rate, the background atom scattering rate, and the detuning of the closed-channel molecules from the open-channel free atom threshold energy.

However, some renormalization of these parameters is clearly required. This is because in writing the Hamiltonian the tightly bound closed-channel molecules have been taken to be point particles, and the interatomic couplings treated as zero-range δ functions. This is invalid at small distances (or, equivalently, at large $\mathbf{k}$) which leads to the so-called ultraviolet divergence resulting in our unrenormalized parameters taking on infinite values. Fortunately we can transform these parameters to renormalized ones, in which the divergent part has been separated out. These

renormalized or "physical" parameters are given by the standard renormalization relations $U_{bg} = \Gamma U_{bg}^{(p)}$, $\alpha = \Gamma\alpha^{(p)}$, and $\nu = \nu^{(p)} + \Gamma(\alpha^{(p)})^2 \sum_{\mathbf{k}} (2\epsilon_{\mathbf{k}})^{-1}$ where $\Gamma^{-1} = 1 - U^{(p)} \sum_{\mathbf{k}} (2\epsilon_{\mathbf{k}})^{-1}$. The physical parameters can be expressed in terms of empirically measurable values such as the scattering length. In particular, $U_{bg}^{(p)} = 4\pi\hbar^2 a_{bg}/m$ and $\nu^{(p)} = \mu_{co}(B - B_0)$. The atom-scattering rate U_s is related to the atom-molecule coupling and the detuning by $U_s = -(\alpha^{(p)})^2/\nu^{(p)} = -(\alpha^{(p)})^2/\mu_{co}(B - B_0)$. We also have $U_s = 4\pi\hbar^2 a_s/m \approx -4\pi\hbar^2 a_{bg} W/m(B - B_0)$ where the last approximation is from equation (1.19) close to resonance. Thus, we find $(\alpha^{(p)})^2 = 4\pi\hbar^2 a_{bg}\mu_{co} W/m$. In subsequent sections we generally drop the superscript (p) when it is clear we're referring to the physical parameters.

1.3 Optical Lattices and Superlattices

Optical lattices have been described as "artificial crystals of atoms bound by light." That is, instead of a naturally occurring crystal where atoms are arranged periodically due to interatomic forces, in an optical lattice the periodic arrangement of atoms results from their interactions with an optical standing wave. The standing wave is created by combining two laser beams of equal wavelength propagating in opposite directions. In practice this is usually achieved by reflecting a single laser beam back on itself with a fixed mirror. A one-dimensional lattice consisting of only a single retroreflected beam produces confinement in sufficiently low-energy atoms along the direction of the beam, while leaving them unconfined in the other directions. One can add additional lasers orthogonal to the first, so as to produce confinement in two or three dimensions. (Changing the angle between the beams can produce different lattice geometries, such as the triangular lattice, but in this work we will focus on the case of a square lattice.)

1.3.1 Dissipative Forces and Gradient Forces

Optical lattices in general exert two types of forces on atoms: dissipative forces and gradient forces.[63, 64] Dissipative forces can be understood as arising from the scattering of the incident field into unoccupied modes of the vacuum field. Because such scattering is irreversible, these forces are non-conservative. Gradient forces, in contrast, are conservative forces which can be understood as arising from scattering from one traveling component of the incident field into the counterpropagating component. An alternative but equivalent explanation is that the standing wave field produces a spatially modulated Stark shift in the atoms' energy, and the force arises as the gradient of this energy shift.

Much of the early work on what has come to be known as optical lattices focused on the use of the dissipative force to achieve cooling. In particular, the optical molasses introduced by Chu et al. in 1985 was essentially an optical lattice, with identical counterpropagating laser beams along three orthogonal axes.[65] However at the time the emphasis was on reducing the speed of the atomic motion, and thus the temperature. Ordering in real space was only observed after the discovery of sub-Doppler cooling by W. D. Phillips group a few years later.[66]

The optical molasses uses the Doppler cooling method proposed by Hänsch and Schawlow in 1975.[67] If the beams are tuned slightly below the resonant frequency for an atomic transition, then those beams that oppose the atomic velocity are blue-shifted towards resonance while the beams that align with the atom's velocity are red-shifted further from resonance. This means that light is scattered at a greater rate from those beams that oppose the atom's velocity. Because there is no preferred outgoing direction of the scattered light, the average force is in the direction of the incident light. This produces a net force in opposition to the atomic motion, and

thus, cooling.

Calculations using the two-level approximation to the atom show that there is a limit on the cooling in optical lattices attainable via the dissipative force (the Doppler limit), and typical lattice depths are not such that the atoms can be localized to particular wells without additional cooling. In fact, sub-Doppler cooling was found to be achievable in optical lattices.[66] In contrast to Doppler cooling, this sub-Doppler cooling, due to the "Sisyphus effect", can only be understood by consideration of more than two levels of the atom.[68, 69] In brief: For certain choices of the beam polarizations (notably the lin$\perp$lin polarization in which the two beams are given orthogonal linear polarizations), atoms in two different internal states will feel different standing wave potentials, such that the maxima of one potential are at the minima of the other. Cooling is then achieved as the atoms continually climb to the top of a potential well (losing kinetic energy on the way) only to be optically pumped into the other state and thus the bottom of the well.

In contrast, if the fields are far-detuned from any atomic transition, it is the gradient force that dominates. In particular, if we consider the interaction between an optical field oscillating with angular frequency ω and two atomic levels with frequency separation ω_0, so that the detuning is $\delta = \omega_0 - \omega$, then for large δ the dissipative force is proportionate to $|\Omega_0|^2/\delta^2$ and the gradient force is proportionate to $|\Omega_0|^2/\delta$, where Ω_0 is the Rabi frequency.[64] Thus for sufficiently large $|\delta|$ the dissipative force can be neglected, while the gradient force can still be nonnegligible for large enough values of $|\Omega_0|$. Ordinarily the light force experienced by an atom with velocity $\mathbf{v}$ depends on the Doppler shifted frequency of the light, so that instead of a detuning δ we have $\delta \pm \mathbf{k}\cdot\mathbf{v}$ (where the standing wave is formed by counterpropagating plane waves with wavevectors $\mathbf{k}$, $-\mathbf{k}$). However, for $|\delta| \gg |\mathbf{k}\cdot\mathbf{v}$ the gradient force is

essentially the same for atoms of any velocity, namely:

$$\mathbf{F}(\mathbf{r}) = -\frac{\hbar\mathbf{k}\left|\Omega_0\right|^2}{4\delta}\sin\left(2\mathbf{k}\cdot\mathbf{r}\right) \tag{1.22}$$

This satisfies $\mathbf{F} = -\nabla\left(\Delta E\right)$ for the spatially varying energy shift

$$\Delta E = -\frac{\hbar\mathbf{k}\left|\Omega_0\right|^2}{4\delta}\cos^2\left(\mathbf{k}\cdot\mathbf{r}\right) \tag{1.23}$$

Thus we see that all the atoms experience the same periodic potential, and in particular we note that the amplitude of this potential can be readily controlled by changing the amplitude of the beams (which is proportionate to the Rabi frequency Ω_0, while the spacing between minima is just controlled by the beams' wavelength.

The far off-resonant trap is of particular importance in trapping ultracold atoms which have been cooled well below the Doppler limit. While the dispersive force can be used for trapping, as in the magneto-optical trap (MOT), the scattering of photons into the vacuum field modes produces a recoil in the atom (in a random determined direction) and leads to heating. As this recoil energy is well below the Doppler limit, it only becomes relevant for sub-Doppler cooling. In order to avoid this recoil heating, the sub-Doppler cooled atoms must be trapped by some conservative force. While magnetic trapping is possible for certain states (the low-field seeking states), those states whose energy is reduced in *high* magnetic fields cannot be magnetically trapped, as this would require the magnetic field to have a local maximum, which is forbidden by Maxwell's equations. In fact, the hyperfine states of ^{40}K and ^{6}Li associated with the commonly utilized Feshbach resonances are high-field seeking (see figure 1.1), and thus for experiments with ultracold atoms in these states a far-off resonant optical trap is required in the final stage. Typical experiments utilize Doppler cooling in a MOT in an earlier stage, followed by forced evaporative cooling in a far off-resonant trap or magnetic trap (with the states transferred to magnetically

trappable states as necessary) to achieve a degenerate fermi gas. Because of the aforementioned suppression of scattering for fermions at low temperatures, either two interacting fermion spin-species or else some sympathetic cooling by interactions with bosons is required so as to maintain thermal equilibrium during the evaporative step.

1.3.2 Optical Superlattices

While even the simple optical lattice described above offers substantial control over the many-body physics through the continuously-tunable lattice depth and lattice spacing, further control can be achieved by superimposing additional lattice beams. This is exactly the definition of an optical superlattice: a superposition of multiple optical standing waves. In the most basic case, we simply combine two standing waves one of which has twice the wavelength of the other. Thus we have

$$V(x) = -V_L \sin^2\left(\frac{\pi x}{a}\right) - V_S \sin^2\left(\frac{2\pi x}{a} - \phi\right) \tag{1.24}$$

where V_L and V_S are the depths of the individual lattices with lattice spacings a and $a/2$, respectively, and ϕ is the phase difference between these two lattices. This leads to a lattice with alternating higher and lower barriers. Specifically, if the two lattice beams are in phase, we just have an array of double wells (see figure 1.2(a)), where the double well central barriers can be tuned separately from the barriers between double wells. If instead the two standing waves are out of phase, the double wells become asymetrical, with the minimum of one well higher than the other (see figure 1.2(b)). This energy bias between the neighboring wells is controlled by the phase shift between the two simple lattices, which is itself a tunable parameter.

In particular, the optical superlattice was used in recent experiments to study superexchange interactions[70] and second order tunneling[71]. In these experiments

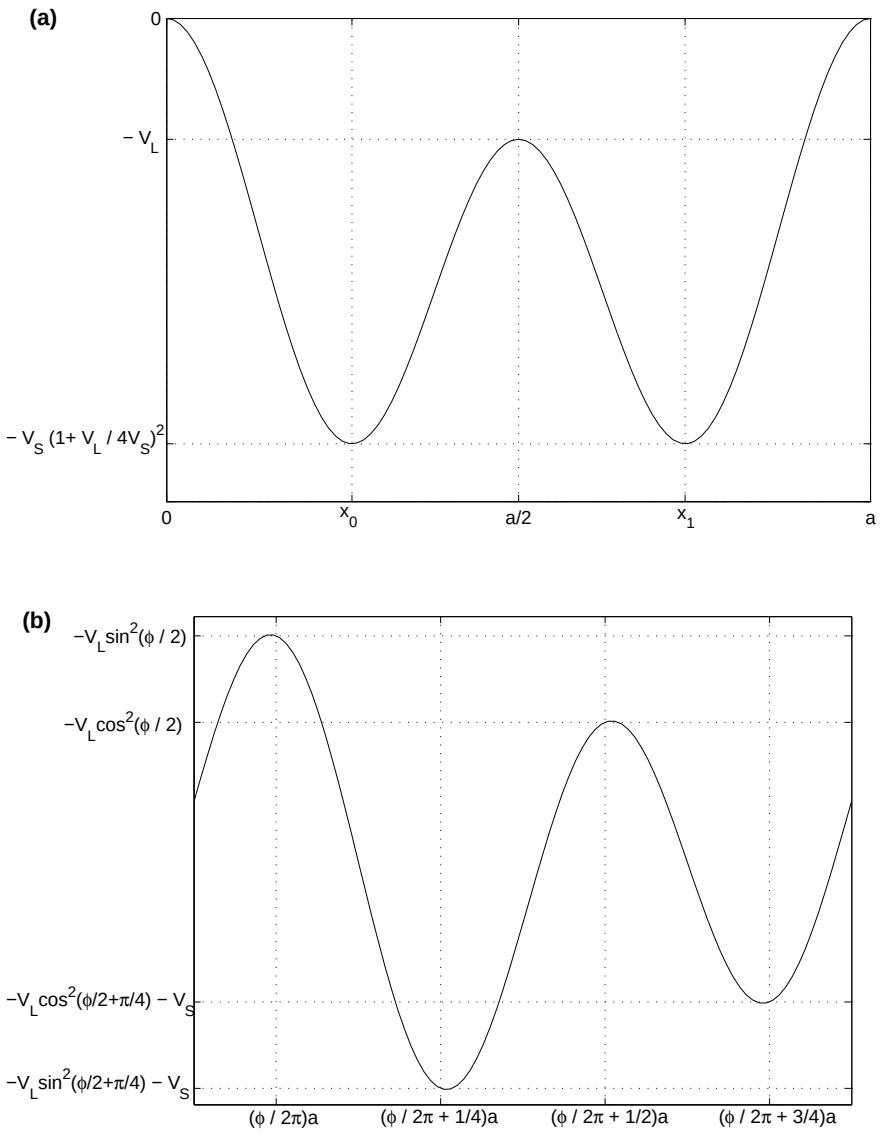

Figure 1.2: The super-lattice potential $-V_L \sin^2\left(\frac{\pi x}{a}\right) - V_S \sin^2\left(\frac{2\pi x}{a} - \phi\right)$ vs. x, for $0 \leq x \leq a$. In these figures we take $V_S = 3V_L$, but the formulas shown are general. **(a)** The $\phi = 0$ case: For $4V_S > V_L$ there are two minima located at $x_0 = \frac{a}{2\pi}\cos^{-1}\left(-\frac{V_L}{4V_S}\right)$ and $x_1 = a - x_0$. The height of the central barrier is $V_S\left(1 - \frac{V_L}{4V_S}\right)^2$. **(b)** The $\phi > 0$ case: The phase difference shifts the positions of the minima and introduces a bias between the two wells. For $V_S > V_L$ the positions of the wells are approximated by the expressions shown in the figure, so that the bias between the minima is $V_L \sin(\phi)$. In this figure we take $\phi = \frac{\pi}{4}$.

the standing waves were produced by a 765 nm Titanium-Sapphire laser and a 1530 nm fibre laser. The difference in wavelength can be measured by recording the beat note between the two (after frequency-doubling part of the long-wavelength beam), and a feedback circuit allows the fibre laser's frequency to be adjusted, so as to tune the frequency difference over a 1 GHz range. If both the long-wavelength and short-wavelength beam are retroreflected by the same mirror, this fixes the phase of each at that point. By placing that mirror well *beyond* the atomic cloud (25 cm beyond in the Mainz experiment), one ensures that the two beams will have gained a phase difference over the course of traversing that difference, and that phase difference depends on the tunable frequency difference between the two. In contrast, because the atomic cloud itself extends over a much shorter region in space, the phase difference between the beams is roughly constant over the atoms.

1.4 Chapter Summary and Thesis Outline

In this chapter we have introduced the physical system to be studied in this thesis, that of two-component ultracold fermionic atoms in an optical lattice, with strong, tunable interatomic interactions due to a Feshbach resonance controlled by an external magnetic field. We note that this system can be described by a generalization of the famous Hubbard model. This general Hubbard model contains all the terms of the usual Hubbard model plus additional terms representing correlated tunneling – that is, an enhanced tunneling among atoms of one hyperfine spin-state if additional atoms of the opposite spin are present on either site. The derivation of this Hamiltonian we reserve for the subsequent chapter. Here we instead have focused on the origins of Hubbard's original model, with particular emphasis on the approximations used in its derivation. (We took a brief detour to discuss the Bloch and Wannier state

formalism, which will be of use throughout this thesis.) We noted in particular that the optical lattice system under consideration breaks many of Hubbard's key assumptions. That it is nevertheless well-described by a single-band Hubbard like model may at this point be quite surprising. The remainder of this introductory chapter outlined certain key experimental techniques, namely the use of Feshbach resonance, and the implementation of optical lattices and in particular the superlattices which further break the discrete translational symmetry of the original lattice.

The remainder of this dissertation will cover the following general topics:

- We review the origins of the generalized Hubbard model (GHM) as an effective Hamiltonian for strongly interacting fermions in an optical lattice. Specifically, we present both a direct derivation of this Hamiltonian[3] and a separate argument that this is in fact the most general possible Hamiltonian for the system that respects certain key symmetries such as the $SU(2)$ spin symmetry, and given certain conditions on the lattice depth.[24]

- We derive the two body-states allowed by the GHM. We discuss two motivations of this search, one being to simplify comparisons between the GHM parameters and the full two-body wavefunction as given by the Schrödinger equation for a periodic potential. This presents a possible means for examining the relationship between the GHM parameters and the experimentally controllable parameters such as lattice depth and applied magnetic field. The other motivation is to extrapolate the many-body physics from that of the two-body solutions, in analogy to the standard BCS theory.

- We propose a means of experimentally measuring the GHM parameters and empirically confirming that the model has the form of the generalized Hubbard model. This proposal uses an optical superlattice to subdivide the lattice into

pairs of neighboring sites, such that interactions are highly suppressed except within these pairs. In similar technique has been used in recent experiments on optical lattice bosons.[70, 71] Because the physics of the GHM is exactly solvable in the two-site system, this allows us to unambiguously compare the experimental signatures to the predictions of the theory.

- We consider the case of a lattice subdivided into four-site square plaquettes, such that atomic tunneling and interactions between different plaquettes are highly suppressed. Such a configuration can be achieved with an optical superlattice. We exactly determine the eigenstates and eigenenergies of this system for various filling numbers, taking particular note of changes in the symmetry of the plaquette states as we adjust the dressed molecule detuning (a parameter controlled by the magnetic field). The four-site plaquette is of particular interest because it is the smallest grouping of lattice sites that can exhibit d-wave rotational symmetry, and is thus a potential building block for many-body states with d-wave excitations.

- We examine the generalized Hubbard model on a lattice of weakly coupled four-site plaquettes. This is realizable in experiments by a superlattice configuration similar to that of the uncoupled-plaquette case, but with the potential barrier between plaquettes somewhat reduced. The weakness of the interplaquette coupling relative to the intraplaquette interactions allows the system to be studied by means of degenerate perturbation theory. This yields an effective Hamiltonian for which the vacuum state and excitations correspond to the states of the generalized Hubbard model on non-interacting plaquettes. We compare these results to similar results for the ordinary Hubbard model in the highly-plaquettized limit, noting the importance of symmetry in fixing the form of the

effective Hamiltonian. Lastly, we consider a mean field treatment of this effective Hamiltonian, and make comparisons to the d-wave superconducting state with nodal quasiparticles which occurs in high-T_c superconductors.

CHAPTER II

Generalized Hubbard Model for Fermions in an Optical Lattice near Feshbach Resonance

In the previous chapter we briefly reviewed the Hubbard model, as well as the use of optical lattices and Feshbach resonance in experiments with ultracold atoms. Before moving on to discuss new results concerning the general Hubbard model as it applies to strongly-interacting fermions in optical lattices, it is useful to first review the theoretical argument for believing the model describes this system, as given in References [3, 24]. That is the focus of this chapter. We will present a direct derivation of this Hamiltonian, and will show by a different approach that the general Hubbard model is in fact the most general Hamiltonian allowed for this system by considerations of the Hilbert space and spin symmetry.

2.1 Field Operator Hamiltonian

We consider fermionic atoms prepared in two hyperfine states (labeled with spin index $\sigma = \uparrow, \downarrow$). These might for instance be the $|F = 1/2, m_F = 1/2\rangle$ and $|F = 1/2, m_F = -1/2\rangle$ states of ^{6}Li, or the $|F = 9/2, m_F = -9/2\rangle$ and $|F = 9/2, m_F = -7/2\rangle$ states of ^{40}K. In each case, there is a wide Feshbach resonance (near $B = 834$G for ^{6}Li and $B = 202$G for ^{40}K) near which atoms in these two states couple to a tightly bound diatomic Feshbach molecule. We take the atoms to

have been loaded into a far-detuned optical lattice generated by counterpropagating laser beams in each orthogonal direction, each with equal amplitude and with wave number $k_0 = 2\pi/\lambda$.

We can split the full Hamiltonian of this system into two parts, $H = H_0 + H_I$, where H_0 is due to the kinetic energy of the particles and their interactions with the lattice potential, and H_I is due to the interactions between the particles. Expressed in terms of field operators $\Psi_\sigma^{(a)}(\mathbf{r})$ for atoms and $\Psi^{(m)}(\mathbf{r})$ for bare molecules (so named to differentiate them from the dressed molecules we introduce subsequently), the Hamiltonian is given by:

$$H_0 = \sum_\sigma \int \Psi_\sigma^{(a)\dagger}(\mathbf{r}) \left(T_a + V_a\right) \Psi_\sigma^{(a)}(\mathbf{r}) d^3\mathbf{r} + \int \Psi^{(m)^\dagger}(\mathbf{r}) \left(T_m + V_m + \nu_b\right) \Psi^{(m)}(\mathbf{r}) d^3\mathbf{r} \tag{2.1}$$

$$H_1 = \alpha \int \Psi^{(m)\dagger}(\mathbf{r}) \Psi_\uparrow^{(a)}(\mathbf{r}) \Psi_\downarrow^{(a)}(\mathbf{r}) d^3\mathbf{r} + H.c. + U_{bg} \int \Psi_\downarrow^{(a)\dagger}(\mathbf{r}) \Psi_\uparrow^{(a)\dagger}(\mathbf{r}) \Psi_\uparrow^{(a)}(\mathbf{r}) \Psi_\downarrow^{(a)}(\mathbf{r}) d^3\mathbf{r} \tag{2.2}$$

The kinetic energy is $T_a = 2T_m = -\hbar^2\nabla^2/2m$ (where m is the mass of the atoms), the lattice potential energy is $V_a = V_m/2 = V_0\left(\sin^2 k_0 x + \sin^2 k_0 y + \sin^2 k_0 z\right)$, and ν_b is the detuning of the bare molecules relative to the free atom threshold in the open channel. The values of the atom-molecule coupling rate α and the background scattering rate of the atoms U_{bg} can be determined from empirical measurements of the s-wave scattering length:

$$a_s = a_{bg}\left(1 - \frac{W}{B - B_0}\right) \tag{2.3}$$

Measuring a_s for different magnetic field strengths B is sufficient to determine the background scattering length a_{bg}, the resonance width W and the magnetic field B_0 at which the resonance occurs. (Indeed, all these parameters have been measured

for the Feshbach resonances of ^{6}Li and ^{40}K referred to above.[72, 73]) As shown in the previous chapter, we can express α and U_{bg} in terms of these measured values as $\alpha = \sqrt{4\pi\hbar^2\mu_{co}W\left|a_{bg}\right|/m}$ and $U_{bg} = 4\pi\hbar^2 a_{bg}/m$.

2.2 Wannier Function Expansion of H_0 and H_I

At this point we wish to transform from a Hamiltonian in terms of spatial coordinates to one in terms of lattice sites. This is accomplished by expanding the field operators in terms of Wannier functions:

$$\Psi_\sigma^{(a)}(\mathbf{r}) = \sum_{i\mathbf{p}} a_{i\mathbf{p}\sigma} w_{\mathbf{p}}^{(a)}(\mathbf{r}-\mathbf{r}_i) \tag{2.4}$$

$$\Psi^{(m)}(\mathbf{r}) = \sum_{i\mathbf{p}} b_{i\mathbf{p}} w_{\mathbf{p}}^{(m)}(\mathbf{r}-\mathbf{r}_i) \tag{2.5}$$

where $w_{\mathbf{p}}^{(a)}(\mathbf{r}-\mathbf{r}_i)$ and $w_{\mathbf{p}}^{(m)}(\mathbf{r}-\mathbf{r}_i)$ are the Wannier functions for atoms and molecules, respectively, centered at site $\mathbf{r}_i$ and for lattice bands $\mathbf{p} = (p_x, p_y, p_z)$. (We take the Wannier functions to be products of the single-dimensional Wannier functions, $w_{\mathbf{p}}^{(a)}(\mathbf{r}-\mathbf{r}_i) = w_{p_x}^{(a)}(x-x_i)\, w_{p_y}^{(a)}(y-y_i)\, w_{p_z}^{(a)}(z-z_i)$.) $a_{i\mathbf{p}\sigma}$ and $b_{i\mathbf{p}}$ are the annihilation operators for the corresponding modes. With this expansion, H_0 becomes

$$H_0 = \sum_{i\mathbf{p}} \left(\epsilon_{\mathbf{p}}^{(m)} + \nu_b\right) b_{i\mathbf{p}}^\dagger b_{i\mathbf{p}} + \sum_{i\mathbf{p}\sigma} \epsilon_{\mathbf{p}}^{(a)} a_{i\mathbf{p}\sigma}^\dagger a_{i\mathbf{p}\sigma} + \sum_{i\mathbf{p}} \sum_{j\in N(i)} \left(t_{\mathbf{p}}^{(m)} b_{i\mathbf{p}}^\dagger b_{j\mathbf{p}} + \sum_\sigma t_{\mathbf{p}}^{(a)} a_{i\mathbf{p}\sigma}^\dagger a_{j\mathbf{p}\sigma} \right) \tag{2.6}$$

Here $N(i)$ represents nearest neighbors of i, and we have assumed that the lattice is sufficiently deep that we can neglect next-nearest-neighbor terms. We can estimate the single-site terms with a harmonic approximation to the potential well. This yields: $\epsilon_{\mathbf{p}}^{(a)} = \epsilon_{\mathbf{p}}^{(m)} \approx \left[2\left(p_x + p_y + p_z\right) + 3\right]\sqrt{V_0 E_r}$ where $E_r = \hbar^2 k_0^2/2m$ is the atom recoil energy. Meanwhile the tunneling rates $t_{\mathbf{p}}^{(a)}$ and $t_{\mathbf{p}}^{(m)}$ can be determined by computing the band structure using variational methods.[48]

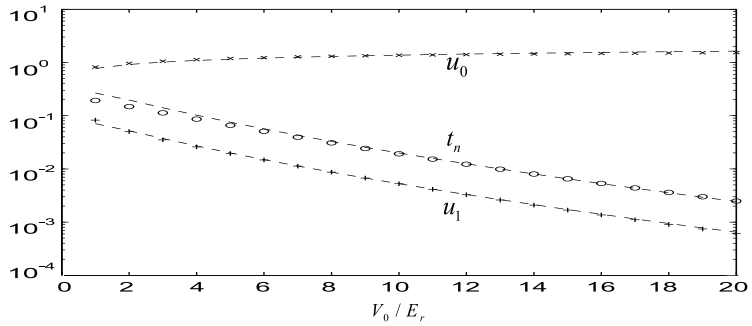

Figure 2.1: Normalized atom tunneling rate $t_n \equiv t_{\mathbf{0}}^{(a)}/E_r$ and normalized overlaps of atomic and molecular Wannier functions: $u_0 \equiv \sqrt{\lambda/2}\int \left(w_0^{(m)}(x)\right)^* \left(w_0^{(a)}(x)\right)^2 dx$ (on-site), $u_1 \equiv \sqrt{\lambda/2}\int \left(w_0^{(m)}(x)\right)^* w_0^{(a)}(x) w_0^{(a)}(x+\lambda/2)dx$ (neighboring site) all calculated in the lowest band and plotted vs. the lattice depth (in units of recoil energy) V_0/E_R. The marked datapoints indicate the exact numerical results, while the dotted lines are fits to the formulas $t_n \approx (3.5/\sqrt{\pi})\,(V_0/E_r)^{3/4}\exp\left(-2\sqrt{V_0/E_r}\right)$, $u_0 \approx 0.77\,(V_0/E_r)^{1/4}$, and $u_1 \approx 0.52\,(V_0/E_r)^{3/4}\exp\left(-2\sqrt{V_0/E_r}\right)$ The nearest-neighbor atom-molecule coupling rate in the lowest band is given by $c_{1;\mathbf{000}}^{(am)} = \alpha\,(\lambda/2)^{(-3/2)}\,u_0^2 u_1$, and we observe that for the broad Feshbach resonance (and thus large α) in typical experiments $c_{1;\mathbf{000}}^{(am)}$ exceeds $t_{\mathbf{0}}^{(a)}$[Source: Reference [3]]

We likewise expand H_I in terms of Wannier functions, keeping both on-site and nearest neighbor terms, while taking longer-range terms to be negligible. This differs from earlier work, in which nearest neighbor terms were also neglected.[17–20]. In fact, for typical wide Feshbach resonance the atom-molecule coupling rate α is great enough that it can contribute nearest neighbor interactions which exceed the tunneling rate $t_a^{(m)}$. As shown in figure 2.1, the ratio between the nearest-neighbor atom-molecule coupling rate and the atom tunneling rate in the lowest band is well-approximated by $c_{1;\mathbf{00},\mathbf{0}}/t_{\mathbf{0}}^{(a)} \approx 0.44\left(\alpha\lambda^{-3/2}/E_r\right)\sqrt{V_0/E_r}$. We estimate $c_{1;\mathbf{00},\mathbf{0}}/t_{\mathbf{0}}^{(a)} \approx 10\sqrt{V_0/E_r}$ for ${}^6Li$ and $c_{1;\mathbf{00},\mathbf{0}}/t_{\mathbf{0}}^{(a)} \approx 1.4\sqrt{V_0/E_r}$ for ${}^{40}K$, where in this estimation we take the following parameters for ${}^6Li$ (${}^{40}K$): $W = 180$G (8G), $a_{bg} = -2000a_B$ ($170a_B$), $\lambda = 1\mu$m (0.8μm) and $\mu_{co} \approx 2\mu_B$ (where a_B is the Bohr radius and μ_B is the Bohr magneton). Thus, the atom-molecule couplings between neighboring sites cannot be neglected in consideration of the multi-site physics. With

the Wannier function expansion, the interaction Hamiltonian is thus:

$$\begin{aligned} H_I = &\sum_{i\mathbf{pss'}} \left(c^{(am)}_{0;\mathbf{pss'}} b^\dagger_{i\mathbf{p}} a_{i\mathbf{s}\uparrow} a_{i\mathbf{s'}\downarrow} + \text{H.c.} \right) + \sum_{i\mathbf{pqss'}} c^{(aa)}_{0;\mathbf{pqss'}} a^\dagger_{i\mathbf{p}\downarrow} a^\dagger_{i\mathbf{q}\uparrow} a_{i\mathbf{s}\uparrow} a_{i\mathbf{s'}\downarrow} \\ &+ \sum_{i\mathbf{pss'}} \sum_{j\in N(i)} \left[c^{(am)}_{1;\mathbf{pss'}} b^\dagger_{i\mathbf{p}} \left(a_{i\mathbf{s}\uparrow} a_{j\mathbf{s'}\downarrow} - a_{i\mathbf{s}\downarrow} a_{j\mathbf{s'}\uparrow} \right) + \text{H.c.} \right] \\ &+ \sum_{i\mathbf{pss'}} \sum_{j\in N(i)} \left[c^{(am)}_{2;\mathbf{pss'}} b^\dagger_{i\mathbf{p}} a_{j\mathbf{s}\uparrow} a_{j\mathbf{s'}\downarrow} + \text{H.c.} \right] \end{aligned} \tag{2.7}$$

where $c^{(am)}_{0;\mathbf{pss'}} \equiv \alpha \int w^{(m)*}_{\mathbf{p}}(\mathbf{r}) w^{(a)}_{\mathbf{s}}(\mathbf{r}) w^{(a)}_{\mathbf{s'}}(\mathbf{r}) d^3\mathbf{r}$, $c^{(aa)}_{0;\mathbf{pqss'}} \equiv U_{bg} \int w^{(a)*}_{\mathbf{p}}(\mathbf{r}) w^{(a)*}_{\mathbf{q}}(\mathbf{r}) w^{(a)}_{\mathbf{s}}(\mathbf{r}) w^{(a)}_{\mathbf{s'}}(\mathbf{r}) d^3\mathbf{r}$, $c^{(am)}_{1;\mathbf{pss'}} \equiv \alpha \int w^{(m)*}_{\mathbf{p}}(\mathbf{r}) w^{(a)}_{\mathbf{s}}(\mathbf{r}) w^{(a)}_{\mathbf{s'}}(\mathbf{r}+\delta\mathbf{r}) d^3\mathbf{r}$, $c^{(am)}_{2;\mathbf{pss'}} \equiv \alpha \int w^{(m)*}_{\mathbf{p}}(\mathbf{r}+\delta\mathbf{r}) w^{(a)}_{\mathbf{s}}(\mathbf{r}) w^{(a)}_{\mathbf{s'}}(\mathbf{r}) d^3\mathbf{r}$. Here $\delta\mathbf{r}$ gives the difference in the positions of two neighboring sites.

2.3 Effective Single-Band Hamiltonian

The Hamiltonian derived thus far seems very complicated. It includes on-site and nearest-neighbor couplings between atoms and bare molecules in many lattice bands. Fortunately, this Hamiltonian can be greatly simplified by taking advantage of a large separation between the various energy scales of the system. In particular, for typical experiments the band gap $E_{bg} \sim 2\sqrt{V_0 E_R}$ and the on-site interaction energy $E_{on} \sim c^{am}_{0;pss'}$ are much larger than the atom tunneling rate $E_t \sim t^{(a)}_p$ and off-site interaction energy $E_{off} \sim c^{am}_{1;pss'}$. (For instance, for ^{40}K with a typical lattice depth of $V_0 = 10E_R$, these are estimated as $E_{on} = 23E_R$, $E_{bg} = 6.3E_R$, $E_{off} = 0.09E_R$, and $E_t = 0.02E_R$.[3])

Taking $(E_{on}, E_{bg}) \gg (E_{off}, E_t)$, we can solve the single-site problem while initially neglecting the intersite interactions. Considering the single-site terms from both H_0

and H_I, we see that the single-site Hamiltonian is

$$H_i = \sum_{\mathbf{p}} \left[\left(\epsilon^{(m)}_{\mathbf{p}} + \nu_b\right) b^\dagger_{i\mathbf{p}} b_{i\mathbf{p}} + \sum_\sigma \epsilon^{(a)}_{\mathbf{p}} a^\dagger_{i\mathbf{p}\sigma} a_{i\mathbf{p}\sigma} + \sum_{j\in N(i)} \left(t^{(m)}_p b^\dagger_{i\mathbf{p}} b_{j\mathbf{p}} + \sum_\sigma t^{(a)}_{\mathbf{p}} a^\dagger_{i\mathbf{p}\sigma} a_{j\mathbf{p}\sigma} \right) \right]$$
$$+ \sum_{\mathbf{pss'}} \left(c^{(am)}_{0;\mathbf{pss'}} b^\dagger_{i\mathbf{p}} a_{i\mathbf{s}\uparrow} a_{i\mathbf{s'}\downarrow} + \text{H.c.} \right) + \sum_{\mathbf{pqss'}} c^{(aa)}_{0;\mathbf{pqss'}} a^\dagger_{i\mathbf{p}\downarrow} a^\dagger_{i\mathbf{q}\uparrow} a_{i\mathbf{s}\uparrow} a_{i\mathbf{s'}\downarrow} \tag{2.8}$$

For a single atom in lattice band $\mathbf{p}$, the energy is just $\epsilon^{(a)}_{\mathbf{p}}$. For two atoms of opposite spin on a single site, the atom-molecule coupling results in a state which is a superposition of a pair of open-channel atoms and a closed-channel bare molecule. We refer to these two-atom eigenstates of the single-site Hamiltonian as "dressed molecules". The dressed molecule states (numbered by an index μ) can be written as $\Psi_{i\mu} = d^\dagger_{i\mu} |0\rangle$, where $|0\rangle$ is the vacuum state and $d^\dagger_{i\mu}$ is the dressed molecule creation operator defined by $d^\dagger_{i\mu} = \sum_{\mathbf{p}} \chi_{\mu p} b^\dagger_{ip} + \sum_{pq} \gamma_{\mu pq} a^\dagger_{ip\downarrow} a^\dagger_{iq\uparrow}$. The coefficients $\chi_{\mu p}$ and $\gamma_{\mu pq}$ are determined by solving the Schrödinger equation $H_i |\Psi_{i\mu}\rangle = E_\mu |\Psi_{i\mu}\rangle$ (where E_μ is the corresponding eigenenergy) and from the normalization condition $\sum_p \chi^*_{\mu p} \chi_{\mu' p} + \sum_{pq} \gamma^*_{\mu pq} \chi_{\mu' pq} = \delta_{\mu\mu'}$. This sort of problem has been solved in Ref. [16], taking a harmonic approximation to the potential and applying an appropriate renormalization procedure. (The need for renormalization can be seen as a consequence of treating dressed molecules as point-particles, which results in an ultraviolet divergence.) Note that the eigenenergy E_μ implicitly depends on the applied magnetic field B, due to the contribution from ν_b.

Because the separation between eigenenergies E_μ is on the order of the band gap, if any particular energy E_{μ_0} is tuned (via the magnetic field) close to the two-atom free energy of a particular band p_0, it will be far from the two-atom free energy for all other bands. That is, if $\left| E_{\mu_0} - 2\epsilon^{(a)}_{p_0} \right| \ll E_{bg}$, then the multi-site terms of the Hamiltonian (which are much smaller than the band gap) can couple atoms in band p_0 only to the dressed molecule state d_{μ_0}, and vice versa. This means that if the

system is prepared with all atoms initially in the band p_0, then only four different single-site states are possible: $|0\rangle$, $|\sigma\rangle \equiv a^\dagger_{ip_0\sigma}|0\rangle$ for $\sigma =\uparrow,\downarrow$, and $|d\rangle \equiv d^\dagger_{i\mu_0}|0\rangle$. For example, the atoms might be prepared in the lowest band and coupled to the lowest energy dressed molecule eigenstate. Here we have assumed that the average filling number $\bar{n}$ is less than 2, so that there are only one or two atoms per site (sites with more than two particles being separated by an energy difference on the order of the band gap).

We can thus project the full Hamiltonian onto the Hilbert space spanned by tensor products of these four single site states. That is, we apply the projector $P = \bigotimes_i P_i$ where $P_i = |0\rangle_i\langle 0| + |\uparrow\rangle_i\langle\uparrow| + |\downarrow\rangle_i\langle\downarrow| + |d\rangle_i\langle d|$. The full Hamiltonian $H_{eff} \equiv PHP$ takes the form

$$H_{eff} = \sum_i \Delta(B) d_i^\dagger d_i + \sum_{i,j\in N(i)} \left[t_d P d_i^\dagger d_j P + \sum_\sigma \left(t_a P a_{i\sigma}^\dagger a_{j\sigma} P + t_{da} d_i^\dagger d_j a_{j\sigma}^\dagger a_{i\sigma} \right) \right] + \sum_{i,j\in N(i)} \left[g d_i^\dagger \left(a_{i\uparrow} a_{j\downarrow} - a_{i\downarrow} a_{j\uparrow} \right) + \text{H. c.} \right] \tag{2.9}$$

where $\Delta(B) \equiv E_{\mu_0}(B) - 2\epsilon^{(a)}_{\mathbf{p}_0}$, $g \equiv \gamma^*_{\mu_0\mathbf{p}_0\mathbf{p}_0} t^{(a)}_{\mathbf{p}_0}/2 + \sum_{\mathbf{q}} \chi^*_{\mu_0\mathbf{q}} c^{(am)}_{1;\mathbf{q},\mathbf{p}_0,\mathbf{p}_0}$, $t_a \equiv t^{(a)}_{\mathbf{p}_0}$, $t_{da} \equiv -\sum_{\mathbf{q}} |\gamma_{\mu_0\mathbf{q}\mathbf{p}_0}|^2 t^{(a)}_{\mathbf{q}} - 2\text{Re}\left(\sum_{\mathbf{q},\mathbf{s}} \chi^*_{\mu_0\mathbf{q}} c^{(am)}_{1;\mathbf{q}\mathbf{p}_0\mathbf{s}} \gamma_{\mu_0\mathbf{s}\mathbf{p}_0} \right)$ and $t_d \equiv \sum_{\mathbf{q}} |\chi_{\mu_0\mathbf{q}}|^2 t^{(m)}_{\mathbf{q}} + 2\text{Re}\left(\sum_{\mathbf{q},\mathbf{s},\mathbf{s}'} \chi^*_{\mu_0\mathbf{q}} c^{(am)}_{2;\mathbf{q}\mathbf{s}\mathbf{s}'} \gamma_{\mu_0\mathbf{s}'\mathbf{s}} \right)$. To simplify the notation we have omitted the indices $\mathbf{p}_0$ and μ_0 on the operators $a_{i\sigma}$ and d_i in H_{eff}, as H_{eff} is effectively a single-band model. (It is important to remember, however, that the dressed molecule state is actually a multiband superposition.) We include the explicit dependence of Δ on the magnetic field B (which controls the energy of the dressed molecule state.)

2.4 Generalized Hubbard Model

The Hamiltonian H_{eff} can be seen as describing a resonance between local dressed molecule states $d_i^\dagger|0\rangle$ and two-site atomic valence bonds $\left(a^\dagger_{i\uparrow}a^\dagger_{j\downarrow} - a^\dagger_{i\downarrow}a^\dagger_{j\uparrow}\right)|0\rangle$. In

this section we show that it can be mapped to a more familiar form, that of the generalized Hubbard model which has been studied in various contexts in condensed matter physics. [26–39] In order to facilitate this mapping, we first re-express the projection P in a more convenient way. In the Hamiltonian H_{eff}, the states outside the subspace spanned by $\{|0\rangle, |\uparrow\rangle, |\downarrow\rangle, |d\rangle\}$ have already been projected out, so the only effect of the explicit projection operators P appearing in H_{eff} is to prevent double occupancy of any site. (Because the dressed molecule is the exact solution for the case of two atoms on one site, the idea of a site containing *both* a dressed molecule and a single atom state would be nonsensical.) The condition of no double occupancy can be equivalently expressed using the slave boson formalism.[74, 75]

We introduce slave boson creation operator $b_i^\dagger$ representing the "creation" of an empty site, $|0\rangle \equiv b_i^\dagger |0\rangle$. With each empty site treated as occupied by a slave boson, the condition of no double occupancy is simply $b_i^\dagger b_i + a_{i\uparrow}^\dagger a_{i\uparrow} + a_{i\downarrow}^\dagger a_{i\downarrow} + d_i^\dagger d_i = I$. We therefore no longer require the projector P, and can instead rewrite the Hamiltonian so that a slave boson is created (annihilated) whenever any lattice site becomes unoccupied (occupied) by atoms or molecules. The Hamiltonian H_{eff} expressed in slave boson form is:

$$H_{sb} = \sum_i \Delta(B) d_i^\dagger d_i + \sum_{i,j\in N(i)} \left[t_d d_i^\dagger b_i b_j^\dagger d_j + \sum_\sigma \left(t_a a_{i\sigma}^\dagger b_i b_j^\dagger a_{j\sigma} + t_{da} d_i^\dagger d_j a_{j\sigma}^\dagger a_{i\sigma} \right) \right] + \sum_{i,j\in N(i)} \left[g d_i^\dagger b_j^\dagger \left(a_{i\uparrow} a_{j\downarrow} - a_{i\downarrow} a_{j\uparrow} \right) + \text{H. c.} \right] \tag{2.10}$$

Because the single-site Hilbert space has only four basis states $\{|0\rangle, |\uparrow\rangle, |\downarrow\rangle, |d\rangle\}$, we can map this to the single-site Hilbert space of the Hubbard model, given by $\left\{ |0\rangle, |\uparrow\rangle, |\downarrow\rangle, |\downarrow\uparrow\rangle \equiv a_{i\downarrow}^\dagger a_{i\uparrow}^\dagger |0\rangle \right\}$. Specifically, we map a site occupied by a dressed molecule to one occupied by two atoms, by taking $d_i^\dagger |0\rangle \to a_{i\downarrow}^\dagger a_{i\uparrow}^\dagger |0\rangle$. Of course, as we have noted above, the physical composition of the dressed molecule is not simply

two atoms in a single band occupying the same site. It is a complex superposition of two open-channel atoms and a closed-channel molecule distributed over many bands. Nevertheless, we can *mathematically* map the dressed molecule to a double-occupation by single-band atoms. This means that whenever a doubly-occupied site occurs in this new description, the correct *physical* interpretation will be that the site is occupied by a dressed molecule.

Under such a mapping (see Appendix A), the Hamiltonian becomes:

$$H = \sum_{\langle i,j\rangle,\sigma} \left[t_a + g_1\left(n_{i\bar{\sigma}} + n_{j\bar{\sigma}}\right) + g_2 n_{i\bar{\sigma}} n_{j\bar{\sigma}}\right] a^\dagger_{i\sigma} a_{j\sigma} + \text{H.c.} + \sum_i \Delta n_{i\uparrow} n_{i\downarrow} - \mu\left(n_{i\uparrow} + n_{i\downarrow}\right) \tag{2.11}$$

where $g_1 = g - t_a$, $g_2 = t_{da} - 2g + t_a$, $n_{i\sigma} = a^\dagger_{i\sigma} a_{i\sigma}$, and $\bar{\sigma} = \uparrow, \downarrow$ for $\sigma = \downarrow, \uparrow$ We have dropped the slave boson operators b_i, which previously were needed to prevent double occupancy of the lattice sites. In the transformed language double occupancy is allowed, as it represents the existence of a dressed molecule. The previous condition that a site cannot be occupied by both a dressed molecule and a single atom is now a restriction against *triple* occupancy, and this restriction is automatically satisfied by the Pauli exclusion principle and the fact that the atoms are restricted to two possible spin states. (The slave bosons did continue to play an important role, for instance in requiring that the t_a term in H_eff cannot contribute to the atom tunneling out of a doubly occupied site, since as noted the double-occupied site is really occupied by a single dressed molecule. This has been accounted for by mapping $b^\dagger_i a_{i\sigma} \to a_{i\sigma}\left(1 - n_{i\bar{\sigma}}\right)$, as shown in Appendix A.)

We have also dropped the t_d term corresponding to dressed molecule tunneling. In the transformed language, this would correspond to two atoms hopping in unison from a site to one of its neighbors. We are justified in neglecting this term because t_d depends on the parameters $t^{(m)}_{\mathbf{q}}$ and $c^{(am)}_{2;\mathbf{q}ss'}$, which are substantially smaller at typical

lattice depths than the corresponding parameters $t_{\mathbf{q}}^{(a)}$ and $c_{1;\mathbf{qss}'}^{(am)}$ that contribute the other nearest neighbor terms in the Hamiltonian. The relative smallness of the t_d term can be understood from the fact that it involves twice as much mass tunneling through the potential barrier between sites, and this tunneling is exponentially suppressed with increasing mass. Put another way, the Wannier functions for the molecules are more sharply peaked than for atoms, due to the difference in the particles' mass, and this results in a reduction of the overlap between Wannier functions on neighboring sites. Specifically, for $t_{\mathbf{0}}^{(a)}$ and $c_{1;\mathbf{000}}^{(am)}$ (where here we consider the lowest band $vect0$) both vary with the same exponential factor $\exp\left(-2\sqrt{V_0/E_R}\right)$.[3] Because the molecules feel twice the potential V_0 and have half the recoil energy E_R, this produces an additional factor $\exp\left(-2\sqrt{V_0/E_R}\right)$ in the molecule tunneling relative to the atom tunneling. For a typical lattice depth $V_0 = 10E_R$, this reduces the molecular tunneling by a factor of ~ 0.002.

We see that the Hamiltonian (2.11) is that of the generalized Hubbard model, with correlated tunneling given by the g_1 and g_2 terms. (In the special case $g_1 = g_2 = 0$, this is just the Hamiltonian of the standard Hubbard model). This Hamiltonian has been studied previously in condensed matter physics [26–39], where it is natural to consider extensions of the Hubbard model to cases where some of the terms Hubbard found negligible are actually large enough to be of importance. This can for instance be due to a modification of the atomic orbitals due to the on-site interactions between the electrons. Here the origins of this generalized Hubbard model are quite different, since (as we emphasized in the previous chapter) nearly all the crucial assumptions made by Hubbard in deriving his model, such as the restriction to a single band, do not apply. Nevertheless, we see precisely the generalized Hubbard model Hamiltonian arising as a mathematically equivalent model to one in which many lattice bands are

populated by strong on-site interactions. The fact that the same Hamiltonian can describe two such different systems is at first quite surprising. As we will see in the next section the generalized Hubbard model is in fact the most general model that satisfies certain restrictions on the system symmetry and its Hilbert space. The broad applicability of the generalized Hubbard model to diverse physical systems can be viewed as a consequence of this fact.

2.5 Generalized Hubbard Model as a Consequence of Symmetry

Above, we showed how the Hamiltonian for fermions in an optical lattice near Feshbach resonance can be determined by starting from the two-channel model expressed in terms of field operators, expanding these field operators in terms of Wannier functions, and computing the various overlap integrals of these functions. The resulting Hamiltonian, given by the sum of equations (2.6) and (2.7), is quite complicated, but as we saw it was greatly simplified by projecting the state of each single site onto the Hilbert space spanned by the states $\{|0\rangle, |\uparrow\rangle, |\downarrow\rangle, |d\rangle\}$. This projection was justified by observing that the dressed molecule states (that is, the eigenstates for two particles on a single site) are separated by energies on the order of the bandgap, while the couplings between atoms on different sites are all much less than the band gap. This makes it possible to restrict the possible states to include only atoms in that band and one particular dressed molecule state that couples to that band.

Here we take what can be considered the opposite approach. Rather than first determining the multi-site Hamiltonian and then simplifying it based on a restriction of the single-site Hilbert space, we instead *start* with the assumption that the space of allowed single-site states is $\{|0\rangle, |\uparrow\rangle, |\downarrow\rangle, |d\rangle\}$, and then ask the question: What is the most general Hamiltonian (respecting certain essential symmetries) that can

act on these states? In particular, we assume a global $SU(2)$ symmetry for the spin components. Furthermore, the number of particles must be conserved for each spin component. This is equivalent to imposing conservation on the total number of particles along with conservation of the z-component of spin. Finally, the atomic interactions are taken to be sufficiently short range that couplings between more than two sites, or between non-neighboring sites, can be neglected.

Even this rather minimal set of assumptions is enough to significantly limit the terms that can occur in the Hamiltonian. Conservation of particle number excludes terms that only create or only destroy a single particle in state $|\uparrow\rangle$ or $|\downarrow\rangle$, and conservation of the z-component of spin prohibits changing a single $|\uparrow\rangle$ into a $|\downarrow\rangle$ or vice versa. If the dressed molecule state were not allowed, the only allowed terms of the Hamiltonian would thus be ones that describe $|\uparrow\rangle$ atoms or $|\downarrow\rangle$ tunneling between different sites. Terms in which an $|\uparrow\rangle$ is changed to a $|\downarrow\rangle$ and $|\downarrow\rangle$ is simultaneously changed to an $|\uparrow\rangle$ are also allowed, but this case is equivalent to an $|\uparrow\rangle$ and a $|\downarrow\rangle$ each tunneling to the site formerly occupied by the other. Terms in which two particles can interact without changing positions are also allowed, but these can equivalently be viewed as one particle virtually tunneling to the site of the other and back again. Because of the short-range of the atomic interactions, a barrier that suppresses such virtual tunnelings likewise suppresses these intersite interactions.

With the inclusion of dressed molecules, the total number of $|\uparrow\rangle$ and $|\downarrow\rangle$ atoms can be changed, but only if the numbers of each change by the same amount, and for each pair of $|\uparrow\rangle$ and $|\uparrow\rangle$ states destroyed (created) a dressed molecule is created (destroyed). Because the dressed molecule is *not* simply an atom in state $|\uparrow\rangle$ and an atom in state $|\downarrow\rangle$, these processes, unlike those described above, are not simply rearrangements of the atoms in state $|\uparrow\rangle$ and state $|\downarrow\rangle$. Nevertheless, the dressed molecule is composed

of two atoms in the hyperfine states denoted by $\uparrow$ and $\downarrow$ (albeit in a superposition over many bands), so it is possible to categorize the dressed molecule creating and destroying terms in the Hamiltonian by the number of atoms that these terms transfer from one site to another.

With this in mind, we take the Hamiltonian to have the form $H = \sum_i H_i + \sum_{\langle i,j\rangle}\left(H_{ij}^{(1)} + H_{ij}^{(2)}\right)$, where $\langle i,j\rangle$ represents pairs of neighboring sites, and where H_i is the single-site Hamiltonian, $H_{ij}^{(1)}$ represents two-site terms that involve the tunneling of one atom between the sites, and $H_{ij}^{(2)}$ represent the two site terms that involve two real or virtual tunnelings. (That is, $H_{ij}^{(2)}$ includes both the case where two atoms tunnel between sites i and j, and the case where a single atom virtually tunnels from one site to another and back again, leaving the configuration of atoms unchanged.) Terms in which a molecule is created or destroyed by moving one atom are grouped into $H_{ij}^{(1)}$, as are terms that exchange an atom with a molecule (since these two states can be swapped by transferring a single atom). Terms in which a molecule moves from site to site are grouped into $H_{ij}^{(2)}$. Because of the short range of the interactions, the terms involving more tunnelings decay at a significantly greater rate with increase in the lattice depth. Terms involving more than two tunnelings thus become negligibly small, as did the terms involving more than two sites. Likewise, tunneling between non-adjacent sites is highly suppressed.

We can write the terms and H_i, $H_{ij}^{(1)}$, and $H_{ij}^{(2)}$ in the slave-boson formalism introduced in the previous section, where the constraint of no double occupancy is enforced by the condition $b_i^\dagger b_i + a_{i\uparrow}^\dagger a_{i\uparrow} + a_{i\downarrow}^\dagger a_{i\downarrow} + d_i^\dagger d_i = I$. Since there can be no double occupancy, the single-site Hamiltonian H_i just gives the energy for a state $|\uparrow\rangle$, $|\downarrow\rangle$, or $|d\rangle$ on site i, relative to the energy of an unoccupied (i.e., slave-boson occupied) site. Furthermore, because of the $SU(2)$ symmetry of the spin components, the states

$|\uparrow\rangle$ and $|\downarrow\rangle$ must be degenerate in energy. This means the most general form of the single site Hamiltonian is $H_i = -\mu \sum_\sigma a_{i\sigma}^\dagger a_{i\sigma} + (\Delta - 2\mu)\, d_i^\dagger d_i$, where the single atom energy is incorporated into the chemical potential μ and Δ gives the energy of the dressed molecule relative to two single atoms.

The terms of $H_{ij}^{(1)}$ and $H_{ij}^{(2)}$ are likewise fixed by the symmetry requirements. As described above, $H_{ij}^{(1)}$ includes only the tunneling of a single atom between adjacent sites, the exchange of an atom and a molecule on adjacent sites, and conversion of a molecule into a pair of atoms of opposite spin on adjacent sites. Moreover, because of the $SU(2)$ symmetry, the Hamiltonian is invariant under exchange of $\uparrow$ and $\downarrow$. Thus, the form of $H_{ij}^{(1)}$ must be:

$$H_{ij}^{(1)} = \sum_\sigma \left(t_a a_{i\sigma}^\dagger b_i b_j^\dagger a_{j\sigma} + t_{da} d_i^\dagger a_{i\sigma} a_{j\sigma}^\dagger d_j \right) + g \left(d_i^\dagger b_j^\dagger + b_i^\dagger d_j^\dagger \right) \left(a_{i\uparrow} a_{j\downarrow} - a_{i\downarrow} a_{j\uparrow} \right) + \text{H. c.} \tag{2.12}$$

In particular, the relative signs of the terms with coefficient g are determined by the fact that the Hamiltonian is symmetric under exchange of $\uparrow$ and $\downarrow$, and also symmetric under exchange of the two sites i and j. Note that b_i and d_i satisfy bosonic commutation relations, while $a_{i\uparrow}$ and $a_{i\downarrow}$ satisfy fermionic anti-commutation relations. It is also important to note that the dressed molecule operators change sign under exchange of the spins $\uparrow$ and $\downarrow$, due to the fact that the dressed molecule is composed of anti-commuting fermions of each spin.

As described above, $H_{ij}^{(2)}$ included terms involving two atoms tunneling between two sites. This includes the dressed molecule tunneling term, where two atoms tunnel in unison from one site to another. It also includes the case where one atom virtually tunnels from one site to the other and back again. This results in terms which are diagonal in the position basis. The third possibility is that one atom tunnels from one site to another, and a different atom tunnels back. This produces a Heisenberg

term, as dictated by the $SU(2)$ symmetry. Thus, $H_{ij}^{(2)}$ is given by:

$$H_{ij}^{(2)} = \left(t_d d_i^\dagger b_i b_j^\dagger d_j + \text{H. c.}\right) + x_d n_{di} n_{dj} + x_a n_i n_j + x_s \mathbf{s}_i \cdot \mathbf{s}_j + x_b n_{bi} n_{bj} \tag{2.13}$$

where $n_{di} \equiv d_i^\dagger d_i$, $n_i \equiv a_{i\uparrow}^\dagger a_{i\uparrow} + a_{i\downarrow}^\dagger a_{i\downarrow}$, $n_{bi} \equiv b_i^\dagger b_i$ and

$$(\mathbf{s}_i)_\alpha \equiv \frac{1}{2} \begin{pmatrix} a_{i\uparrow}^\dagger & a_{i\downarrow}^\dagger \end{pmatrix} \sigma_\alpha \begin{pmatrix} a_{i\uparrow} \\ a_{i\downarrow} \end{pmatrix} \tag{2.14}$$

where $\alpha = x, y, z$ and the σ_α are the Pauli matrices.

Here we have included the $H_{ij}^{(2)}$ terms of the Hamiltonian for the sake of completeness, but in fact for a sufficiently deep lattice these terms can be neglected. This is the case since for short-ranged interactions the terms involving two atoms tunneling between sites decay much faster than the single-tunneling terms with increase of the lattice potential barrier. Dropping the double-tunneling terms, the Hamiltonian becomes $H = \sum_i H_i + \sum_{\langle i,j \rangle} H_{ij}^{(1)}$. Thus,

$$\begin{aligned} H = &\sum_i \left[(\Delta - 2\mu)\, d_i^\dagger d_i - \mu \sum_\sigma a_{i\sigma}^\dagger a_{i\sigma} \right] \\ &+ \sum_{\langle i,j \rangle} \left[\sum_\sigma \left(t_a a_{i\sigma}^\dagger b_i b_j^\dagger a_{j\sigma} + t_{da} d_i^\dagger a_{i\sigma} a_{j\sigma}^\dagger d_j \right) + g \left(d_i^\dagger b_j^\dagger + b_i^\dagger d_j^\dagger \right) \left(a_{i\uparrow} a_{j\downarrow} - a_{i\downarrow} a_{j\uparrow} \right) + \text{H. c.} \right] \end{aligned} \tag{2.15}$$

This matches equation (2.9) with $t_d = 0$ and with the addition of a chemical potential μ (which we took to zero above, but which must be included for consideration of a varying number of particles). As we have seen above and in Appendix A, this Hamiltonian takes the form of the generalized Hubbard model if we mathematically map the dressed molecule state to a doubly-occupied state: $d_i^\dagger |0\rangle \rightarrow a_{i\downarrow}^\dagger a_{i\uparrow}^\dagger |0\rangle$.

2.6 Chapter Summary

In this chapter we have presented the Hamiltonian for fermions in an optical lattice near a broad Feshbach resonance, and shown that it can be mathematically mapped

to the generalized Hubbard model (which has been studied previously in the context of condensed matter physics). We have presented two separate derivations of this Hamiltonian, one from field theory of the two-channel model of Feshbach resonance, and the other based on a set of more basic assumptions about the system, such as the $SU(2)$ symmetry of the spin components and the short range of the atomic interactions. This latter derivation helps to clarify why the generalized Hubbard model has such general applicability, while the former derivation provides us with explicit expressions for the coefficients of each term in the Hamiltonian.

Despite the fact that we have obtained explicit expressions for the coefficients of each term in the Hamiltonian, calculation of these values remains difficult. The explicit expressions contain sums over many bands for both the atoms and bare molecules, which not only pose numerical difficulties but also complicate the renormalization procedure necessary to obtain the dressed molecule solutions. In the next chapter, we explore the two-body solution of the generalized Hubbard model, motivated in part by the desire to find a simpler way to determine the parameters of the model from the experimentally controllable parameters. In the subsequent chapter, we propose an experimental scheme to measure the parameters of the generalized Hubbard model in this system. These chapters also reflect our strategy of attempting to first examine the generalized Hubbard model in more restricted cases before attempting to consider the substantially more complicated many-body case.

CHAPTER III

Two-Body Bound States of the Generalized Hubbard Model

In this chapter we solve the two-body problem for the generalized Hubbard model. As seen in BCS theory, an understanding of the two-body problem can be essential in understanding the many-body physics. Additionally, studying the two-body physics offers a possible route to determining the dependence of the lattice parameters on the experimentally controllable parameters such as lattice depth and magnetic field strength.

3.1 Introduction

In previous chapters we showed how fermions in an optical lattice in the unitary regime are described by a generalized Hubbard model, governed by the parameters t_a, Δ, μ, g_1, and g_2. As we have seen, it is difficult to calculate the dependence of the Hamiltonian parameters (in particular the correlated hopping terms g_1 and g_2) on the controllable parameters such as magnetic field B and lattice depth V.

We can simplify this problem by restricting our attention to the two-body problem – that is, the case of a lattice containing only two atoms. By determining the two-body bound states from the lattice Hamiltonian, we can express the binding energy and wave function as functions of the lattice parameters. Likewise, by directly solving the Schrödinger equation (in continuous spatial coordinates) for two

interacting particles in a periodic potential, one can determine the dependence of the binding energy and wave function on the magnetic field and lattice depth. In this way, the controllable parameters can be related to the parameters of the general Hubbard model. (Note however that the parameter g_2 cannot be determined in this way, as it represents a three-body effect not relevant to the two-body problem.)

Here we solve the two-body problem for the general Hubbard model. (As this result is the focus of this chapter, we opt to go over the derivation in some detail rather than confining the details to an appendix.) The related problem of solving the Schrödinger equation for two interacting particles in a periodic potential has been explored by other members of our research group.

3.2 The Two-Body Hamiltonian

For the case of two atoms, the general Hubbard Hamiltonian takes a somewhat simpler form:

$$H = \sum_i \Delta n_{i\uparrow} n_{i\downarrow} + \sum_{\langle i,j\rangle,\sigma} \left[-t_a + g_1 \left(n_{i\bar{\sigma}} + n_{j\bar{\sigma}}\right)\right] a^\dagger_{i\sigma} a_{j\sigma} \tag{3.1}$$

In particular, the three-body term governed by g_2 disappears. The chemical potential μ is likewise irrelevant since the number of particles is fixed at two.

It is convenient for the subsequent calculation to first transfer this Hamiltonian from position space to $\mathbf{k}$-space. That is, instead of annihilation (creation) operators a_i ($a_i^\dagger$) representing spatially localized states given by Wannier functions, we transfer to $a_\mathbf{k}$ ($a_\mathbf{k}^\dagger$) representing Bloch states with wave-vector $\mathbf{k}$. The benefit of this is that the Hamiltonian conserves the total crystal momentum $\mathbf{k}$ (due to the discrete translational symmetry of the lattice), and thus its eigenstates can be assumed to be states of definite $\mathbf{k}$.

The transfer to **k**-space is accomplished by applying the transformation

$$a_i = \frac{1}{\sqrt{N}} \sum_{\mathbf{k}} \mathrm{e}^{-\mathrm{i}\mathbf{k}\cdot\mathbf{r}_i} a_{\mathbf{k}} \tag{3.2}$$

to every annihilation operator (and applying the conjugate transformation to each creation operator), where the sum is taken over all k in the first Brillouin zone. Here $\mathbf{r}_i$ is the position of site i and N is the total number of lattice sites (which is also the number of sites in the first Brillouin zone in **k**-space). This produces a sum over wave vector for each operator in the Hamiltonian. The resulting expression can be simplified by replacing the summed exponentials with the Kronecker delta, defined by:

$$\delta_{\mathbf{k},\mathbf{k}'} = \frac{1}{N} \sum_{i} \mathrm{e}^{\mathrm{i}(\mathbf{k}-\mathbf{k}')\cdot\mathbf{r}_i} \tag{3.3}$$

This replacement removes all explicit sums over lattice sites from our Hamiltonian. Also, since $\delta_{\mathbf{k},\mathbf{k}'} = 0$ for $\mathbf{k} \neq \mathbf{k}'$ this allows us to further reduce the total number of summations, eliminating many of the sums over wave-vector. Thus the k-space Hamiltonian simplifies to:

$$H = -t_a \sum_{\mathbf{k},\sigma} \epsilon_{\mathbf{k}} a^{\dagger}_{\mathbf{k}\sigma} a_{\mathbf{k}\sigma} + \frac{1}{N} \sum_{\mathbf{k},\mathbf{k}',\mathbf{q}} U_{\mathbf{q},\mathbf{k},\mathbf{k}'}(\Delta, g_1) a^{\dagger}_{\mathbf{k}+\mathbf{q}/2,\uparrow} a^{\dagger}_{-\mathbf{k}+\mathbf{q}/2,\downarrow} a_{-\mathbf{k}'+\mathbf{q}/2,\downarrow} a_{\mathbf{k}'+\mathbf{q}/2,\uparrow} \tag{3.4}$$

where a is the lattice spacing, $\epsilon_{\mathbf{k}} = 2\cos(k_x a) + 2\cos(k_y a)$ for $\mathbf{k} = (k_x, k_y)$, and

$$\begin{aligned} U_{\mathbf{q},\mathbf{k},\mathbf{k}'}(\Delta, g_1) = \Delta + g_1 \big[& 4\cos(q_x a/2)\left(\cos(k_x a) + \cos(k'_x a)\right) \\ & + 4\cos(q_y a/2)\left(\cos(k_y a) + \cos(k'_y a)\right)\big] \end{aligned}$$

3.3 Two-Particle Eigenkets and Schrödinger's equation

We can define the eigenket for two particles with total momentum **q** as

$$|\psi\rangle = \frac{1}{\sqrt{N}} \sum_{\mathbf{k}} c_{\mathbf{k}} a^{\dagger}_{\mathbf{k}+\mathbf{q}/2,\uparrow} a^{\dagger}_{-\mathbf{k}+\mathbf{q}/2,\downarrow} |0\rangle \tag{3.5}$$

where $\{c_{\mathbf{k}}\}$ are complex coefficients satisfying the normalization condition $\sum_{\mathbf{k}} |c_{\mathbf{k}}|^2 = N$. Applying the Schrödinger equation $H|\psi\rangle = E|\psi\rangle$, we have:

$$\begin{aligned} &\frac{1}{\sqrt{N}} \sum_{\mathbf{k}} -t_a c_{\mathbf{k}} \left(\epsilon_{\mathbf{k}+\mathbf{q}/2} + \epsilon_{-\mathbf{k}+\mathbf{q}/2}\right) a^\dagger_{\mathbf{k}+\mathbf{q}/2,\uparrow} a^\dagger_{-\mathbf{k}+\mathbf{q}/2,\downarrow} |0\rangle \\ +&\frac{1}{N\sqrt{N}} \sum_{\mathbf{k},\mathbf{k}'} c_{\mathbf{k}'} U_{\mathbf{q},\mathbf{k},\mathbf{k}'}(\Delta, g_1) a^\dagger_{\mathbf{k}+\mathbf{q}/2,\uparrow} a^\dagger_{-\mathbf{k}+\mathbf{q}/2,\downarrow} |0\rangle \\ =&\frac{1}{\sqrt{N}} \sum_{\mathbf{k}} E c_{\mathbf{k}} a^\dagger_{\mathbf{k}+\mathbf{q}/2,\uparrow} a^\dagger_{-\mathbf{k}+\mathbf{q}/2,\downarrow} |0\rangle \end{aligned} \tag{3.6}$$

To simplify this equation, we define

$$A_{\mathbf{q}/2,\mathbf{k}} = 4\cos(q_x a/2)\cos(k_x a) + 4\cos(q_y a/2)\cos(k_y a) \tag{3.7}$$

and note that $\epsilon_{\mathbf{k}+\mathbf{q}/2} + \epsilon_{-\mathbf{k}+\mathbf{q}/2} = A_{\mathbf{q}/2,\mathbf{k}}$ and $U_{\mathbf{k},\mathbf{k}',\mathbf{q}}(\Delta, g_1) = \Delta + g_1\left(A_{\mathbf{q}/2,\mathbf{k}} + A_{\mathbf{q}/2,\mathbf{k}'}\right)$. From the Schrödinger equation we now have a relation for $c_{\mathbf{k}}$:

$$\left(E + t_a A_{\mathbf{q}/2,\mathbf{k}}\right) c_{\mathbf{k}} = \left(\Delta + g_1 A_{\mathbf{q}/2,\mathbf{k}}\right) \frac{1}{N} \sum_{\mathbf{k}'} c_{\mathbf{k}'} + g_1 \frac{1}{N} \sum_{\mathbf{k}'} A_{\mathbf{q}/2,\mathbf{k}'} c_{\mathbf{k}'} \tag{3.8}$$

3.4 Solving for the Eigenenergies E and Eigenstate components $c_{\mathbf{k}}$

Equation (3.8) provides a set of equations (one for each $\mathbf{k}$ in the first Brillouin zone), which together with the normalization condition $\frac{1}{N}\sum_{\mathbf{k}} |c_{\mathbf{k}}|^2 = 1$ are enough to completely determine the unknowns $c_{\mathbf{k}}$ and E. Here we have written these equations for a general two-body state for one atom of each spin-state and with total crystal momentum $\mathbf{q}$. Note that $c_{\mathbf{k}}$ and E also implicitly depend on $\mathbf{q}$.

To solve the set of equations (3.8), we define variables X and Y (also implicitly $\mathbf{q}$-dependent) by $X \equiv \frac{1}{N}\sum_{\mathbf{k}'} c_{\mathbf{k}'}$ and $Y \equiv \frac{1}{N}\sum_{\mathbf{k}'} A_{\mathbf{q}/2,\mathbf{k}'} c_{\mathbf{k}'}$. This yields an explicit expression for each $c_{\mathbf{k}}$:

$$c_{\mathbf{k}} = \frac{\Delta + g_1 A_{\mathbf{q}/2,\mathbf{k}}}{E + t_a A_{\mathbf{q}/2,\mathbf{k}}} X + \frac{g_1}{E + t_a A_{\mathbf{q}/2,\mathbf{k}}} Y \tag{3.9}$$

The full state is thus determined by only the three unknowns X, Y, and E. To determine the values of these variables, we sum the equations (3.9) to yield:

$$X = \frac{1}{N}\sum_{\mathbf{k}} \frac{\Delta + g_1 A_{\mathbf{q}/2,\mathbf{k}}}{E + t_a A_{\mathbf{q}/2,\mathbf{k}}} X + \frac{1}{N}\sum_{\mathbf{k}} \frac{g_1}{E + t_a A_{\mathbf{q}/2,\mathbf{k}}} Y \tag{3.10}$$

$$Y = \frac{1}{N}\sum_{\mathbf{k}} \frac{A_{\mathbf{q}/2,\mathbf{k}}\left(\Delta + g_1 A_{\mathbf{q}/2,\mathbf{k}}\right)}{E + t_a A_{\mathbf{q}/2,\mathbf{k}}} X + \frac{1}{N}\sum_{\mathbf{k}} \frac{g_1 A_{\mathbf{q}/2,\mathbf{k}}}{E + t_a A_{\mathbf{q}/2,\mathbf{k}}} Y \tag{3.11}$$

Together with the normalization condition these equations are enough to fully determine X, Y, and E. To simplify equations (3.10) and (3.11) it is convenient to define

$$I_n \equiv \frac{1}{N}\sum_{\mathbf{k}} \frac{\left(A_{\mathbf{q}/2,\mathbf{k}}\right)^n}{E + t_a A_{\mathbf{q}/2,\mathbf{k}}} \tag{3.12}$$

where in the limit of large N

$$I_n \to \frac{a^2}{4\pi^2}\int_{-\pi}^{\pi}\int_{-\pi}^{\pi} \frac{\left(A_{\mathbf{q}/2,\mathbf{k}}\right)^n}{E + t_a A_{\mathbf{q}/2,\mathbf{k}}} dk_x dk_y \tag{3.13}$$

Thus we have

$$X = \left(\Delta I_0 + g_1 I_1\right) X + g_1 I_0 Y \tag{3.14}$$

$$Y = \left(\Delta I_1 + g_1 I_2\right) X + g_1 I_1 Y \tag{3.15}$$

where we must keep in mind that I_0, I_1, and I_2 are functions of E, in addition to being dependent on the choice of total crystal momentum $\mathbf{q}$.

We first consider the special case of $g_1 = 0$. This corresponds to the standard Hubbard model, with the possible addition of terms like the g_2 term that don't contribute to the two-body physics. In this limit, the value of Y is irrelevant, since we see from equation (3.9) that the corresponding term vanishes in the expression for $c_{\mathbf{k}}$. Equation (3.14) can be solved to eliminate X, which yields $\Delta = 1/I_0$. This equation can be solved numerically for E (since I_0 is a function of E), which then allows us to compute each $c_{\mathbf{k}}$ from (3.9). We see that X is just an overall factor

on the wavefunction, whose phase is irrelevant and whose magnitude is fixed by normalization.

For the case where $g_1 \neq 0$, we proceed by dividing equations (3.14) and (3.15) by X. We introduce the variable $Z \equiv Y/X$. Solving for Z, we have:

$$Z = \frac{1 - \Delta I_0 - g_1 I_1}{g_1 I_0} = \frac{\Delta I_1 + g_1 I_2}{1 - g_1 I_1} \tag{3.16}$$

A little algebra yields a quadratic equation for g_1:

$$\left(I_0 I_2 - I_1^2\right) g_1^2 + 2 g_1 I_1 + \Delta I_0 - 1 = 0 \tag{3.17}$$

Expanding the integrands in I_1 and I_2 in partial fractions, we see that $I_1 = (1 - E I_0)/t_a$ and $I_2 = -E I_1/t_a$. With these replacements, equation (3.17) simplifies to $-(I_1/t_a)\, g_1^2 + 2 I_1 g_1 + \Delta I_0 = 1$. Expressing this equation in a form similar to the $g_1 = 0$ case, we have:

$$\Delta - \left(\frac{t_a I_1}{I_0}\right) \frac{g_1}{t_a} \left(\frac{g_1}{t_a} - 2\right) = \frac{1}{I_0} \tag{3.18}$$

We can see that this exactly reproduces the result for $g_1 = 0$, namely $\Delta = 1/I_0$. For non-zero g_1, we have $\Delta_{eff} = 1/I_0$, where $\Delta_{eff} - \Delta$ is given by the second term in equation (3.18). The effect of the correlated tunneling given by g_1 is to introduce an effective attraction. This can be understood by the fact that the tunneling rate is greater when one atom tunnels into or out of the site occupied by the other atom, and thus it is energetically favorable to have the atoms closer together.

For a given g_1, Δ and t_a, we can numerically solve equation (3.18) to determine the eigenenergy E, since I_0 and I_1 are functions of E. In particular, we take $\mathbf{q} = 0$ and evaluate I_0 and I_1 in the limit of large N, as given by equation (3.13). (The case where $\mathbf{q} = 0$ is of particular interest because in the many-body case it is energetically favorable to form pairs with $\mathbf{q} = 0$, as this allows the greatest number of pairings.)

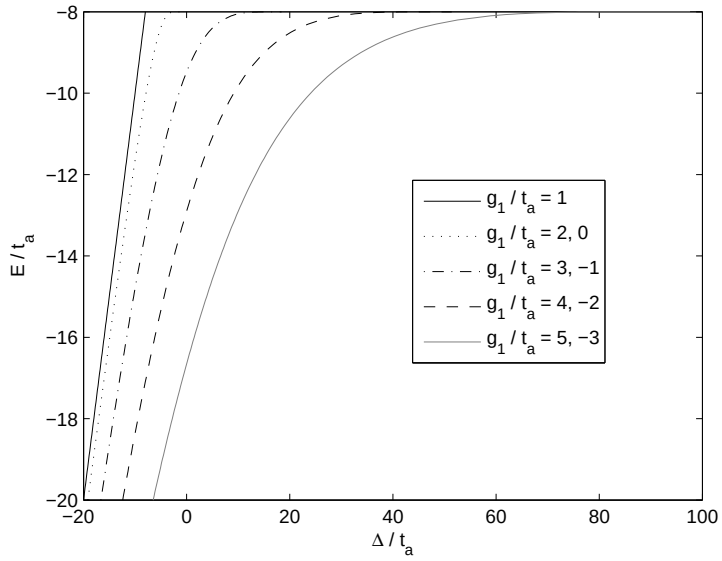

Figure 3.1: Two body boundstate eigenenergy E vs. the on-site interaction energy Δ for various g_1. (Here we take $\mathbf{q} = 0$, where $\mathbf{q}$ gives the total crystal momentum of the pair). The binding energy of the pair is $-8t_a - E$. We note that pair binding is allowed for Δ below some critical value Δ_c (the $E = -8t_a$ axis intercept), and this Δ_c increases with increasing $|g_1 - t_a|$. (Note however that the numerical calculation becomes unreliable in the $E \to -8t_a$ limit due to the divergence of the integral I_0. The values of Δ_c should instead be taken from the analytical formula in the next section.)

Figure 3.1 shows the eigenenergy E as a function of Δ for various values of g_1. Note that the results are identical for $g_1 = t_a + c$ and $g_1 = t_a - c$ (where c is any constant). This can be understood by the fact that the only two-body terms of the Hamiltonian (in the dressed-molecule formulation) that depend on g_1 are the g terms, such as $g d_i^\dagger a_{i\uparrow} a_{j\downarrow}$. Here $g = g_1 - t_a$. Thus reversing the sign of $g_1 - t_a$ is equivalent to reversing the sign of d_i (as the g terms are the only terms in the Hamiltonian with an odd number of dressed molecule operators), while leaving the solution otherwise unchanged.

The binding energy of the two-body bound state is $-8t_a - E$, where $-8t_a$ is the ground state energy of the two atoms in non-interacting case. The main features we note for figure 3.1 are that for a given Δ the energy decreases with increasing $|g_1 - t_a|$, and that a bound state is thus possible at increasing values of Δ, even far

onto the positive-Δ side. This is consistent with the idea that increasing $|g_1 - t_a|$ results in an effective attraction that can cancel out the on-site repulsion $\Delta > 0$. Note however that we should not attempt to use this numerical calculation to determine the critical value of Δ below which pair-binding is allowed for a given g_1. This is because the integrals I_0. I_1 diverge in the limit where $E \to -8t_a$, or equivalently the limit where Δ goes to the critical value. Instead, we determine the critical Δ analytically in the next section.

Figure 3.2 shows the relationship between g_1 and E for various Δ. Again we see that the result is symmetric around $g_1 = 1$. We note in particular that for $\Delta < -8t$, there is a bound state solution for any g_1, with the maximum energy $E = \Delta$ occurring when $g_1 = 1$. This can be understood by the fact that for $g_1 = 1$ the Hamiltonian conserves the number of dressed molecules (since all terms that would violate dressed molecule number conservation have a coefficient $g = g_1 - t_a = 0$). Thus for $g_1 = 1$ the bound state has both atoms bound onto the same site in a dressed molecule with energy Δ. On the other hand, for $\Delta > -8t$ we see that a bound state solution only exists if $|g_1 - t_a|$ is greater than some critical value.

Having numerically determined E, it is straightforward to determine the components $c_{\mathbf{k}}$ of the eigenstate $|\psi\rangle$. Z can be determined from equation (3.16), where I_0, I_1, and I_2 are as given by equation (3.13). Then from equation (3.9), we have:

$$\frac{c_{\mathbf{k}}}{X} = \frac{\Delta + g_1 A_{\mathbf{q}/2,\mathbf{k}} + g_1 Z}{E + t_a A_{\mathbf{q}/2,\mathbf{k}}} \tag{3.19}$$

This determines $c_{\mathbf{k}}$ up to a constant X. The magnitude of X is fixed by the normalization condition $\sum_{\mathbf{k}} c_{\mathbf{k}} = N$, and its phase may be neglected as it contributes only an irrelevant overall phase to $|\psi\rangle$.

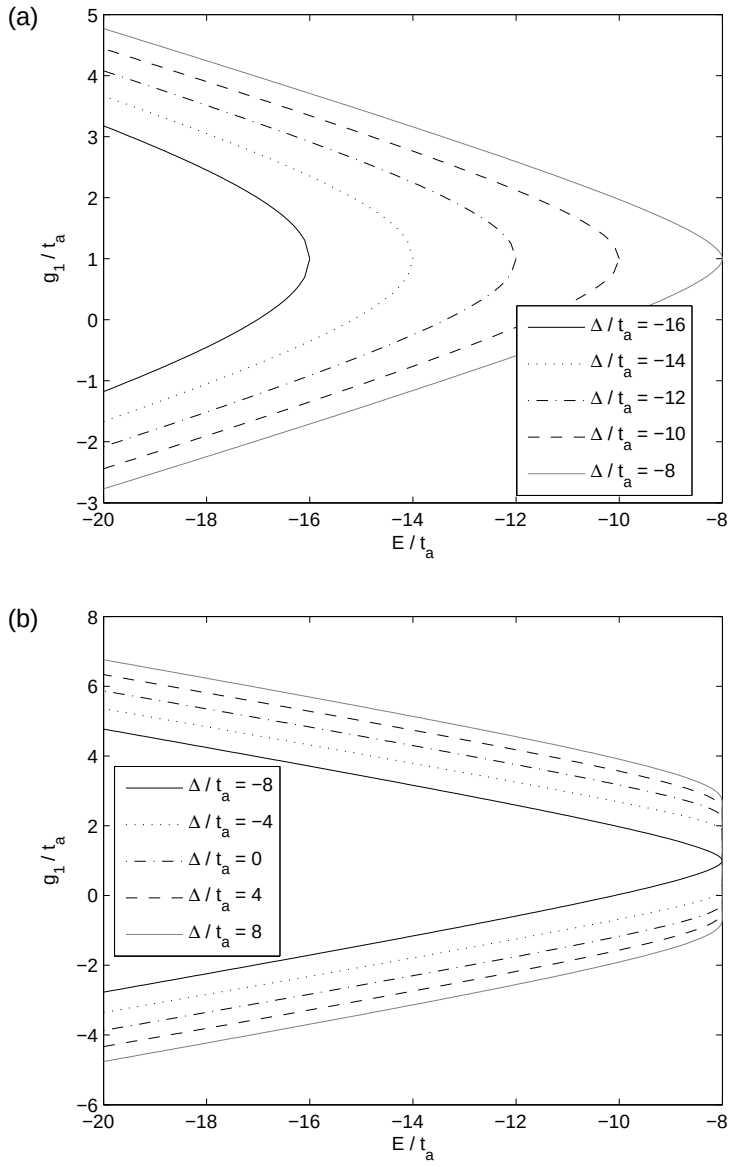

Figure 3.2: Correlated tunneling g_1 vs. eigenenergy E of the two-body boundstates for various Δ. (a) For $\Delta < -8t_a$ a two-body bound state exists for any g_1. Here the energy must satisfy $E \leq \Delta$ (b) $\Delta > -8t_a$, a two-body bound state only exists for sufficiently large $|g_1 - 1|$. The maximum eigenenergy of the two-body bound state is $E = -8t$, corresponding to the limit where the binding energy $-8t - E$ goes to zero. In this limit the integrals diverge, so the numerical calculation becomes unreliable. Instead we give an analytical result in the next section.

3.5 Critical Δ for Pair Binding

In the preceding section we have shown that a bound pair can occur for Δ less than some critical value Δ_c, where the value of Δ_c is dependent on g_1. Moreover, we have shown that we can numerically calculate the binding energy and fully determine the wavefunction for any g_1 and any Δ less than the critical value. However, in the limit where $\Delta \to \Delta_c$, the integrals I_0, I_1, and I_2, diverge, and the numerical calculation can no longer be relied on. In this section, we show that in the $\Delta \to \Delta_c$ limit we can instead determine the critical Δ and fully determine the eigenstate analytically.

From equation (3.18) and the relation $t_a I_1 = (1 - EI_0)$, we have:

$$\Delta - \left(\frac{1}{I_0} - E\right) \frac{g_1}{t_a} \left(\frac{g_1}{t_a} - 2\right) = \frac{1}{I_0} \tag{3.20}$$

In the limit where Δ goes to Δ_c (from below) the eigenenergy becomes just the energy of two unbound atoms $E = -8t_a$ and we can readily see that $I_0 \to -\infty$. Thus we can neglect $1/I_0$ in equation (3.20), which yields:

$$\frac{\Delta_c}{t_a} = 8\frac{g_1}{t_a} \left(\frac{g_1}{t_a} - 2\right) \tag{3.21}$$

As we could see from the numerical results in figures 3.1 and 3.2, Δ_c has a minimum of $-8t_a$ for $g_1 = 1$, and increases with increasing $|g_1 - t_a|$.

We also find that in the $\Delta \to \Delta_c$ limit we have $c_{\mathbf{k}} = 0$ for all $\mathbf{k} \neq 0$. Thus the eigenket is given by $|\psi\rangle = a^\dagger_{0,\uparrow} a^\dagger_{0,\downarrow} |\psi\rangle$. Transforming back to position space, this is just $|\psi\rangle = \sum_{i,j} a^\dagger_{0,\uparrow} a^\dagger_{0,\downarrow} |0\rangle$, which is precisely the state of two non-interacting particles, as we expected.

3.6 Chapter Summary

In this chapter we have studied the two-body problem for the generalized Hubbard model. We found that pair-binding occurs when the on-site interaction Δ is less

than some critical value Δ_c, and that this critical value depends on the parameter g_1. We note in particular that for $|g_1 - t_a| > 1$ pair-binding is possible even for some $\Delta > 0$, in contrast to the standard Hubbard model. This can be understood as a consequence of the g_1 terms contributing an effective attraction that can exceed the repulsion given by the positive Δ.

We have numerically solved for the binding energy and wavefunction of the two-body bound state for varying Δ and g_1, and have given the analytic solution in the limit where the binding energy goes to zero (at which point the numerical solution ceases to converge). As described above, part of the motivation for this is to provide a means for relating the parameters of the generalized Hubbard model (g_1, Δ, etc.), to the experimentally controlled parameters (magnetic field B, lattice depth, etc.). If we can solve the Schrödinger equation for two interacting atoms in a periodic potential near a Feshbach resonance, we can match this solution to the two-body solution of the generalized Hubbard model by comparison of the binding energy. Solving the Schrödinger equation for such a system is itself a non-trivial task. This has been investigated by other members of our group. In the next chapter we present a different approach to determining the parameters of the generalized Hubbard model from the directly controllable parameters, namely an experimental scheme for measuring these values.

After completion of the work presented in this chapter, we discovered that the two-body problem had been previously studied by M. Airoldi and A. Parola for the generalized Hubbard model arising in a condensed matter context.[26] We note that our results are consistent with those of this previous work. In particular, the key equations (3.18) and (3.21) are exactly equivalent to equations (5) and (6) in Airoldi and Parola's paper.

CHAPTER IV

Proposed Experimental Measurement of the Generalized Hubbard Model using a Double-Well Superlattice

In the preceding chapters we have presented a theoretical argument that fermionic atoms in an optical lattice near a wide Feshbach resonance can be described by the generalized Hubbard model (GHM), and we have discussed some approaches to calculating the values of the parameters of this model. Complementary to this approach, we would like to have an experiment to test that this system is described by the GHM, and to empirically determine the parameters of the model. In this chapter we describe such an experimental scheme. Our proposal uses an optical superlattice, such as has been used in recent experiments for demonstration of the spin super-exchange interaction [70, 71, 76]. Those works demonstrate all the necessary controllability of the superlattice required for this measurement scheme.

(This chapter presents our work from Ref. [77])

4.1 Testing The Generalized Hubbard Model

As in the previous chapters, we consider two component fermions (denoted by spin $\sigma = \uparrow, \downarrow$) in an optical lattice near a wide Feshbach resonance. As we saw above and in [24], the Hamiltonian of this system can be mapped to a Generalized Hubbard Model (GHM) Hamiltonian with correlated tunneling. To reiterate the key points of

this derivation: We found that in general many lattice bands get populated due to the strong atomic interaction, but we note (see [3, 24]) that the low energy states at each site are still restricted to only four possibilities: either a vacuum denoted by $|0\rangle$, or a single atom with spin-σ denoted by $a_\sigma^\dagger |0\rangle$, or a dressed molecule in the ground state $|d\rangle$ which consists of superpositions of two-atom states distributed over many bands. All the other states (such as the three-atom states or the dressed molecule excited states) are well separated in energy, and therefore not relevant for low-temperature physics. Based on this low-energy Hilbert space structure and general symmetry arguments, we saw [24] that the effective Hamiltonian takes the form of the GHM:

$$H = \sum_i \left[(U/2)\, n_i \left(n_i - 1 \right) - \mu_i n_i \right] \tag{4.1}$$
$$+ \sum_{\langle i,j \rangle, \sigma} \left[t_a + g_1 \left(n_{i\overline{\sigma}} + n_{j\overline{\sigma}} \right) + g_2 n_{i\overline{\sigma}} n_{j\overline{\sigma}} \right] a_{i\sigma}^\dagger a_{j\sigma} + H.c.$$

where $n_i \equiv \sum_\sigma a_{i\sigma}^\dagger a_{i\sigma}$, $n_{i\overline{\sigma}} \equiv a_{i\overline{\sigma}}^\dagger a_{i\overline{\sigma}}$ ($\overline{\sigma} = \downarrow, \uparrow$ for $\sigma = \uparrow, \downarrow$), U characterizes the effective on-site interaction (defined as the energy shift of $|d\rangle$ with respect to the two-atom state on different sites), μ_i is the chemical potential (we keep its dependence on the site i for convenience of the following discussion, where a global trap induces a site dependent energy shift), t_a is the conventional single-atom tunneling rate, and g_1 and g_2 denote the additional tunneling in the presence of spin-$\overline{\sigma}$ atoms (those two terms come from the multi-band populations in the $|d\rangle$ state and the direct neighboring atomic interaction in the lattice [3]). In this derivation, we have mathematically mapped $|d\rangle$ to the double occupation state $a_{i\uparrow}^\dagger a_{i\downarrow}^\dagger |0\rangle$ [24] (though their physical compositions are different).

Although we believe that strongly interacting fermions in an optical lattice are described by the generalized Hubbard Model, it is important to test this model by comparing its predictions with experimental observations. However, such a com-

parison is usually difficult because of the lack of exact solutions to the GHM and complications in real experimental configurations (such as the inhomogeneity due to the global trap). On the other hand, if instead of considering the full lattice we consider the GHM on a pair of sites, an exact solution is possible. Thus the problem becomes much more tractable if we replace the homogenous optical lattice (that is, with all lattice barriers equal) with an inhomogeneous optical superlattice in which large barriers suppress interactions except within particular pairs of sites.

In the experimental configuration with an inhomogeneous optical superlattice, through manipulation of the lattice barrier and the external magnetic field, we show that one can reconstruct the two-site dynamics from the measured time-of-flight images. The measured dynamics can then be compared with the exact prediction from the general Hubbard model, offering an unambiguous testbed for this complicated system. The proposed measurement also allows a complete empirical determination of all the parameters in the effective GHM.

4.2 The Superlattice and Measurement Scheme

To see whether the effective GHM gives a good description of the low-temperature physics for this system it is important to test the predictions of the GHM experimentally, and as unambiguously as possible. To have an unambiguous test, it is better to design a configuration such that the GHM allows exact solutions. The optical superlattice provides such an opportunity. To have an optical superlattice one adds a 3-dimensional lattice $V_2 = V_{20} \sum_{\alpha=x,y,z} \sin^2(\pi\alpha/2a)$ to a lattice $V_1 = V_{10} \sin^2(\pi z/a - \varphi)$ in one spatial direction (say z), where the periodicity $2a$ of V_2 is twice that of V_1[70, 71, 76]. If V_{10} is sufficiently large relative to V_{20}, the superposition of these two potentials produces a series of double wells along the z

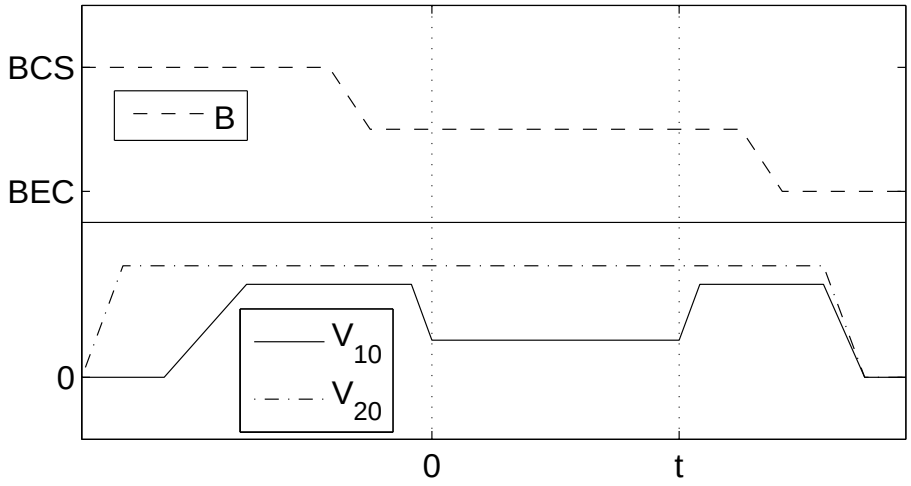

Figure 4.1: The time sequences for the magnetic field (B) and the lattice potentials (V_{10} and V_{20}) to achieve state preparation, controlled dynamics, and detection. (Note that the optical barriers are high during sweeping of the B field.)

direction. The dynamics in each double well are independent of the others provided the barrier between wells (controlled by V_{20}) is sufficiently large. Taking the relative phase φ to be nonzero introduces an energy bias δ_{12} between the minima of each double well.

It is easy to calculate the dynamics in each double well from the GHM. However, it is unclear how to directly measure the dynamics without individual addressing of each well inside the lattice. The conventional time-of-flight (ToF) images involve averages over all the potential wells. These signals are further complicated by the presence of a global harmonic trap $V_g = \sum_{\alpha=x,y,z} m\omega_\alpha^2\alpha^2/2$ inevitable in an optical lattice, which makes each double well slightly different. In the following, we show a scheme that can map out the detailed dynamics in each double well from the measured ToF images even with the presence of these complications.

The scheme here combines the control of both the optical potentials and the magnetic field (see Fig. 4.1 for illustration). First, we need to load each double well with a filling pattern that sets the initial condition of the dynamics. This is achieved

at the BCS limit of the resonance. In this limit, the atoms are free fermions, and we can control the filling pattern by choosing the total number $N = N_\uparrow + N_\downarrow$ and the polarization $P = (N_\uparrow - N_\downarrow)/N$. Then, we turn off all the inter-well dynamics by raising the barrier (controlled by V_{10} and V_{20}) and sweep the magnetic field to the unitarity region. The sweeping speed v is fast compared with the inter-well coupling rate but small compared with the lattice gap of V_1 so that the levels in each single well adiabatically evolve. Near unitarity, we turn on the inter-well dynamics for a duration t by adjusting V_{10} to lower the central barrier of each double well. These dynamics give information on the underlying strongly interacting Hamiltonian. To determine the final state after the dynamics, the central barrier is raised again, and the magnetic field is swept to the BEC limit with a speed similar to v. Depending on the particle number in each well, we have atoms or molecules or their mixture with negligible interaction at the BEC limit. The ToF images for those atoms or molecules are then detected to determine the final state after the dynamics during time t.

4.3 Measuring the Free-Atom Tunneling Rate t_a

To test the prediction of particle-correlated tunneling, we need to compare the free-atom hopping rate t_a with $t_{a2} = t_a + g_1$ and $t_{a3} = t_a + 2g_1 + g_2$, where t_{a2} and t_{a3} correspond respectively to the hopping rates of a spin-$\uparrow$ atom from the site i to j when there is a spin-$\downarrow$ atom on one site or on both sites. Let us first look at how to measure the free-atom hopping rate t_a in the Hamiltonian (4.1). For that purpose, we need one atom per double well. By choosing the polarization $P = 1$ and $V_{10} = 0$ (so we have at this stage single wells rather than double wells), the equilibrium distribution of the free fermions at the BCS limit automatically gives

this configuration. The total atom number N within the global harmonic trap V_g needs to be below

$$N_{max} = (4\pi/3)\left(E_{bg}/2m\omega^2 a^2\right)^{3/2}, \tag{4.2}$$

where $E_{bg} = 2\sqrt{V_{20}\pi^2\hbar^2/8ma^2}$ is the band gap for the lattice V_2 and we have assumed $\omega_x = \omega_y = \omega_z \equiv \omega$. Then, one can adiabatically raise the potential V_{10} with a bias δ_{12} so that the atom sits on the left side well in each double well. After raising V_{10}, δ_{12} is reduced to zero. The system is then moved to the resonance region, and after turn-on of the dynamics for a duration t, the difference between the fraction of atoms in the left-side and the right-side wells over the whole harmonic trap is given by

$$\frac{N_L - N_R}{N} = 1 - \frac{2}{N}\sum_i \left(\frac{t_a}{\hbar\Omega_{1i}}\right)^2 \sin^2(\Omega_{1i}t), \tag{4.3}$$

where $\Omega_{1i} = \sqrt{\Delta_i^2 + 4t_a^2}/2\hbar$, $\Delta_i \approx m\omega^2 a z_i$. The summation of i in Eq. (4.3) is over all the occupied double wells in the global harmonic trap (with z_i the z-coordinate of the center of the double well), and each double well has a slightly different bias Δ_i due to the trap potential V_g. After the dynamics, in order to measure the populations N_L and N_R, the atom of the right-side well can be dumped into an excited vibrational state (corresponding to the second band) of the left-side well by rapidly raising the potential minimum of the right well relative to the left (through control of the phase φ) [70, 71, 76]. The populations in different bands are then mapped out in the BEC limit through measurement of the momentum distribution of free atoms with ToF imaging. From the measured populations N_L and N_R, one can easily determine the tunneling rate t_a. Fig. 4.2 (a) shows the typical time evolution of $N_L - N_R$ from the dynamics, for which the oscillation period is determined by t_a and the damping is due to the inhomogeneity from the global trap. (Note that in this case, the dynamics should be the same as for the bosonic case, and the latter has been measured in

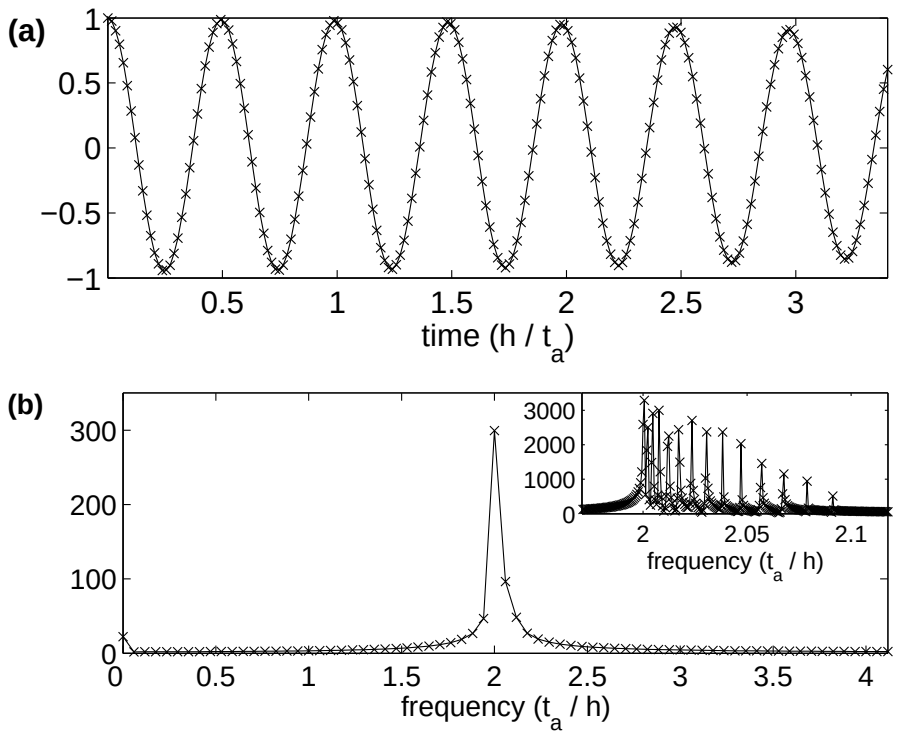

Figure 4.2: Population difference between the left and right wells $(N_L - N_R)/N$ for the case of one atom per double well. **(a):** Population difference vs. time (in the unit of h/t_a). **(b):** Fourier transform of the population difference (frequency in the unit of t_a/h), calculated for a time duration of $20h/t_a$ to give a frequency resolution of $t_a/20h$. The peak occurs at a frequency $\nu = 2t_a/h$. **Inset:** With the time duration increased to give a frequency resolution of $t_a/2000h$, we see that there are actually many peaks, corresponding to the different frequencies Ω_{1i}. Ω_{1i} depends on the z-coordinate and thus each peak corresponds to a different slice of double wells parallel to the z-axis. The slices containing the most occupied double wells are closest to $z = 0$. That is why those peaks (which have the smallest Ω_{1i}) dominate. Because t_a can be determined from the dominant peak, it is not necessary to resolve the other smaller peaks. In calculation of the inhomogeneity effect, we assume a spherical distribution with a diameter of 30 occupied double wells, and take the following typical values for the parameters: $t_a = h \times 170$ Hz, $m = 6.64 \times 10^{-26}$ kg (for ^{40}K), $\omega = 2\pi \times 80$ Hz, and $2a = 765$ nm.

recent experiments [71].) In the frequency domain, the signal peaks at $2t_a$, and the inhomogeneity causes many smaller peaks at frequencies above that of the dominant peak (see Fig. 4.2 (b)).

4.4 Measuring the Particle-Correlated Tunneling Rate t_{a2}

To measure the particle-correlated tunneling rate t_{a2}, we need two atoms per double well, one spin-↑ and one spin-↓. This can be achieved with the equilibrium

distribution of free fermions at the BCS limit by choosing $P \approx 0$, $V_{10} = 0$, and the total atom number $N < 2N_{max}$ (with N_{max} defined in Eq. 4.2). The double well is still turned on with a bias so that both of the atoms are prepared in the left-side well. For the dynamics near resonance with the Hamiltonian (4.1), the state at any time involves a superposition of three components: a double occupation of the left or the right well, and a singlet state of two atoms over the two wells. We can determine t_{a2} as well as the on-site interaction energy U from the difference between the overall fractions of double occupation of the left wells and of the right wells, $(N_{2L} - N_{2R})/(N_{2L} + N_{2R})$. (Here N_{2L} and N_{2R} are the total number of double wells in which the left and right wells, respectively, are doubly occupied.) These fractions can be directly measured at the BEC limit, where the double occupation of a site is mapped to a molecule state, and the molecules in the left and the right wells are distinguished through the band mapping and the measurement of the momentum distribution (similar to the discussion above for the atomic case). The single-atom occupation of a well is mapped to an atomic state at the BEC limit. Because of the large detuning between the atomic and the molecular state, the atomic population do not contribute to the time-of-flight imagining signal of the molecular fraction.

The typical time evolution of $(N_{2L} - N_{2R})/(N_{2L} + N_{2R})$ is shown in Fig. 4.3 (a). In the frequency domain (see Fig. 4.3 (b)), one can see two distinct primary peaks in the Fourier transform, centered at $\left(\sqrt{U^2 + 16t_{a2}^2} \pm U\right)/2$. The smaller peaks from the inhomogeneity of the global harmonic trap do not obscure these two dominant peaks. The frequencies at which these two peaks occur can be understood by the fact that while the oscillation frequency varies from well to well due to the z-dependent bias, there are a greater number of occupied double wells near $z = 0$ than for any other z-coordinate. Thus, the dominant peaks correspond to the zero bias case,

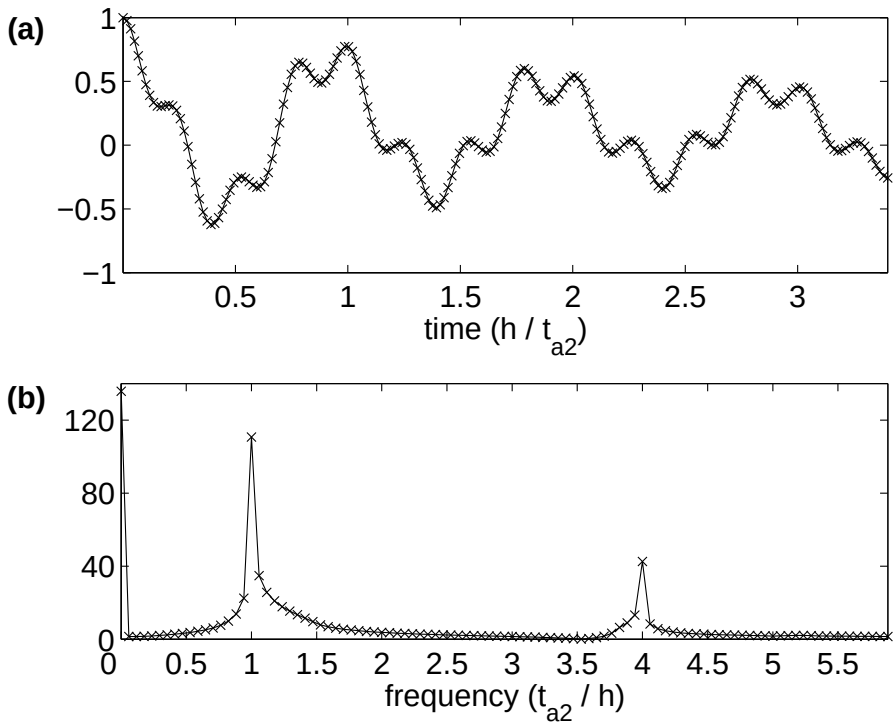

Figure 4.3: The difference between the fractions of doubly occupied left and right wells $(N_{2L} - N_{2R})/(N_{2L} + N_{2R})$ for the case of two atoms per double well. **(a):** Population difference vs. time (in the unit of h/t_{a2}). **(b):** Fourier transform of the population difference (the frequency resolution is 1/20 in the unit of t_{a2}/h. The peaks occur at a frequencies $\nu_1 = \left(\sqrt{U^2 + 16t_{a2}^2} - U\right)/2h$ and $\nu_2 = \left(\sqrt{U^2 + 16t_{a2}^2} + U\right)/2h$ (in the figure we take $U = 3t_{a2}$ as an example). Increasing the frequency resolution would reveal a series of smaller peaks on the high frequency side of the large peaks (as in Fig. 4.2), but it is not necessary to resolve these smaller peaks to determine t_{a2} and U.

where we have

$$\frac{N_{2L}^{(0)} - N_{2R}^{(0)}}{N_{2L}^{(0)} + N_{2R}^{(0)}} = \frac{\Omega_+}{\Omega}\cos\left(\Omega_- t\right) + \frac{\Omega_-}{\Omega}\cos\left(\Omega_+ t\right), \tag{4.4}$$

with $\Omega_\pm = \left(\hbar\Omega_{2i} \pm U\right)/2\hbar$ and $\Omega_{2i} = \sqrt{U^2 + 16t_{a2}^2}/\hbar$.

4.5 Measuring the Hole Tunneling Rate t_{a3}

One can also measure the parameter g_2 in the Hamiltonian (4.1), which requires three atoms per double wells (two spin-↑, one spin-↓). One can consider this case as a single spin-↑ hole in each double well, with a hole hopping rate of t_{a3}. (A key difference between the generalized Hubbard model and the standard Hubbard model

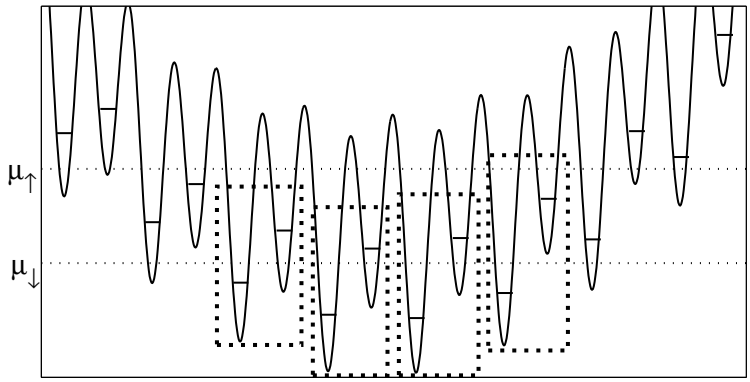

Figure 4.4: The superlattice configuration to achieve three atoms per double well. This is obtained by turning on the lattice potentials V_1 and V_2 simultaneously with relative phase $\varphi > 0$, producing double wells with a non-zero potential bias between the left and right wells. (The overall harmonic potential is exaggerated for illustration purposes). In the figure, the solid line in each well corresponds to the lowest level, the long dotted lines correspond to the Fermi surfaces for ↑-atoms and ↓-atoms (with Fermi energies $\mu_\uparrow$ and $\mu_\downarrow$), which differ due to the polarization $P > 0$, and the dotted rectangles indicate those double wells that are occupied by two ↑-atoms and one ↓-atom. The $\mu_\uparrow$ and $\mu_\downarrow$ are chosen such that ↓-atoms only occupy the left wells while ↑-atoms occupy both wells. This is the initial configuration needed to measure the hole hopping rate t_{a3}. There is also the possibility of additional ↑-atoms further from the center of the trap, but the measured molecule signal is only sensitive to double wells containing *both* ↑-atoms and ↓-atoms. With the conditions given in the text, we insure that the only such double wells are those with two ↑-atoms and one ↓-atom.

is that in the GHM holes and atoms tunnel at different rates, violating particle-hole symmetry.) This hopping rate can be measured by the same method as for measurement of the free atom hopping rate t_{a1}. To prepare three atoms per double wells, one can consider the free fermion distribution at the BCS limit in an asymmetric double-well lattice with a bias δ_{12} controlled by the phase shift φ. We would like to have two atoms (one spin-↑ and one spin-↓) in the deep wells and one spin-↑ atom in the shallow wells as shown in Fig. 4.4. This can be achieved by choosing the polarization P and bias δ_{12} so that the atom numbers satisfy $N_\uparrow > \left(2\sqrt{2}+1\right) N_0$ and $N_\downarrow < N_0$, where $N_0 = (4\pi/3)\left(\delta_{12}/2m\omega^2 a^2\right)^{3/2}$. These relations were derived by requiring that $N_\uparrow$ be great enough that every double well which contains a ↓-atom must also contain at least two ↑-atoms (so that the molecule signal corresponds only to double wells containing three atoms), and also requiring that no double well con-

tain more than one ↓-atom. (Note that it is not sufficient to require a polarization $P \geq 1/3$, since this could be achieved with an inner core of double wells containing one ↑-atom and one ↓-atom, surrounded by a shell of double wells containing only an ↑-atom.) $N_\uparrow$ must also be small enough that there are no more than two ↑ atoms per double well in the center of the trap. This condition can be met along with the above conditions provided the band gap of the lattice is sufficiently great.

4.6 Testing Our Assumptions for the Single-Site Hilbert Space

A key assumption in deriving the Hamiltonian (4.1) is that in the strongly interacting region there is a significant energy gap (of the order of the band gap) which separates the four low energy states on each site from the other higher energy states [3, 24]. With the superlattice technique, one can directly test this assumption and measure the energy gap. Given this energy gap, if we fill each site with two atoms, there will be no dynamics as long as the atomic tunneling rate between the two sites is small compared with the band gap energy. To fill each site with two atoms (one spin-↑, one spin-↓), we can start with the free-fermion distribution in the BCS limit, choosing the polarization $P \approx 0$ and total atom number $N < 4N_{max}$ (with N_{max} as defined in Eq. 4.2). We then adiabatically turn on V_1 and V_2 simultaneously while keeping a constant ratio $V_{10}/V_{20} > 1$. With this filling pattern, we should see no dynamics in the strongly interacting region, so the atomic distribution over the two sites (which will be mapped to the molecular population distribution in the BEC limit) will not change with the evolution time t. One can also tilt the double-well lattice by tuning the bias δ_{12}, and measure what is the critical δ_{12} to turn on the two-site dynamics in the population distribution. The measured critical δ_{12} will give an estimate of the energy gap to excite the system to the high energy states.

4.7 Chapter Summary

In this chapter we have described a scheme to test in a controllable fashion the predictions of an effective Hamiltonian for strongly interacting atoms in an optical lattice. With the superlattice technique, one can directly test the key assumption in derivation of the Hamiltonian, and can measure the physical parameters to confirm the particle-correlated tunneling. This scheme provides a quantitative testbed to compare theory with experiments in the strongly interacting region. Comparison of the few-site physics in an optical superlattice provides a general method to test model Hamiltonians for the atomic gas system. Slight modifications of the scheme here can also be used to test the theoretical model Hamiltonians in other configurations, including the multi-component Fermi gases.

In this chapter we focused on the case of interactions only between groups of two sites, as this provides the simplest case in which all the parameters of the model can be measured. Of course, we are interested not only in measuring the parameters of the generalized Hubbard model but also in examining its predictions for the many-body physics. In subsequent chapters, we consider what happens when larger numbers of lattice sites are allowed to interact.

CHAPTER V

Low Energy Eigenstates of the Generalized Hubbard Hamiltonian in a Plaquette Superlattice

In previous sections we have described how for fermions in an optical lattice near a Feshbach resonance, the effective interaction is easily larger than the band gap. It is in general quite difficult to understand the many-body physics of such a strongly interacting system. An examination of the physics of a few particles or a few sites serves as a valuable starting point. Having solved the two-particle and two-site cases above, we here move on to the next simplest case, that of a single four-site square plaquette. This case can be realized in experiments using an optical superlattice which suppresses interactions between plaquettes. (This is similar to the superlattice described in the previous chapter and demonstrated in recent experimental work [70, 71, 76], except here such a superlattice is applied along two orthogonal directions.)

This case is of particular interest because it is the smallest system that can exhibit d-wave rotational symmetry, such as has been found for the order parameter of the cuprate high-temperature superconductors.[78–81] Studying d-wave superfluidity in optical lattices may be instructive in understanding the high T_c superconductors, particularly as the effective Hamiltonian for strongly interacting optical lattice fermions resembles the model Hamiltonians used in studying strongly interacting electrons in

condensed matter systems.

We show that for the generalized Hubbard model the single plaquette states are in general described by superpositions of atomic resonating valence bonds and dressed molecules. As one scans the magnetic field, level crossings are found between states with different symmetry properties, which may correspond to quantum phase transitions in the many-body case.

(This chapter presents our work as published in Ref. [82])

5.1 The Effective Hamiltonian

In this effective Hamiltonian, whenever two atoms come to the same lattice site, they form a dressed molecule state (a single-site Cooper pair), which corresponds to an exact eigenstate constructed from the single-site physics. The effective Hamiltonian then describes the interaction between these dressed molecules and the atoms over different lattice sites. The explicit form of the Hamiltonian is as follows [3]

$$\begin{aligned} H_{eff} &= \sum_i \Delta(B) d_i^\dagger d_i + \sum_{i;j\in N(i)} t_d P d_i^\dagger d_j P \\ &+ \sum_{i;j\in N(i)} \sum_\sigma \left(t_a P a_{i\sigma}^\dagger a_{j\sigma} P + t_{da} d_i^\dagger d_j a_{j\sigma}^\dagger a_{i\sigma} \right) \\ &+ \sum_{i;j\in N(i)} \left(g d_i^\dagger \left(a_{i\uparrow} a_{j\downarrow} - a_{i\downarrow} a_{j\uparrow} \right) + h.c. \right) \end{aligned} \tag{5.1}$$

where $a^\dagger$ and $d^\dagger$ represent creation operators for fermionic atoms and bosonic dressed molecules, respectively; $\sigma = \uparrow, \downarrow$ labels two internal spin states; and i labels the lattice sites (with $j \in N(i)$ labeling the sites adjacent to i). P represents a projection of the state at every lattice site i onto the four-dimensional subspace with basis $\left\{ |0\rangle_i, a_{i\uparrow}^\dagger |0\rangle_i, a_{i\downarrow}^\dagger |0\rangle_i, d_i^\dagger |0\rangle_i \right\}$. The parameters g, t_d, t_a, and t_{da} depend on the physical properties of the atomic system as well as the multi-band properties of the optical lattice (see the explicit expressions in [3]). The parameter Δ corresponds to

an eigenenergy of the two-body physics from a single site, and can be tuned over a wide range of values by varying the applied magnetic field B [16]. Although in this chapter we use the form of the Hamiltonian given by equation (5.1), we should keep in mind that this is mathematically equivalent to the generalized Hubbard model.[24]

5.2 Why Study This Hamiltonian on Four-Site Plaquettes?

In this paper, we make use of the above effective Hamiltonian H_{eff} to study the physics of this strongly correlated system with interactions among a few lattice sites. In particular, we focus on investigation of the states of a single plaquette, which is a basic unit of the two-dimensional square lattice. This study has two purposes. First, understanding the states of atoms at a single plaquette is a necessary step towards the challenging goal of understanding the physics of this strongly interacting gas in a quasi-two-dimensional optical lattice. It is shown in Ref. [3] that the effective Hamiltonian H_{eff} reduces to the well-known t-J model [83] and the XXZ model [84] in certain limits of the parameter values, so the physics associated with H_{eff} should be rich and parameter-dependent. In this work, we would like to understand the influence of the parameters on a few body physics, and that understanding will provide an intuition for taking appropriate approximations towards the many-body physics. In particular, from the few-body physics, we construct states which will provide the lowest order eigenstates of perturbation theory for the case of weak coupling between the plaquettes. Even in the case of the homogeneous lattice (where the interplaquette coupling is not weak), the states on small clusters of cites might be used as the basic entries for an effective many-body theory through the contractor renormalization procedure (a real-space renormalizaton group method for high dimensions) [85, 86]. We will see that even for a single plaquette, the behavior of the states has been pretty

rich. The eigenstates involve resonating valence bonds and superposition of dressed molecules, and are highly entangled over different lattice sites. With variation of the parameters in the Hamiltonian H_{eff}, there are several level crossings for the lowest eigenstate with change of the state symmetry properties, which may correspond to a quantum phase transition for larger systems.

Second, the study of the physics of a single plaquette is also of practical relevance. For atoms in an optical superlattice, the physics can be dominated by the interactions within single plaquettes. A simple optical superlattice can be formed by adding two standing wave laser beams with commensurate wave vectors [87, 88]. The potential, say, along the x direction, has the form $V(x) = -\left[V_1 sin^2\left(k_1 x\right) + V_2 sin^2\left(k_2 x\right)\right]$. If we choose the wave vector $k_2 = 2k_1 = 2\pi/L$ and require $0 < V_1 < 4V_2$, then we have potential barriers of two different heights (see FIG. 5.1). The minima occur at $x = nL \pm x_0$ (for integer n), where

$$x_0 = \frac{L}{2\pi} cos^{-1}\left(\frac{-V_1}{4V_2}\right) \tag{5.2}$$

The lower and higher potential barriers V_{low} and V_{high} are given respectively by

$$\begin{aligned} V_{low} &= \left(1 - \frac{V_1}{4V_2}\right)^2 V_2 \\ V_{high} &= \left(1 + \frac{V_1}{4V_2}\right)^2 V_2. \end{aligned} \tag{5.3}$$

The barrier V_{high} can be significantly larger than V_{low} if we choose V_1 close to $4V_2$, and such a high barrier turns off the interactions except for the ones between the sites separated by V_{low}. If we apply this optical superlattice potential along both the x and y directions and a deep lattice potential along the z direction, we then have interactions dominantly within the single plaquettes in the x-y plane. With strongly interacting atoms in this optical superlattice potential, one can test the predictions

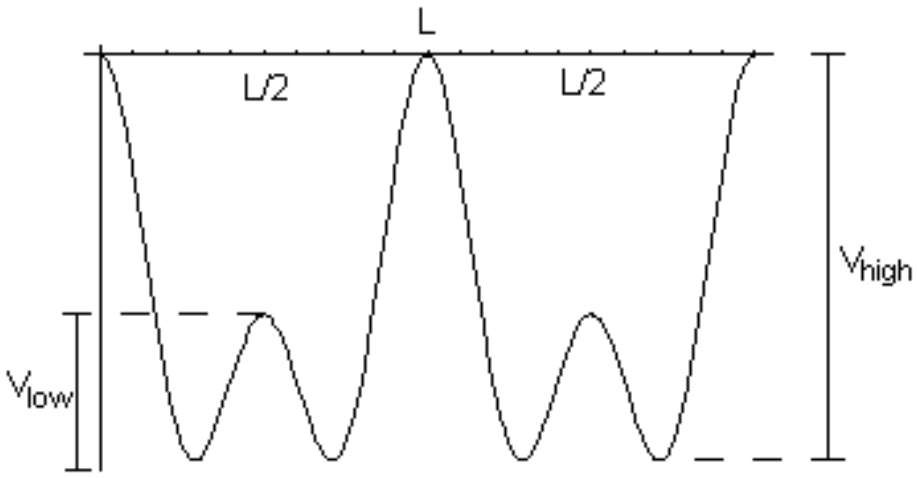

Figure 5.1: Superlattice potential vs. x for $V(x) = -\left(V_1 sin^2\left(\frac{\pi x}{L}\right) + V_2 sin^2\left(\frac{2\pi x}{L}\right)\right)$

from the effective Hamiltonian H_{eff}, and detect the exotic entangled states emerging from the ground state configurations of H_{eff}.

We should also point out that the effective Hamiltonian H_{eff} includes the Hubbard model as a particular case. The Hubbard model is given by the Hamiltonian [86, 89]

$$H_{Hub} = -t \sum_{<i,j>,\sigma} \left(a^\dagger_{i\sigma} a_{j\sigma} + H.c. \right) + U \sum_i n_{i\uparrow} n_{i\downarrow}, \tag{5.4}$$

where $n_{i\sigma} = a^\dagger_{i\sigma} a_{i\sigma}$. Specifically, H_{eff} can be written in the form of H_{Hub} if we substitute $d^\dagger_i$ with $a^\dagger_{i\uparrow} a^\dagger_{i\downarrow}$ and make a particular choice of the parameters in H_{eff} with $t_a = -t$, $t_{da} = t$, $g = t$, $t_d = 0$, and $\Delta = U$. So, one can see that H_{eff} extends the well-known Hubbard model H_{Hub} in a nontrivial way. Note that for strongly interacting atoms near a broad Feshbach resonance, the parameters g and t_{da} are significantly different from the atomic tunneling rate t due to the multi-band populations and the direct neighboring collisions. From the expressions of these parameters in Ref. [3], we estimate that typically $|t_d| << |t_a| << |t_{da}| \sim |g|$. This is because t_a corresponds to atomic tunneling in the single lowest band, whereas t_{da} and g correspond to interactions involving the dressed molecule states (which are superpositions of states in multiple upper bands). For the numerical calculations in

this work, we typically take $t_d \sim 0$, $-t_a \sim 0.1|g|$–$0.3|g|$, and $t_{da} \sim |g|$–$2|g|$. (Note from the form of H_{eff} that the sign of g is essentially irrelevant, as it can be incorporated into the definition of $d^\dagger$.) The parameter Δ is sensitive to the external magnetic field, and can be scanned from the value much smaller than $-|g|$ to the value much larger than $|g|$.

The atomic states within each plaquette critically depend on the atom number and the spin configuration in that plaquette. In the following, we will consider all the different nontrivial cases with different numbers of spin $\uparrow$ and $\downarrow$ atoms occupying the four-site plaquette.

5.3 Four atoms per plaquette: two $\uparrow$, two $\downarrow$

Over most of the typical range of the parameter values, the plaquette occupied by two $\uparrow$ and two $\downarrow$ atoms has two distinct types of ground states, with a level crossing occurring at some critical value of Δ. These two types of states can be distinguished by how they transform under a 90° rotation in the plane of the plaquette. Under such a rotation, the ground state wavefunction for Δ less than (greater than) the critical value is multiplied by a factor of $+1$ (-1). Thus, we say that the phase on the negative side of the transition has s-wave symmetry, and that on the positive side has d-wave symmetry.

The ground states of each of these two types change smoothly with changes in the parameter Δ. Thus, we can identify particular energy eigenstates as the "s-wave state" and the "d-wave state" over the full range of Δ, even as the exact form of the eigenstate changes. (Note that these are not the *only* eigenstates with s-wave and d-wave symmetry – here we use these terms to refer solely to those states which are the ground states when the system is in the corresponding parameter regions.)

The energies of the s-wave and d-wave states can be easily calculated through exact diagonalization, and they are plotted in FIG. 5.2(a), which illustrates the crossover between them. (For this figure, we scan Δ and set the other parameters of H_{eff} to their typical values with $t_{da} = 1.5|g|$ and $t_a = -0.2|g|$.) The energy gap between the ground state and 1st excited state is shown in FIG. 5.2(b)).

To understand the properties of the ground state, it is important to have its explicit expression. Although one can calculate this explicit expression through numerical exact diagonalization, the state is in general a superposition of many basis-vectors (36 vectors in this case), with all the superposition coefficients varying with Δ. It is troublesome to understand the state's properties from this lengthy expression. To overcome this problem, we describe the s-wave and d-wave states more compactly, in a way that illustrates their rotational symmetry, by means of a pictorial representation which we define here. The four sites of a plaquette we label as: $\begin{smallmatrix}1 & 2\\ 3 & 4\end{smallmatrix}$. We place various pictures on these sites corresponding to creation operators applied at those sites. The whole picture represents the product of these operators, applied to the vacuum state $|0\rangle$. For instance,  placed on two sites (either horizontally, vertically, or diagonally) represents a normalized singlet between those two sites. So, if the sites are labeled i and j, this represents $\frac{1}{\sqrt{2}}\left(a^\dagger_{i\uparrow}a^\dagger_{j\downarrow} - a^\dagger_{i\downarrow}a^\dagger_{j\uparrow}\right)$. (Note that the order of i and j does not matter, as the anti-commutation of $a^\dagger_i$ and $a^\dagger_j$ makes the singlet symmetric under exchange of i and j.) represents a dressed molecule. (I.e., if located at site i , this picture corresponds to $d^\dagger_i$.) represents an unoccupied site. The creation operators that make up a singlet are always grouped together; other than that, the order of the operators is irrelevant, as the singlets and dressed molecules commute. As an example, the picture  represents $\frac{1}{\sqrt{2}}\left(a^\dagger_{1\uparrow}a^\dagger_{3\downarrow} - a^\dagger_{1\downarrow}a^\dagger_{3\uparrow}\right) d^\dagger_2 |0\rangle$.

The full Hilbert space for two $\uparrow$ and two $\downarrow$ atoms on a plaquette is 36-dimensional.

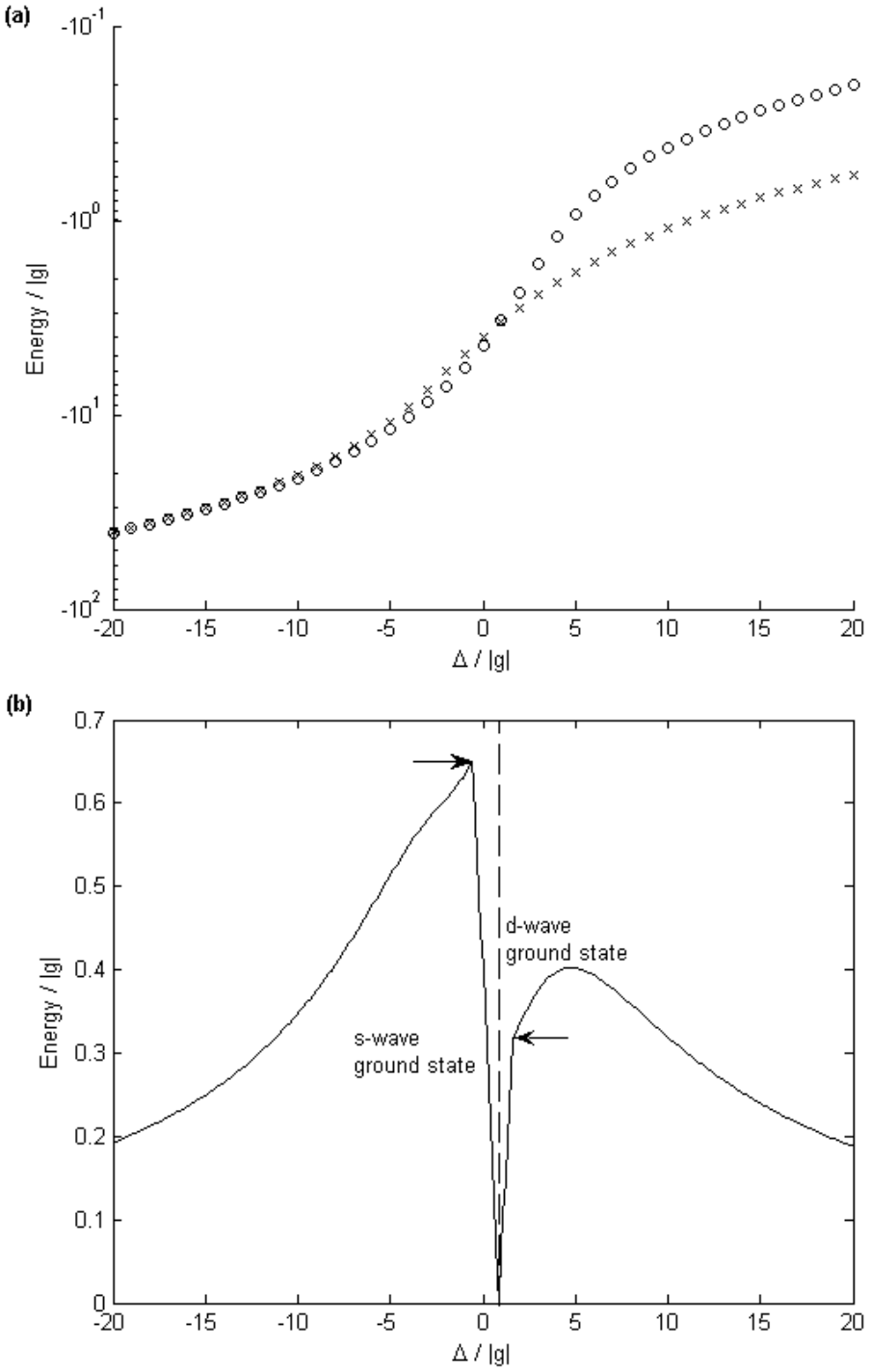

Figure 5.2: Energy vs. Δ for a plaquette occupied by two $\uparrow$ and two $\downarrow$ atoms. Other parameters are $t_{da} = 1.5|g|$, $t_a = -0.2|g|$, $t_d = 0$ (a): Eigenenergies of the s-wave ($\circ$) and d-wave (x) states. (b): Energy difference (gap) between ground state and first excited state. The gap vanishes at the level crossing point. Because the eigenenergies vary smoothly with Δ, the curve is smooth except at the level crossing points for the ground state (where the gap is zero) and for the first excited state (indicated by arrows)

However, the s-wave state (over the full range of Δ) can be conveniently expressed as a vector in a 4-dimensional subspace of the full space, with basis vectors:

$|1\rangle_s = \frac{1}{2\sqrt{3}}$ 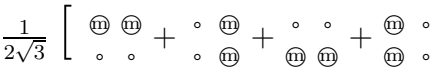

$|2\rangle_s = \frac{1}{2\sqrt{2}}$ 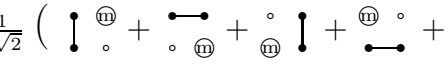

$|3\rangle_s = \frac{1}{2}$ 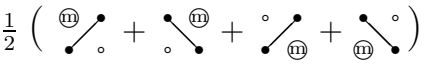

$|4\rangle_s =$ 

The d-wave state (as Δ varies) can be written as a vector in a 3-dimensional subspace with basis vectors:

$|1\rangle_d = \frac{1}{2}$ 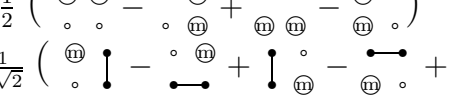

$|2\rangle_d = \frac{1}{2\sqrt{2}}$ 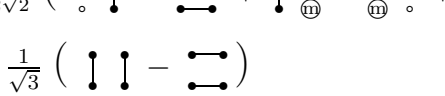

$|3\rangle_d = \frac{1}{\sqrt{3}}$ 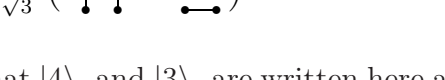

Note that $|4\rangle_s$ and $|3\rangle_d$ are written here as sums of *non-orthogonal* terms; however, this form makes their rotational symmetry readily apparent. The states $|4\rangle_s$ and $|3\rangle_d$ are the resonating valence bond (RVB) states for atoms on a single plaquette [83, 86], with s and d wave symmetries, respectively. For a larger lattice, the RVB states are in general superpositions of many different spin-singlet distribution patterns [90].

Thus the s-wave and d-wave ground states, respectively, are:

$$|\psi\rangle_s = s_1 |1\rangle_s + s_2 |2\rangle_s + s_3 |3\rangle_s + s_4 |4\rangle_s , \tag{5.5}$$

$$|\psi\rangle_d = d_1 |1\rangle_d + d_2 |2\rangle_d + d_3 |3\rangle_d , \tag{5.6}$$

They are superpositions of many different distribution patterns of the dressed molecules and the atomic valence bonds (spin singlets). The values of the superposition coefficients are shown in FIG. 5.3 as a function of the ratio $\Delta/|g|$. Note that in the limiting case $\Delta/|g| >> 1$, the effective Hamiltonian H_{eff} reduces to the t-J model [3]. Indeed, one can see from FIG. 5.3 that the state $|\psi\rangle_d$ in that limit tends

to the ground state $|3\rangle_d$ of the t-J model on a plaquette [83].

Projected onto these subspaces, H_{eff} (with $t_d \simeq 0$) expressed in terms of the bases shown above becomes:

$$H_s = \begin{pmatrix} 2\Delta & -2\sqrt{3}g & 0 & 0 \\ -2\sqrt{3}g & \Delta & \sqrt{2}\,(t_a + t_{da}) & -2g \\ 0 & \sqrt{2}\,(t_a + t_{da}) & \Delta & 0 \\ 0 & -2g & 0 & 0 \end{pmatrix} \tag{5.7}$$

for the s-wave state, and:

$$H_d = \begin{pmatrix} 2\Delta & -2g & 0 \\ -2g & \Delta & -2\sqrt{3}g \\ 0 & -2\sqrt{3}g & 0 \end{pmatrix} \tag{5.8}$$

for the d-wave state. The lowest energy eigenstates of these two Hamiltonians are the s-wave and d-wave states (respectively) of the full Hamiltonian H_{eff}. (See solid lines on FIG. 5.3.)

For a small portion of the range of the parameter values $t_{da}/|g|$ and $t_a/|g|$ there is an additional type of ground state, which occurs for Δ between the s-wave and d-wave states above. For this type, the ground state also has s-wave rotational symmetry. However, the states $\uparrow$ and $\downarrow$ are in a triplet configuration, rather than the singlet occurring in the other two types of states $|\psi\rangle_s$ and $|\psi\rangle_d$. The region of the parameter space for which this triplet phase occurs is shown in FIG. 5.4. The eigenenergies of the s-wave singlet, s-wave triplet, and d-wave singlet states are shown in FIG. 5.5(a) for $t_{da} = 2|g|$, $t_a = -0.3|g|$ (which is within the range where the triplet ground state occurs.) The gap between the ground state and first excited state for $t_{da} = 2|g|$, $t_a = -0.3|g|$ is shown in FIG. 5.5(b).

The s-wave triplet state can be written as a linear combination of three states:

$|1\rangle_{trip} = \frac{1}{2\sqrt{2}}$ 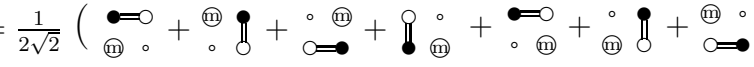

$|2\rangle_{trip} = \frac{1}{2}$ 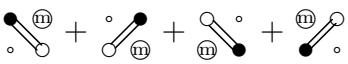

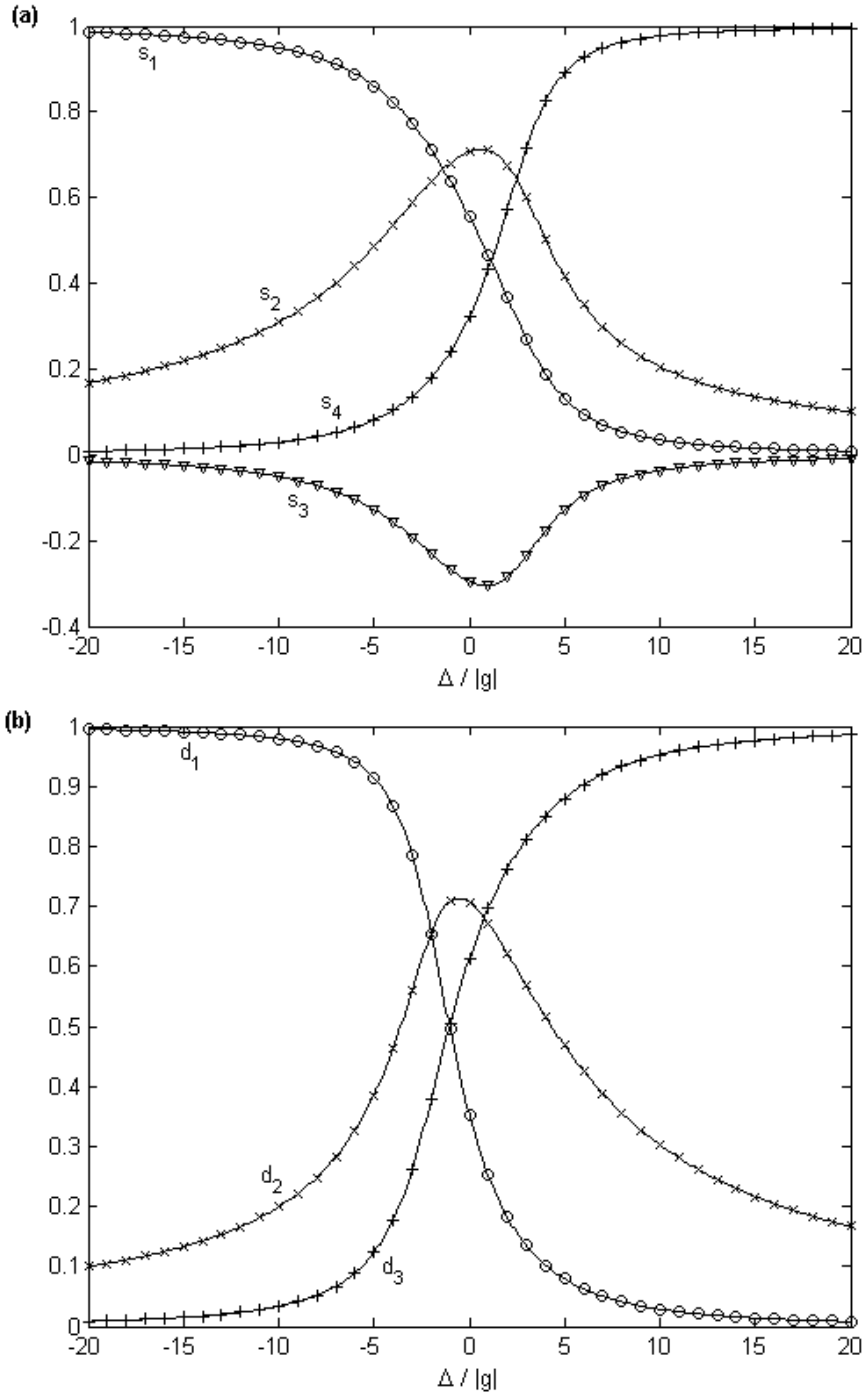

Figure 5.3: The ground-state configuration vs. the detuning Δ for a plaquette occupied by two $\uparrow$ and two $\downarrow$ atoms. ($t_{da} = 1.5|g|$, $t_a = -0.2|g|$, $t_d = 0$) (a) Components of the s-wave state (s_1: $\circ$, s_2: x, s_3: $\bigtriangledown$, s_4 : +). (b) Components of the d-wave state (d_1: $\circ$, d_2: x, d_3: +). The marked data points were computed from the full Hamiltonian H_{eff}, whereas the solid lines were computed from the projected Hamiltonians H_s and H_d, respectively.

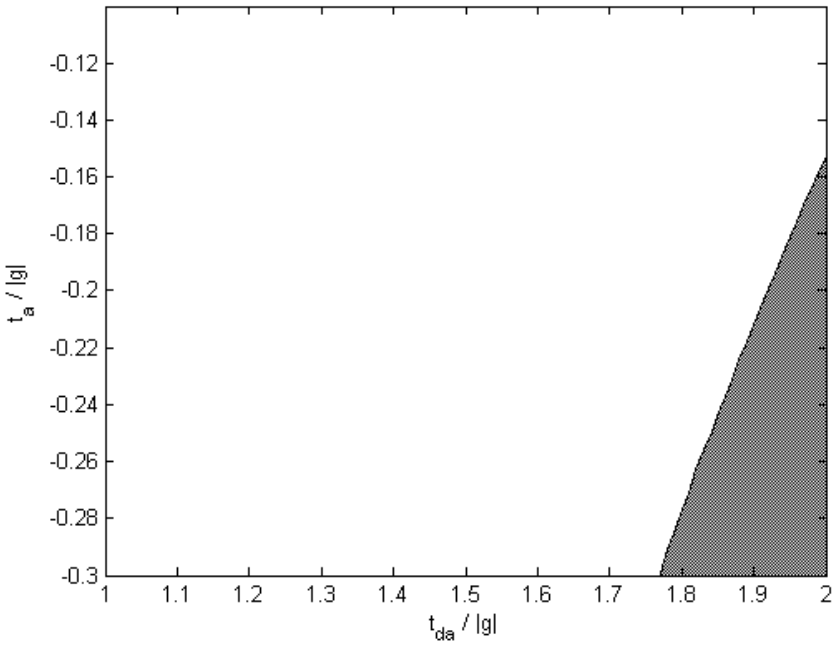

Figure 5.4: In the typical range of $t_{da}/|g|$ and $t_a/|g|$, the s-wave triplet ground state of the plaquette with 2 $\uparrow$ and 2 $\downarrow$ atoms occurs for parameter values within the shaded region.

$|3\rangle_{trip} = \frac{1}{2\sqrt{2}}$ ( )

Here represents the triplet $\frac{1}{\sqrt{2}}\left(a^\dagger_{i\uparrow}a^\dagger_{j\downarrow} + a^\dagger_{i\downarrow}a^\dagger_{j\uparrow}\right)$, where i is the site of the black-filled circle, and j is the site of the white-filled circle. Note that unlike the singlet, the triplet is not symmetric under exchange of i and j: $\frac{1}{\sqrt{2}}\left(a^\dagger_{i\uparrow}a^\dagger_{j\downarrow} + a^\dagger_{i\downarrow}a^\dagger_{j\uparrow}\right) = -\frac{1}{\sqrt{2}}\left(a^\dagger_{j\uparrow}a^\dagger_{i\downarrow} + a^\dagger_{j\downarrow}a^\dagger_{i\uparrow}\right)$

Projected onto the basis $\left\{|1\rangle_{trip}, |2\rangle_{trip}, |3\rangle_{trip}\right\}$, H_{eff} (with $t_d \simeq 0$) becomes:

$$H_{trip} = \begin{pmatrix} \Delta & \sqrt{2}\,(t_{da} - t_a) & -2\sqrt{2}g \\ \sqrt{2}\,(t_{da} - t_a) & \Delta & 0 \\ -2\sqrt{2}g & 0 & 0 \end{pmatrix} \tag{5.9}$$

and the ground state of this Hamiltonian is the s-wave triplet state. It should also be noted that the s-wave triplet state is the first excited state of H_{eff} in the limit of large positive Δ.

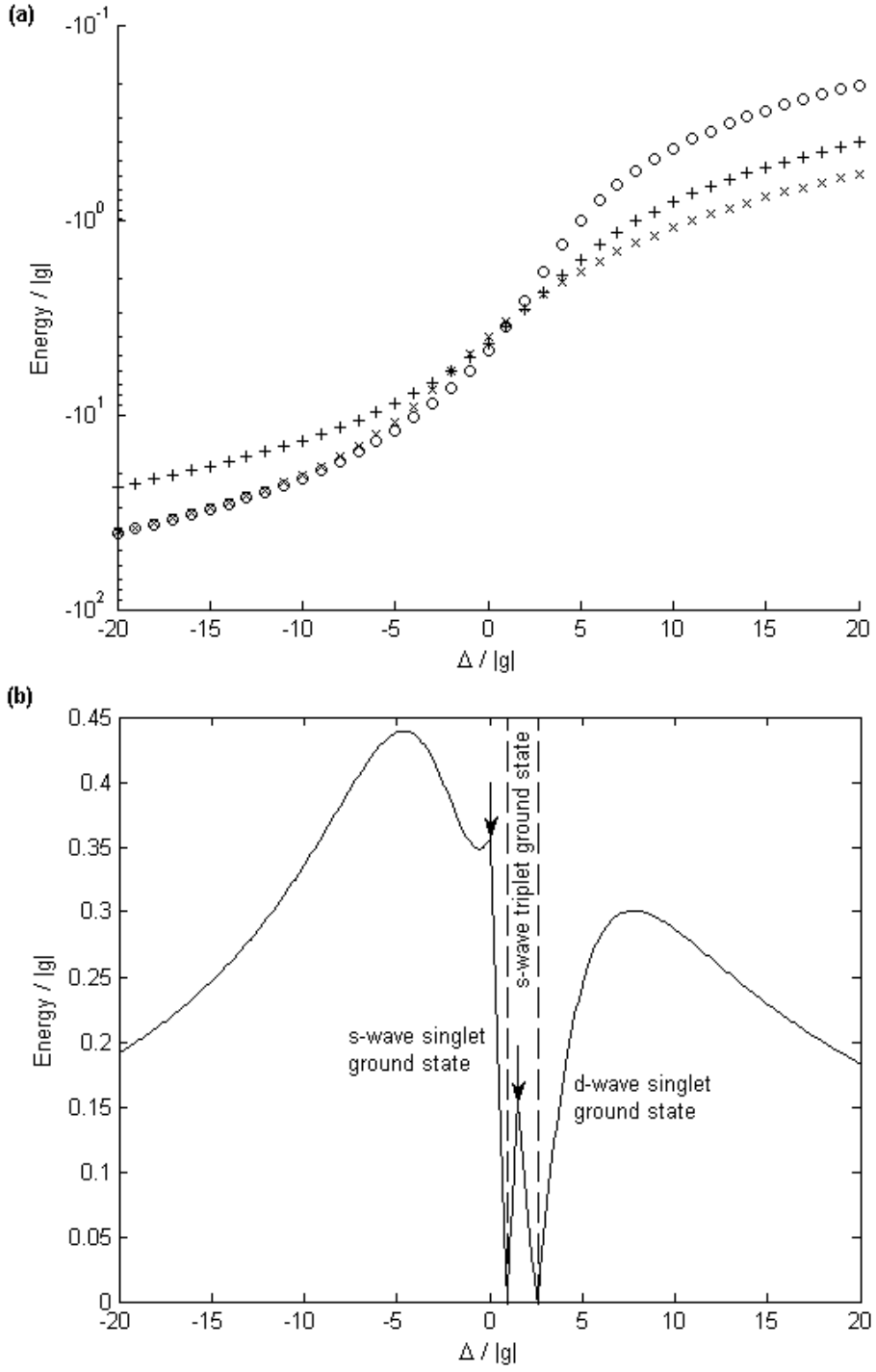

Figure 5.5: Energy vs. Δ for a plaquette occupied by two $\uparrow$ and two $\downarrow$ atoms. Other parameters are $t_{da} = 2|g|$, $t_a = -0.3|g|$, $t_d = 0$ (a): Eigenenergies of the s-wave singlet ($\circ$), d-wave singlet (x), and s-wave triplet (+) states. (b): Energy difference between ground state and first excited state. Crossovers in the first excited state are indicated by arrows.

5.4 Four atoms per plaquette: three ↑, one ↓

The plaquette occupied by three ↑ and one ↓ atoms has only one type of ground state over the full range of Δ. The ground state has s-wave symmetry (i.e. it is unchanged under 90° rotations in the plane of the lattice). The ground state energy is plotted in FIG. 5.6(a), and the energy difference between the ground state and the first excited state is shown in FIG. 5.6(b). For this figure the other parameters were $t_{da} = 1.5|g|$ and $t_a = -0.2|g|$.

The ground state can be represented compactly in the pictorial representation introduced above. Here we add an additional symbol to represent a single atom in the ↑ state. Because the order of the fermionic creation operators matters, we use ↑ to represent the left creation operator and ⇑ to represent the right creation operator. For instance, $\overset{\textcircled{m}}{\uparrow}\ \overset{\circ}{\Uparrow} = d_1^\dagger a_{3\uparrow}^\dagger a_{4\uparrow}^\dagger |0\rangle$, whereas $\overset{\textcircled{m}}{\Uparrow}\ \overset{\circ}{\uparrow} = d_1^\dagger a_{4\uparrow}^\dagger a_{3\uparrow}^\dagger |0\rangle$.

The ground state is: $|\psi\rangle_{\mathcal{S}} = C_1 |1\rangle_{\mathcal{S}} + C_2 |2\rangle_{\mathcal{S}} + C_3 |3\rangle_{\mathcal{S}}$, where

$|1\rangle_{\mathcal{S}} = \frac{1}{2\sqrt{2}} \left(\begin{smallmatrix} \textcircled{m} & \uparrow \\ \circ & \Uparrow \end{smallmatrix} + \begin{smallmatrix} \circ & \textcircled{m} \\ \Uparrow & \uparrow \end{smallmatrix} + \begin{smallmatrix} \Uparrow & \circ \\ \uparrow & \textcircled{m} \end{smallmatrix} + \begin{smallmatrix} \uparrow & \Uparrow \\ \textcircled{m} & \circ \end{smallmatrix} + \begin{smallmatrix} \circ & \uparrow \\ \textcircled{m} & \Uparrow \end{smallmatrix} + \begin{smallmatrix} \textcircled{m} & \circ \\ \Uparrow & \uparrow \end{smallmatrix} + \begin{smallmatrix} \Uparrow & \textcircled{m} \\ \uparrow & \circ \end{smallmatrix} + \begin{smallmatrix} \uparrow & \Uparrow \\ \circ & \textcircled{m} \end{smallmatrix} \right)$

$|2\rangle_{\mathcal{S}} = \frac{1}{2} \left(\begin{smallmatrix} \textcircled{m} & \uparrow \\ \Uparrow & \circ \end{smallmatrix} + \begin{smallmatrix} \Uparrow & \textcircled{m} \\ \circ & \uparrow \end{smallmatrix} + \begin{smallmatrix} \circ & \Uparrow \\ \uparrow & \textcircled{m} \end{smallmatrix} + \begin{smallmatrix} \uparrow & \circ \\ \textcircled{m} & \Uparrow \end{smallmatrix} \right)$

$|3\rangle_{\mathcal{S}} = \frac{1}{2\sqrt{2}} \left(\begin{smallmatrix} \bullet & \uparrow \\ \Uparrow & \end{smallmatrix} + \begin{smallmatrix} \bullet\!\!-\!\!\bullet & \\ \Uparrow & \uparrow \end{smallmatrix} + \begin{smallmatrix} \Uparrow & \bullet \\ \uparrow & \end{smallmatrix} + \begin{smallmatrix} \uparrow & \Uparrow \\ \bullet\!\!-\!\!\bullet & \end{smallmatrix} \right)$

The values of the coefficients C_1, C_2, C_3 are shown in FIG. 5.7.

Projected onto the three-dimensional subspace of the full Hilbert space with basis vectors $|1\rangle_{\mathcal{S}}$, $|2\rangle_{\mathcal{S}}$, $|3\rangle_{\mathcal{S}}$, H_{eff} (for $t_d \simeq 0$) is:

$$H_{\mathcal{S}} = \begin{pmatrix} \Delta & \sqrt{2}\,(t_a - t_{da}) & -2\sqrt{2}g \\ \sqrt{2}\,(t_a - t_{da}) & \Delta & 0 \\ -2\sqrt{2}g & 0 & 0 \end{pmatrix} \tag{5.10}$$

Thus, the ground state of this Hamiltonian is the ground state of H_{eff}. (See solid lines in FIG. 5.7.)

It should also be noted that the s-wave ground state for 3 ↑, 1 ↓ atoms per plaquette is degenerate with the triplet state for 2 ↑ and 2 ↓ atoms described in

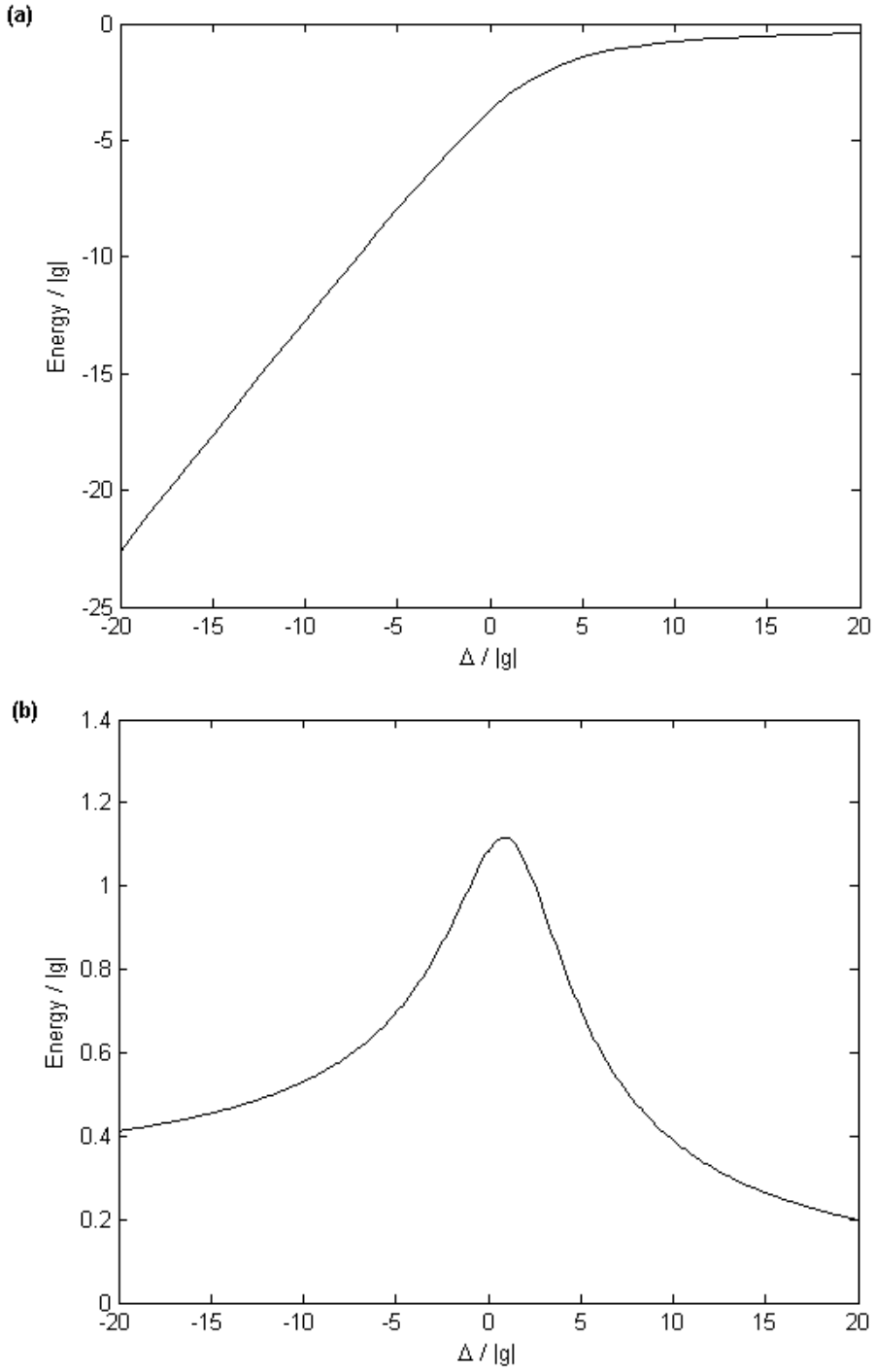

Figure 5.6: Energy vs. Δ for a plaquette occupied by three $\uparrow$ and one $\downarrow$ atoms. Other parameters are $t_{da} = 1.5|g|$, $t_a = -0.2|g|$, $t_d = 0$ (a): Ground state energy. (b): Energy difference between ground state and first excited state.

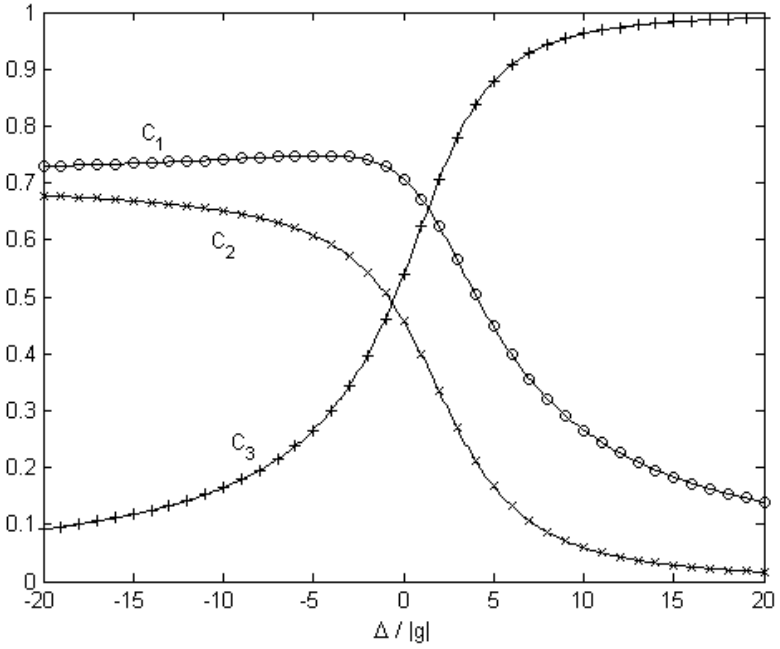

Figure 5.7: Components of the ground state (C_1: $\circ$, C_2: x, C_3: $+$) vs. Δ for a plaquette occupied by three $\uparrow$ and one $\downarrow$ atoms. ($t_{da} = 1.5|g|$, $t_a = -0.2|g|$, $t_d = 0$) The marked datapoints were computed from the full Hamiltonian H_{eff}, whereas the solid lines were computed from the projected Hamiltonian $H_{\mathcal{S}}$.

the previous section. In fact, the 2 $\uparrow$, 2 $\downarrow$ triplet state is identical to the ground state for 3 $\uparrow$ and 1 $\downarrow$ atoms and for 1 $\uparrow$ and 3 $\downarrow$ atoms, except that the triplet $\frac{1}{\sqrt{2}}\left(a^\dagger_{i\uparrow}a^\dagger_{j\downarrow} + a^\dagger_{i\downarrow}a^\dagger_{j\uparrow}\right)$ is replaced with $a^\dagger_{i\uparrow}a^\dagger_{j\uparrow}$ in the 3 $\uparrow$, 1 $\downarrow$ case, and with $a^\dagger_{i\downarrow}a^\dagger_{j\downarrow}$ in the 1 $\uparrow$, 3 $\downarrow$ case.

5.5 Two atoms per plaquette: one $\uparrow$, one $\downarrow$

When occupied by only a single atom of each spin state, the plaquette has a single type of ground state for all values of Δ (for values of the other parameters within the typical range). This state is symmetric under 90° rotations – i.e., it has s-wave symmetry. The ground state energy of this system is plotted in figure 5.8(a). Figure 5.8(b) shows the excitation gap between the ground state and first excited state. Both these figures assume typical values of t_{da} and t_a ($t_{da} = 1.5|g|$, $t_a = -0.2|g|$).

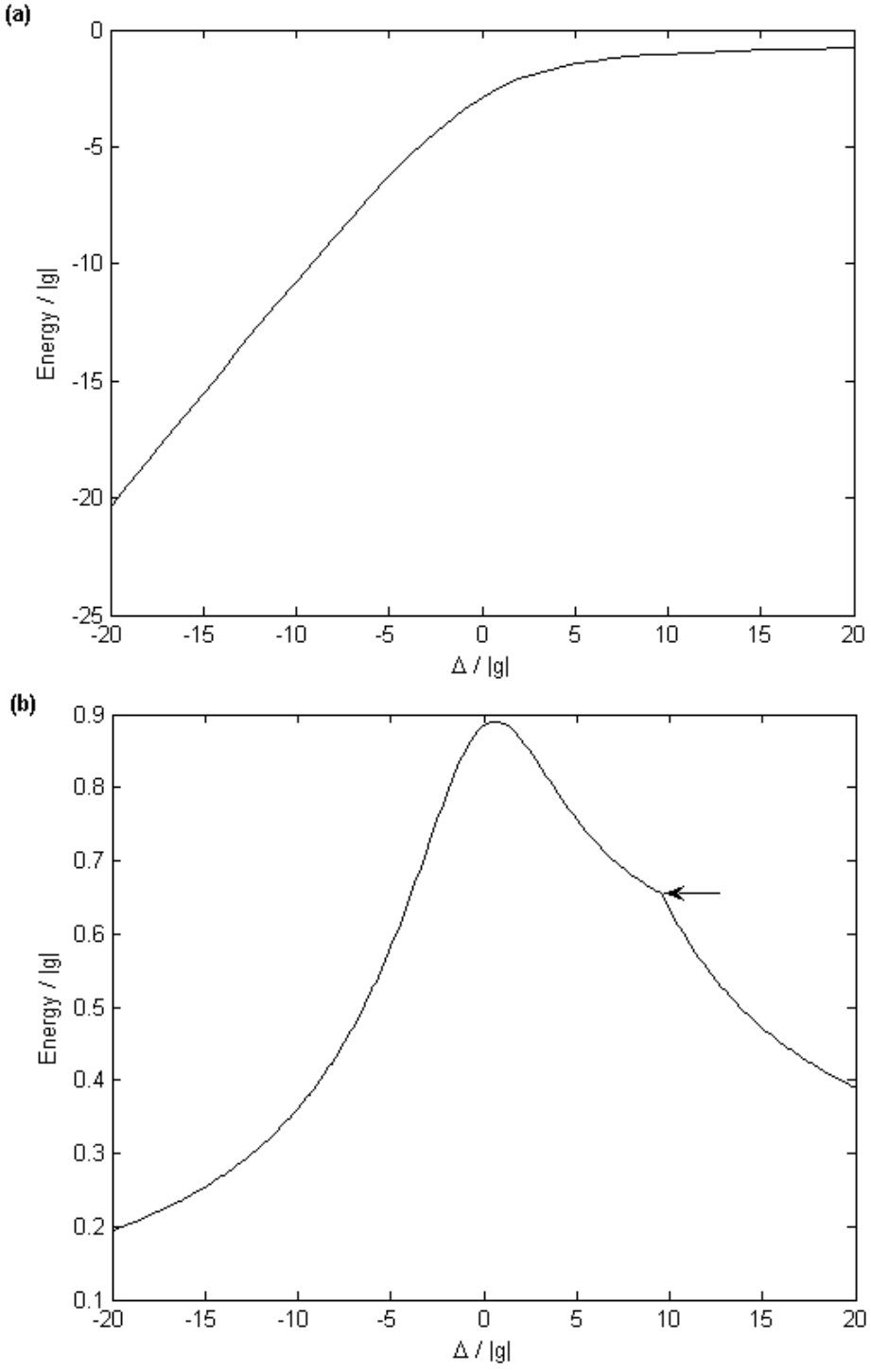

Figure 5.8: Energy vs. Δ for a plaquette occupied by one $\uparrow$ and one $\downarrow$ atom. ($t_{da} = 1.5|g|$, $t_a = -0.2|g|$, $t_d = 0$.) (a): Ground state energy (b): Energy difference between ground state and first excited state. The curve is smooth except at a crossover in the first excited state (indicated by an arrow).

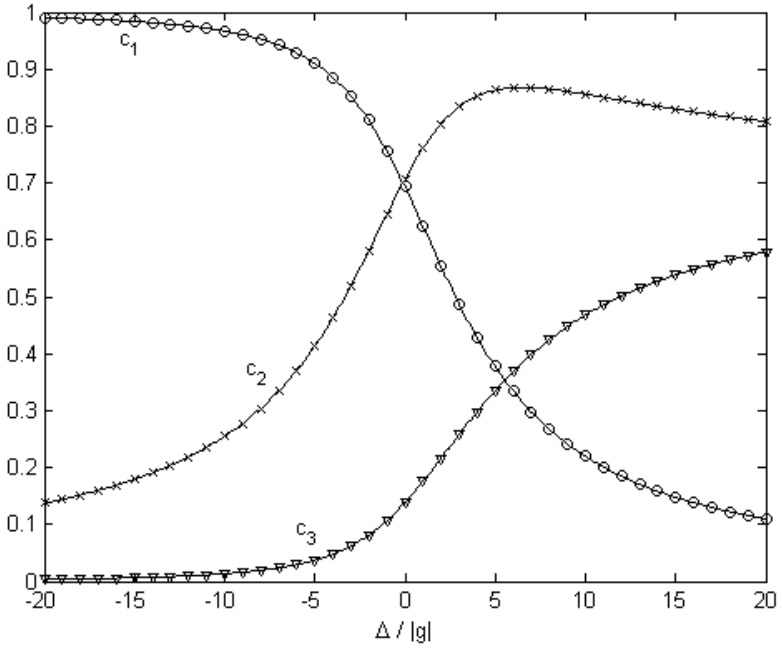

Figure 5.9: Components of the ground state (c_1: $\circ$, c_2: x, c_3: $\triangledown$) vs. Δ for a plaquette occupied by one $\uparrow$ and one $\downarrow$ atom. ($t_{da} = 1.5|g|$, $t_a = -0.2|g|$, $t_d = 0$) The marked datapoints were computed from the full Hamiltonian H_{eff}, whereas the solid lines were computed from the projected Hamiltonian H.

The ground state can be expressed as a vector in a 3-dimensional subspace of the full Hilbert space. The basis vectors of this subspace (in the pictorial representation introduced above) are:

$|1\rangle = \frac{1}{2}\Big($ 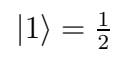 $+$ 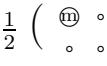 $+$ 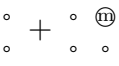 $+$ 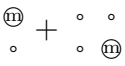 $\Big)$

$|2\rangle = \frac{1}{2}\Big($ 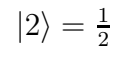 $+$ 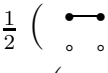 $+$ 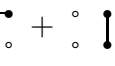 $+$ 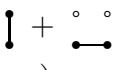 $\Big)$

$|3\rangle = \frac{1}{\sqrt{2}}\Big($ 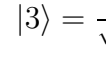 $+$ 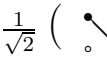 $\Big)$

Thus, the ground state is given by: $|\psi\rangle = c_1 |1\rangle + c_2 |2\rangle + c_3 |3\rangle$, where the values of the coefficients c_1, c_2, c_3 are shown in FIG. 5.9

Projected onto this subspace, H_{eff} (for $t_d \simeq 0$) expressed in the above basis

becomes:

$$H = \begin{pmatrix} \Delta & -2\sqrt{2}g & 0 \\ -2\sqrt{2}g & 0 & 2\sqrt{2}t_a \\ 0 & 2\sqrt{2}t_a & 0 \end{pmatrix} \tag{5.11}$$

Thus, the ground state of this Hamiltonian is the ground state of H_{eff}. (See solid lines on FIG. 5.9.)

5.6 Three atoms per plaquette:two ↑, one ↓

The plaquette with two ↑ atoms and one ↓ atom has three distinct types of ground states for different values of the parameter Δ (with the other parameters in the typical range). However, over a wide range of Δ around $\Delta = 0$ the system is in the same type of ground state. The ground state of this type is two-fold degenerate. (Hence, we will refer to this as the "degenerate state".) The ground state energy and the gap between the ground state and first excited state are shown in FIG. 5.10. (For the full range of Δ values shown in the figure, the system is in the degenerate state.) The degenerate ground states (which we call $|\psi\rangle_+$ and $|\psi\rangle_-$) can be defined in such a way that they are eigenstates of a 90° rotation in the plane of the plaquette, in which case $|\psi\rangle_\pm$ gains a factor of $\pm i$ under such a rotation.

The state $|\psi\rangle_+$ can be expressed as a vector in a particular six-dimensional subspace of the full Hilbert space. We define the basis vectors of this subspace in the pictorial representation introduced above. However, because the order of the fermionic creation operators matters, we use three symbols ↑, ⇑, ∧ (↓, ⇓, ∨) to represent the first, second, and third creation operator for atoms in the ↑ (↓) state. E.g., $\begin{smallmatrix} \wedge & \circ \\ \Downarrow & \uparrow \end{smallmatrix} = a^\dagger_{4\uparrow} a^\dagger_{3\downarrow} a^\dagger_{1\uparrow} |0\rangle$. Represented in this way, the six basis vectors are:

$|1\rangle_+ = \frac{1}{2}\Big[\Big(\begin{smallmatrix} ⓜ & \uparrow \\ \circ & \circ \end{smallmatrix} - \begin{smallmatrix} \circ & \circ \\ \uparrow & ⓜ \end{smallmatrix}\Big) - i\Big(\begin{smallmatrix} \circ & ⓜ \\ \circ & \uparrow \end{smallmatrix} - \begin{smallmatrix} \uparrow & \circ \\ ⓜ & \circ \end{smallmatrix}\Big)\Big]$

$|2\rangle_+ = \frac{1}{2}\Big[\Big(\begin{smallmatrix} \uparrow & ⓜ \\ \circ & \circ \end{smallmatrix} - \begin{smallmatrix} \circ & \circ \\ ⓜ & \uparrow \end{smallmatrix}\Big) - i\Big(\begin{smallmatrix} \circ & \uparrow \\ \circ & ⓜ \end{smallmatrix} - \begin{smallmatrix} ⓜ & \circ \\ \uparrow & \circ \end{smallmatrix}\Big)\Big]$

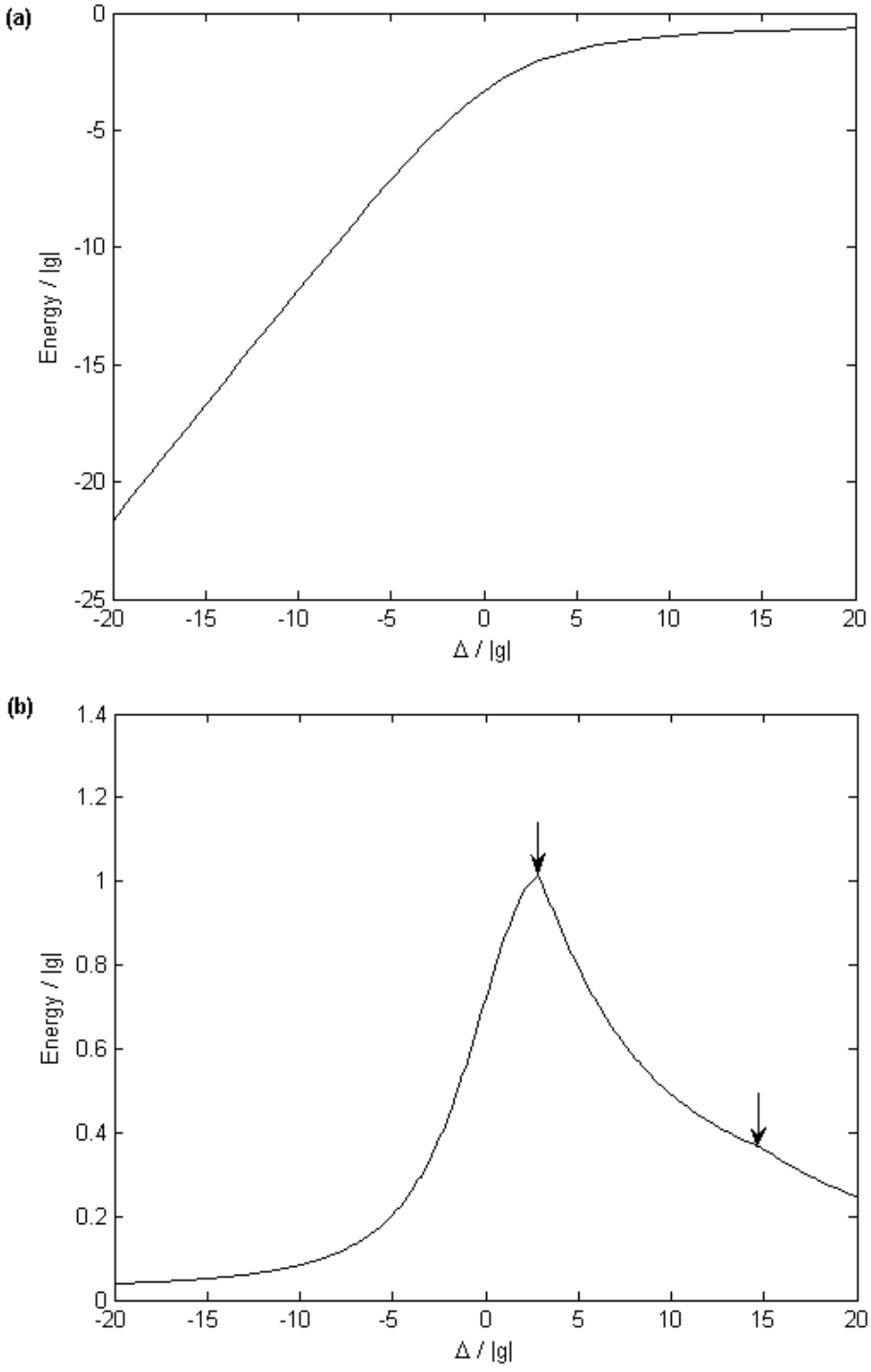

Figure 5.10: Energy vs. Δ for a plaquette occupied by two $\uparrow$ and one $\downarrow$ atoms. ($t_{da} = 1.5|g|$, $t_a = -0.2|g|$, $t_d = 0$) (a): Ground state energy (b): Energy difference between ground state and first excited state. Crossovers in the first excited state (at which points the curve is not smooth) are indicated by arrows.

$$|3\rangle_+ = \tfrac{1}{2}\Big[\Big(\begin{smallmatrix}\ominus & \circ\\ \circ & \uparrow\end{smallmatrix} \begin{smallmatrix}-\uparrow & \circ\\ \circ & \ominus\end{smallmatrix}\Big) - i\Big(\begin{smallmatrix}\circ & \ominus\\ \uparrow & \circ\end{smallmatrix} \begin{smallmatrix}-\circ & \uparrow\\ \ominus & \circ\end{smallmatrix}\Big)\Big]$$

$$|4\rangle_+ = \tfrac{1}{2}\Big[\Big(\begin{smallmatrix}\uparrow & \Downarrow\\ \circ & \wedge\end{smallmatrix} \begin{smallmatrix}-\wedge & \circ\\ \Downarrow & \uparrow\end{smallmatrix}\Big) - i\Big(\begin{smallmatrix}\circ & \uparrow\\ \wedge & \Downarrow\end{smallmatrix} \begin{smallmatrix}-\Downarrow & \wedge\\ \uparrow & \circ\end{smallmatrix}\Big)\Big]$$

$$|5\rangle_+ = \tfrac{1}{2}\Big[\Big(\begin{smallmatrix}\downarrow & \Uparrow\\ \circ & \wedge\end{smallmatrix} \begin{smallmatrix}-\wedge & \circ\\ \Uparrow & \downarrow\end{smallmatrix}\Big) - i\Big(\begin{smallmatrix}\circ & \downarrow\\ \wedge & \Uparrow\end{smallmatrix} \begin{smallmatrix}-\Uparrow & \wedge\\ \downarrow & \circ\end{smallmatrix}\Big)\Big]$$

$$|6\rangle_+ = \tfrac{1}{2}\Big[\Big(\begin{smallmatrix}\Uparrow & \vee\\ \uparrow & \circ\end{smallmatrix} \begin{smallmatrix}-\circ & \uparrow\\ \vee & \Uparrow\end{smallmatrix}\Big) - i\Big(\begin{smallmatrix}\uparrow & \Uparrow\\ \circ & \vee\end{smallmatrix} \begin{smallmatrix}-\vee & \circ\\ \Uparrow & \uparrow\end{smallmatrix}\Big)\Big]$$

and the state $|\psi\rangle_+$ is given by:

$$\begin{aligned} |\psi\rangle_+ &= A\,|1\rangle_+ + A^*\,|2\rangle_+ + B\,|3\rangle_+ + C\,|4\rangle_+ \\ &\quad + D\,|5\rangle_+ + D^*\,|6\rangle_+ \end{aligned} \tag{5.12}$$

for some complex coefficients A, B, C, and D. Note that under a 90° clockwise rotation $|n\rangle_+ \to i\,|n\rangle_+$ for each n, and thus $|\psi\rangle_+ \to i\,|\psi\rangle_+$. The state $|\psi\rangle_-$ can be expressed as a vector in a six-dimensional subspace of the full Hilbert space with basis vectors

$$|n\rangle_- = |n\rangle_+^* \tag{5.13}$$

for $n = 1, ..., 6$. $|\psi\rangle_-$ is given by:

$$\begin{aligned} |\psi\rangle_- &= A^*\,|1\rangle_- + A\,|2\rangle_- + B^*\,|3\rangle_- + C^*\,|4\rangle_- \\ &\quad + D^*\,|5\rangle_- + D\,|6\rangle_- = |\psi\rangle_+^* \end{aligned} \tag{5.14}$$

The complex coefficients A, B, C, and D can be written as:

$$\begin{aligned} A &= |A|\,e^{i\phi_A},\ D = |D|\,e^{i\phi_D} \\ B &= |B|\,e^{i\pi/4},\ C = |C|\,e^{i\pi/4} \end{aligned} \tag{5.15}$$

where $|A|$, $|B|$, $|C|$, $|D|$, ϕ_A, and ϕ_D depend on the parameters of H_{eff}. The coefficients are determined up to an arbitrary overall phase, which here was chosen to fix the phases of B and C as shown. (B and C were found to have the same phase.)

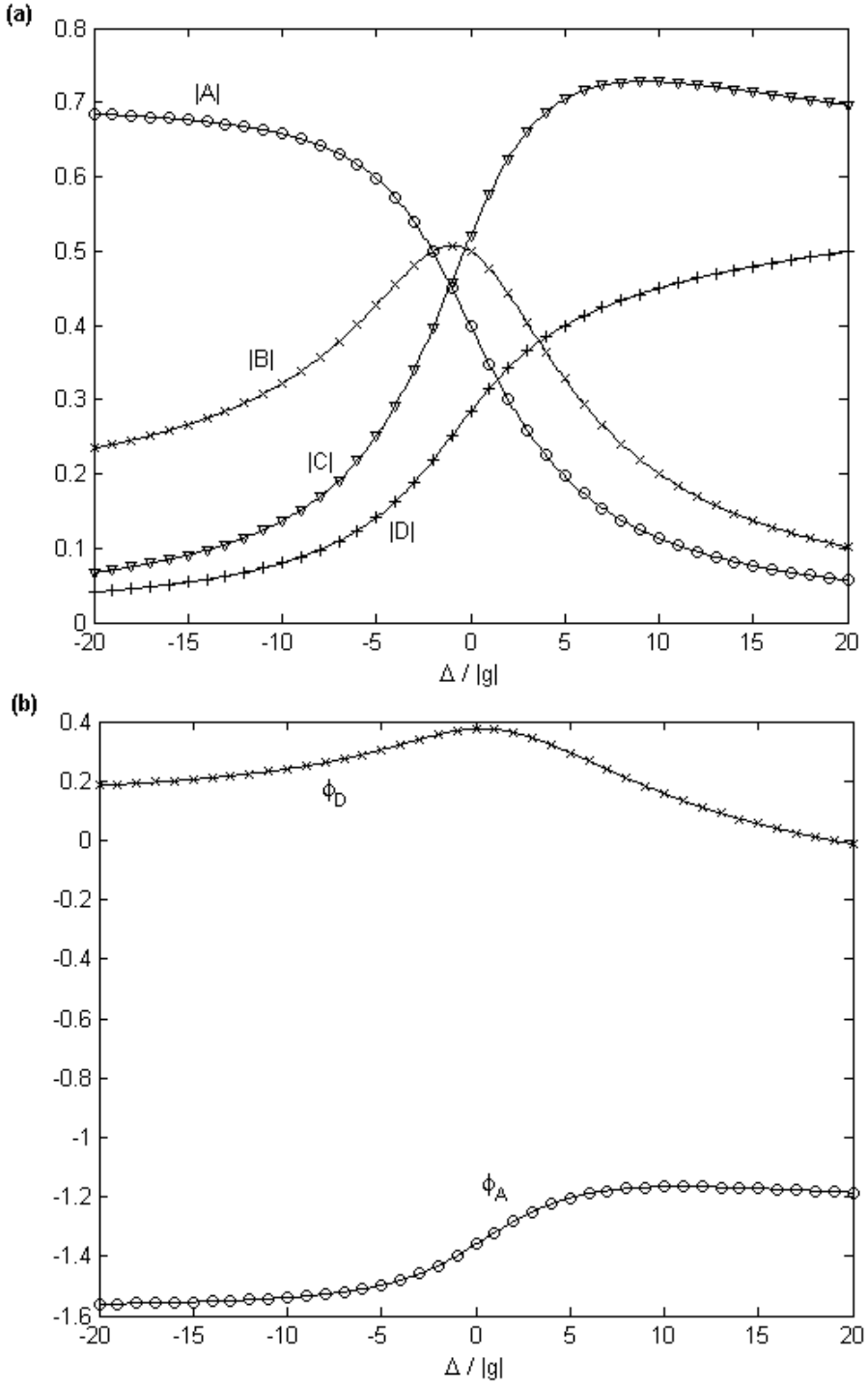

Figure 5.11: Ground state parameters vs. Δ for a plaquette occupied by two $\uparrow$ and one $\downarrow$ atoms. ($t_{da} = 1.5|g|$, $t_a = -0.2|g|$, $t_d = 0$) (a): Amplitudes ($|A|$: $\circ$, $|B|$: x, $|C|$: $\bigtriangledown$, $|D|$: +). (b): Phases (ϕ_A: $\circ$, ϕ_D: x). The overall phase was chosen to give $B = |B|\, e^{i\pi/4}$ and $C = |C|\, e^{i\pi/4}$. The marked datapoints on (a) and (b) were computed from the full Hamiltonian H_{eff}, whereas the solid lines were computed from the projected Hamiltonian H_+.

For typical values of $t_a = -0.2|g|$, $t_{da} = 1.5|g|$, $t_d = 0$, the values of these parameters (vs. Δ) are shown in FIG. 5.11.

Projected onto the subspace with basis $\{|1\rangle_+, |2\rangle_+, |3\rangle_+, |4\rangle_+, |5\rangle_+, |6\rangle_+\}$, H_{eff} (expressed in that basis) is (for $t_d \simeq 0$):

$$H_+ = \begin{pmatrix} \Delta & t_{da} & t_a & -ig & ig & 0 \\ t_{da} & \Delta & -it_a & g & 0 & ig \\ t_a & it_a & \Delta & -2g & g & -ig \\ ig & g & -2g & 0 & -it_a & t_a \\ -ig & 0 & g & it_a & 0 & -t_a \\ 0 & -ig & ig & t_a & -t_a & 0 \end{pmatrix} \tag{5.16}$$

The ground state of H_+ is thus $|\psi\rangle_+$. (See solid lines in FIG. 5.11.) Projected onto the subspace with basis $\{|1\rangle_-, |2\rangle_-, |3\rangle_-, |4\rangle_-, |5\rangle_-, |6\rangle_-\}$, H_{eff} is given by:

$$H_- = H_+^* = H_+^T \tag{5.17}$$

(Note that in this equation H_+ is still expressed in the basis in which it was defined above.) Thus the ground state of H_- is $|\psi\rangle_+^* = |\psi\rangle_-$.

For Δ far to the negative side ($\Delta < -92.9\,|g|$ for $t_{da} = 1.5|g|$, $t_a = -0.2|g|$, $t_d = 0$), the system of two $\uparrow$ atoms and one $\downarrow$ atom on a plaquette has a non-degenerate d-wave ground state. This state can be expressed as a vector in a 3-dimensional subspace of the full Hilbert space of this system, with basis vectors:

$|1\rangle_{left} = \frac{1}{2\sqrt{2}}$ 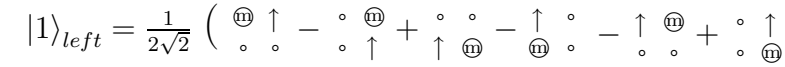

$|2\rangle_{left} = \frac{1}{2}$ 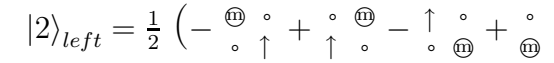

$|3\rangle_{left} = \frac{1}{2}$ 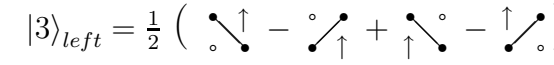

$= \frac{1}{2}$ 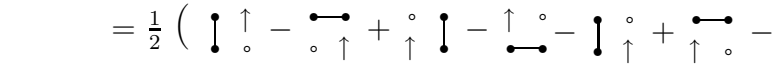

Note that there is some ambiguity in which spins to group into a singlet and which to write as $\uparrow$, as evidenced by the two forms given for $|3\rangle_{left}$ (the first of which has the advantage of all its terms being orthogonal, but the second of which makes more obvious how the Hamiltonian connects it to components $|1\rangle_{left}$ and $|2\rangle_{left}$).

H_{eff} (for $t_d \simeq 0$) projected onto this subspace expressed in the basis $\left\{|1\rangle_{left}, |2\rangle_{left}, |3\rangle_{left}\right\}$ is:

$$H_{left} = \begin{pmatrix} \Delta - t_{da} & -\sqrt{2}t_a & -g \\ -\sqrt{2}t_a & \Delta & -\sqrt{2}g \\ -g & -\sqrt{2}g & t_a \end{pmatrix} \tag{5.18}$$

Thus, the ground state of this Hamiltonian is the ground state of H_{eff} in the left-most region ($\Delta < -92.9\,|g|$).

For Δ far to the positive side ($\Delta > 97.9\,|g|$ for $t_{da} = 1.5|g|$, $t_a = -0.2|g|$, $t_d = 0$), the system has a non-degenerate s-wave ground state. Furthermore, in this state the ground state wavefunction and energy are constant for changing Δ. In the pictorial representation this ground state is given by:

$|\psi\rangle_{right} = \frac{1}{2\sqrt{6}}$ 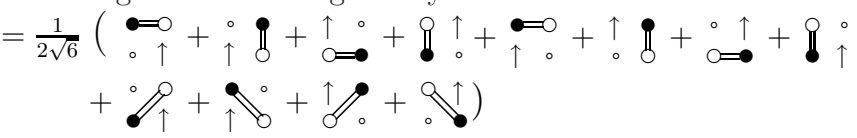

The energy of this state is $H_{right} = 2t_a$.

It should be noted that the case of 1 $\uparrow$, 2 $\downarrow$ atoms on a plaquette is equivalent to the 2 $\uparrow$, 1 $\downarrow$ case under exchange of $\uparrow$ and $\downarrow$ spins. The Hamiltonian H_{eff} is invariant under such a spin exchange, except for a change in the sign of g. This is equivalent to replacing $d^\dagger$ with $-d^\dagger$. Thus, the eigenenergies of these two cases are identical, and the eigenstates are identical except for a change in the sign of the components which include a dressed molecule.

5.7 Summary and discussion

In the above, we have investigated the ground state properties of the system with different numbers of spin ↑ and ↓ atoms occupying the four-site plaquette in an optical superlattice. All the other cases can be reduced to one of the configurations considered above, or to a trivial case, through the particle-hole exchange. (Cases where all particles are in the same spin state are non-interacting, and thus trivial.) For instance, for five atoms with three spin-↓ and two spin-↑, one has two spin-↑ and one spin-↓ holes in that plaquette. So, the states are equivalent to those in the case with two spin-↑ and one spin-↓ atoms, but with exchange of the parameters t_{da} and t_a in the effective Hamiltonian H_{eff}. The sign of g also changes, but as noted above this is equivalent to replacing $d^\dagger$ with $-d^\dagger$. Thus this change has no effect on the eigenenergies, and the eigenstates only experience a change in the sign of those components where the plaquette is occupied by an odd number of dressed molecules. In addition, if particle-hole exchange changes the number of atoms by N, then the eigenenergies are shifted by $\frac{N}{2}\Delta$.

From this investigation, we have seen that even on a single plaquette, the Hamiltonian H_{eff} exhibits a number of different types of ground state configurations, possessing various forms of rotational symmetry (s-wave, d-wave, etc.). There are level crossings between these different types of ground states as the detuning Δ is varied. The change of the ground state symmetry from s-wave to d-wave as one scans the parameter Δ from negative to positive regions may be a general feature and not limited to a single plaquette. For a large lattice, this symmetry change might correspond to a quantum phase transition from the s-wave to the d-wave superfluidities (for a review, see Ref. [50]). The states found in this work on a single plaque-

tte also can be used to construct the zeroth-order eigenstates for a lattice of many weakly coupled plaquettes, where the interaction between plaquettes can be treated perturbatively (as discussed in the next chapter). These states also provide some basic entries for constructing the effective many-body Hamiltonian for atoms in a quasi-two-dimensional optical lattice through the contractor renormalization method [85, 86]. When the average filling number of the lattice is close to a half with hole doping, one expects that the basic degrees of freedom from each plaquette are the ground state configurations specified in Sec. II, the fermionic hole excitations given by the states in Sec. V, the bosonic hole-pair excitations specified in Sec. IV, and the bosonic spin excitations given by the states in Sec. III and II. The effective many-body Hamiltonian will then describe the interaction between these basic degrees of freedom. So, it is our hope that the investigation of the single-plaquette physics here will make it possible to better understand the physics of strongly interacting fermions on larger lattices.

CHAPTER VI

d-wave Superfluidity in the Generalized Hubbard Model with Weakly Coupled Plaquettes

In the previous chapters we have shown how strongly-interacting fermions in an optical lattice, under typical experimental conditions, can be described by a generalized Hubbard model (GHM) which includes correlated tunneling. Because the strong interactions make the many-body physics difficult to determine, we have first focused on simpler cases, such as with the particles allowed to interact only within clusters of a few neighboring lattice sites. However, the most interesting questions about this model require us to consider interactions among all the lattices sites. In particular, there has been substantial interest in the question of whether the Hubbard model captures the essentially physics of the high-T_c superconducting cuprates.[90–94] The generalized Hubbard model has also been studied in the context of high-T_c superconductivity [33–36], and of course it includes the ordinary Hubbard model as a special case.

Since the discovery that the excitation gap of the high-T_c superconductors possesses d-wave rotational symmetry[78–81], there has been much interest in whether the Hubbard model supports a d-wave superfluid state.[93, 95–98] Dynamic mean field theory applied to finite clusters provides numerical evidence of a d-wave ground-state for the Hubbard model with a small hole doping.[93] However, density matrix

renormalization group calculations for coupled chains in the same parameter regime indicate a striped groundstate.[94] (The striped state is characterized by spatially modulated expectation values of the hole density $h(x) = \sum_y (1 - \langle n(x,y)\rangle)$ and staggered spin density $s(x) = \sum_y (-1)^{x+y} \langle n_\uparrow(x,y) - n_\downarrow(x,y)\rangle$.) This apparent discrepancy has been taken as evidence that the low energy eigenstates of the Hubbard model include nearly-degenerate d-wave superfluid states and striped states, with the subtle biases of these different numerical methods pushing the result one way or another.[40]

While one could attempt to similarly apply these sophisticated numerical methods to the generalized Hubbard model, we expect that the determination of the groundstate would be likewise sensitive to the choice of which algorithm we use. In principle, it is possible that the presence of the correlated tunneling terms in the GHM might break the near-degeneracy between stripes and d-wave superfluidity, but this is difficult to assess especially without yet knowing how large the correlated hopping terms are in typical experiments. Here we choose instead to focus on a substantially simpler problem, that of an inhomogeneous GHM, where the tunneling rate between plaquettes is much less than the tunneling rate within a plaquette. In the following, we will refer to this case as the plaquettized generalized Hubbard model (PGHM).

6.1 Why Study the Plaquettized GHM?

There are several reasons for considering such a model. First, when the interplaquette tunneling rates are much smaller than the intraplaquette tunneling, it is possible to study the system by the usual methods of degenerate perturbation theory, with the terms of the Hamiltonian that couple different plaquettes serving as the perturbation. Second, the zeroth order eigenstates are just tensor products of

the single-plaquette states, which we determined in the previous chapter. As we saw, there is a region of the parameter space in which the groundstate of the half-filled $(2\uparrow, 2\downarrow)$ plaquettes has d-wave rotational symmetry, but that of the quarter-filled $(1\uparrow, 1\downarrow)$ plaquettes has s-wave symmetry. This means that the hole-pair creation operator that takes the half-filled state to the quarter-filled state must have d-wave symmetry, so that under rotation the hole-pair creation operator produces a factor of -1 to cancel that produced by the half-filled plaquette state.[99]

The significance of this is that we can re-express the PGHM in terms of plaquette excitations, such that a single "site" in this new formulation is one plaquette in the original formulation, and likewise the new "particles" are the excitations between the plaquette states. (To avoid confusion between these two formulations, we will use the subscript P to denote "particles" that are in fact plaquette excitations.) Of course there are many such plaquette states. By keeping only the low-energy states, we produce a Hamiltonian which describes the low-energy effective field theory of the PGHM. As we will see, this Hamiltonian somewhat resembles the original GHM, but with the key difference that it includes bosonic particles with d-wave symmetry (namely the aforementioned hole-pair excitations). Demonstrating d-wave superfluidity in this model is thus as simple as demonstrating that these bosons condense, since such a condensate inherits the d-wave symmetry of the bosons themselves. (In contrast, note that none of the particles in the original GHM possessed d-wave symmetry individually. In fact, the four-site plaquette is the minimal configuration which can support a d-wave state of such particles.)

One additional reason for our interest in the plaquettized GHM is that this configuration can be readily achieved using an optical superlattice. As we saw in previous chapters, the superlattice allows us to create a pattern of alternating high and low

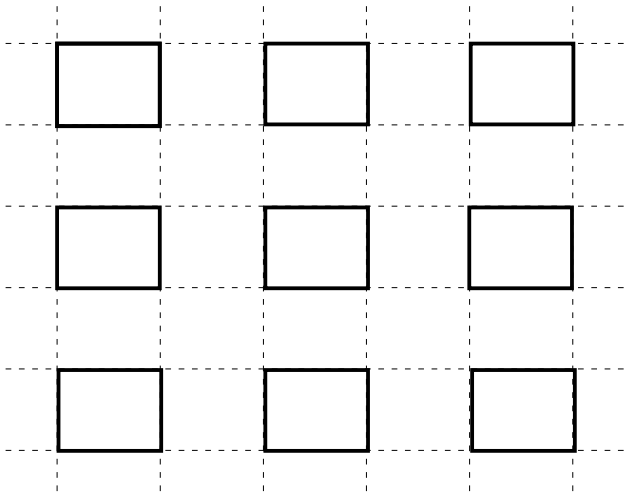

Figure 6.1: Configuration of weakly interacting plaquettes in an optical superlattice. The vertices represent lattice sites, the solid lines represent low potential barriers, and the dotted lines represent high potential barriers.

barriers, with the ability to adjust either barrier height. By applying such a superlattice in two dimensions, with a deep lattice in the third dimension, we can restrict the atoms to move within a two-dimensional plane, with the difference in barrier heights meaning that intra-plaquette couplings are much stronger than couplings between plaquettes. (See figure 6.1) The use of a superlattice in this way is the basis of a recent proposal to create a d-wave superfluid.[100] That work treats the Hamiltonian as a plaquettized version of the standard (non-generalized) Hubbard model, which is valid far from resonance. The plaquettized Hubbard model has also been examined in several recent papers by Kivelson et al.[101–104]

Our work below in particular follows the approach of reference [101], except that here we consider the generalized Hubbard model, while that reference examines the usual ungeneralized version. (Note however that most of this work preceded the erratum [102], which was prompted in part by our private correspondence regarding these results.)

It is true that a d-wave superfluid state can be obtained from the plaquettized Hubbard model. As we will see, this is also true for the PGHM (which includes correlated tunneling terms), However in both the generalized and ungeneralized case this state has a significant difference from the sort of d-wave superfluid state that occurs in high-T_c superconductors, namely that the plaquettized Hubbard model does not support nodal quasiparticles.[102] We will elaborate on this point below, after first discussing the application of perturbation theory to the PGHM.

6.2 Perturbation Theory and the Plaquettized GHM

For fermions near a Feshbach resonance loaded in an optical superlattice such that couplings between plaquettes are suppressed, we have a Hamiltonian similar to the generalized Hubbard model (GHM):

$$\begin{aligned} H = &- \sum_{\langle i,j\rangle,\sigma} \left[t_{a,\langle i,j\rangle} - g_{1,\langle i,j\rangle} \left(n_{i\bar{\sigma}} + n_{j\bar{\sigma}} \right) - g_{2,\langle i,j\rangle} n_{i\bar{\sigma}} n_{j\bar{\sigma}} \right] a^{\dagger}_{i\sigma} a_{j\sigma} + \text{H.c.} \\ &+ \sum_i \Delta n_{i\uparrow} n_{i\downarrow} - \mu \left(n_{i\uparrow} + n_{i\uparrow} \right) \end{aligned} \tag{6.1}$$

The only difference between this plaquettized GHM (PGHM) and the GHM is that the coefficients t_a, g_1, and g_2 all now depend on the particular choice of neighboring sites $\langle i, j\rangle$. In particular, for the PGHM we have $t_{a,\langle i,j\rangle} = t_a$, $g_{1,\langle i,j\rangle} = g_1$ and $g_{2,\langle i,j\rangle} = g_2$ if i and j are within the same plaquette, whereas $t_{a,\langle i,j\rangle} = t'_a$, $g_{1,\langle i,j\rangle} = g'_1$ and $g_{2,\langle i,j\rangle} = g'_2$ if i and j are on neighboring plaquettes. We take the primed coefficients to be much smaller than their unprimed equivalents.

6.2.1 Zeroth Order States

We can separate the Hamiltonian into two parts, $H = H_0 + H'$, where H_0 includes both the single-site terms and the two-site terms with unprimed coefficients, while H' includes the two-site terms with primed coefficients. To zeroth order in H' all

the plaquettes are independent from one another. Thus the eigenstates of the full lattice are just tensor products of the single-plaquette eigenstates of H_0. The zeroth-order states of the full lattice must be highly degenerate (except in cases where all plaquettes are in the same state), because swapping the states of any two plaquettes leaves the energy unchanged.

Since we are interested in the low energy physics, we can restrict the Hilbert space to tensor products of the lowest energy states for each number of particles per plaquette. We call the plaquette ground state energy E_n, where n is the number of particles on the plaquette. If we consider a hole doping x with $0 < x < 1/2$ (that is, an average of between two and four atoms per plaquette) we can further restrict the Hilbert space to tensor products of plaquettes which are occupied by between two and four atoms (or equivalently, states with zero to two holes relative to the half-filled case). States with three or more holes are suppressed so long as $E_1 + E_4 > E_2 + E_3$. This means that for a state with three holes (i.e., with energy E_1), it is energetically favorable to divide those holes among two different plaquettes.

Thus, for consideration of the low-energy physics, the states of the full lattice (to zeroth order in H') can be restricted to tensor products of plaquettes in six possible states. These are the ground state for four particles on a plaquette, the ground state for two particles on a plaquette, and the four-fold degenerate ground state for three particles on a plaquette. As we found in the previous chapter, the lowest energy state for four particles has two $\uparrow$ atoms and two $\downarrow$ atoms, and for a wide range of positive Δ it has d-wave rotational symmetry. We will label this state as the "plaquette vacuum" $|0\rangle_P$. The ground state for two particles we found has one $\uparrow$ and one $\downarrow$ atom, and s-wave rotational symmetry. We label this state $d_P^\dagger |0\rangle_P$, where $d_P^\dagger$ is the hole-pair excitation which as noted above must have d-wave symmetry to

map the d-wave plaquette vacuum to the s-wave hole-pair state. The groundstates for three particles per plaquette have either two $\uparrow$ atoms and one $\downarrow$ atom, or else two $\downarrow$ and one $\uparrow$. For each case, there are two degenerate states, which get a factor of $+\mathrm{i}$ or $-\mathrm{i}$ under a $\pi/2$ rotation. We denote these for states as $a^{\dagger}_{P\sigma\pm}\left|0\right\rangle_P$, where $\sigma =\uparrow$ ($\sigma =\downarrow$) corresponds to the $2\uparrow, 1\downarrow$ ($2\downarrow, 1\uparrow$) case, and $\pm$ corresponds to the rotational symmetry.

It is not necessarily the case that the low energy states of the lattice will have plaquettes in all these states. We must consider the pair-binding energy:

$$\Delta_P = 2E_3 - E_2 - E_4 \tag{6.2}$$

where as above E_n is the lowest energy state for a plaquette with n particles. For $\Delta_P \gg 0$ it is energetically favorable for a pair of holes to occupy the same plaquette, so the plaquette states with three particles are suppressed. Likewise, for $\Delta_P \ll 0$ it is energetically favorable to split holes between different plaquettes, suppressing the states with multiple holes. Only for small Δ_P do each of these plaquette states coexist in the low-energy states of the full lattice. Δ_P can be seen as the effective attraction between hole states.[101]

6.2.2 First-Order Hamiltonian

Because the large potential barriers between plaquettes make all the terms of H' small, the effective low-energy Hamiltonian can be expanded in powers of H' by means of degenerate perturbation theory.[101] In particular, we have:

$$H^{eff} = PH_0P + PH'P + PH'\left(1-P\right)\frac{1}{E_0 - H_0}\left(1-P\right)H'P + \ \ldots \tag{6.3}$$

where P is the projector onto the Hilbert space whose basis is all tensor products $\bigotimes_i \left|\phi_i\right\rangle_P$ where i is the index of a particular plaquette, and $\left|\phi_i\right\rangle_P$ is one of the six low-energy plaquette states on that plaquette.

Here we consider only terms up to first order in H'. In this case, determining the effective Hamiltonian simply requires us to calculate the matrix elements of H' in the basis of zeroth order states. These can be calculated numerically for any choice of parameters of the original Hamiltonian. We observe that many of these matrix elements are equal to one another, and many are in fact zero. This is a consequence of the symmetry of the Hamiltonian. As a result, the effective Hamiltonian (in the language of plaquette excitations) can be expressed in terms of relatively few parameters:

$$\begin{aligned} H_P^{eff} = & \sum_i \left[(\Delta_P - 2\mu)\, d_{Pi}^\dagger d_{Pi} - \mu \sum_{\sigma,s} a_{Pi\sigma s}^\dagger a_{Pi\sigma s} \right] \\ & + \sum_{\langle i,j\rangle,\sigma,s} \mathcal{P} \left[t_{aP}\phi_{ij} a_{Pi\sigma s}^\dagger a_{Pj\sigma\bar{s}} + t_{daP}\phi_{ij} d_{Pi}^\dagger d_{Pj} a_{Pj\sigma s}^\dagger a_{Pi\sigma\bar{s}} + \text{H. c.} \right] \mathcal{P} \\ & + \sum_{\langle i,j\rangle,\sigma,s} \mathcal{P} \left[g_P \phi_{ij} d_{Pi}^\dagger \left(a_{Pi\uparrow s} a_{Pj\downarrow\bar{s}} - a_{Pi\downarrow s} a_{Pj\uparrow\bar{s}} \right) + \text{H. c.} \right] \mathcal{P} \end{aligned} \tag{6.4}$$

Here $s = +, -$, $\bar{s} = -, +$, $\mathcal{P}$ is a projector that prevents double-occupancy, and $\phi_{ij} = +1$ for i, j horizontal nearest neighbors, but $\phi_{ij} = -1$ for i, j vertical nearest neighbors. Note that any term that moves the excitation $a_{Pi\sigma s}^\dagger$ to a neighboring site changes it to $a_{Pi\sigma\bar{s}}^\dagger$. Yet other than this fact and the factors of ϕ_{ij}, this Hamiltonian bears a strong resemblance to the effective single-band Hamiltonian derived in chapter 2, which proved to be equivalent to the Generalized Hubbard model.

Some numerical results for the parameters of this Hamiltonian are given in Figure 6.2 for various values of g_1. Note that for $g_1 = g_2 = 0$ we recover the results for the ungeneralized Hubbard model (see Figure 5 in reference [101]), as expected.

6.3 The Rotational Symmetry Factor ϕ_{ij}

On the results as originally reported for the case of the (non-generalized) Hubbard model[101], the factor ϕ_{ij} was omitted except on the terms we label g_P. This was

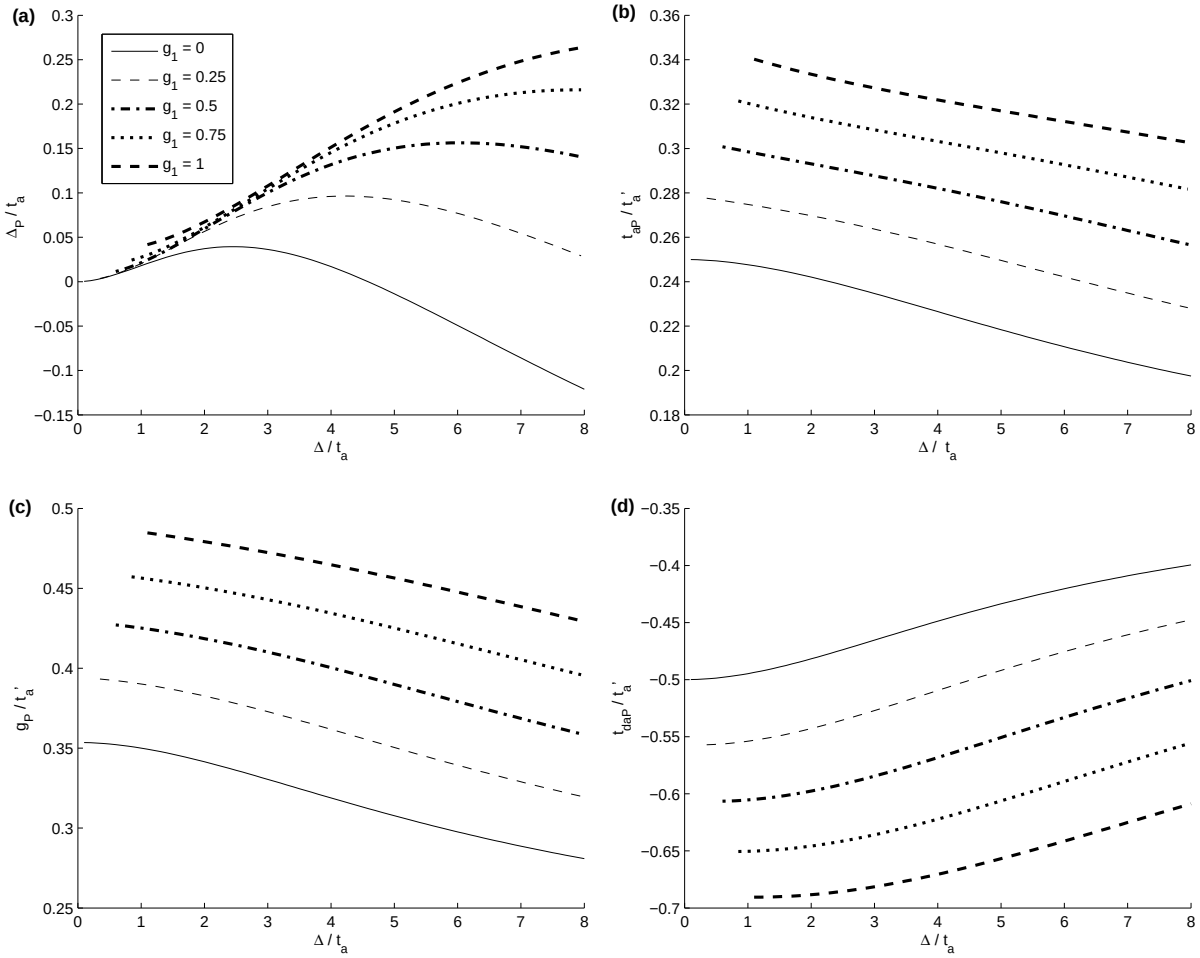

Figure 6.2: Numerical results for the parameters of the Effective Hamiltonian, equation (6.4), for various values of g_1 as given in the legend (in units of t_a). The legend of figure (a) applies to all four figures. Here for simplicity we take $g_1'/t_a' = g_1/t_a$, and $g_2 = g_2' = 0$.

soon corrected[102], in part due to our own correspondence with the authors. As we shall see, the presence of this factor ϕ_{ij} on the other terms of the Hamiltonian has important consequences.

While one can detect the factor ϕ_{ij} through careful calculation of the matrix elements of H', it is fairly easy for sign errors to be introduced into such a calculation, and so we prefer a more definitive argument that this factor does indeed belong on each of the multi-site terms of the Hamiltonian. Such an argument is provided by considering the symmetry of the various operators. Specifically, we expect on general physical grounds that the effective Hamiltonian (6.4) is invariant under a $\pi/2$. However, the various creation and annihilation operators are not rotationally invariant, and thus additional orientation-dependent factors must be introduced to insure the rotational invariance of the full Hamiltonian. This can be understood as the origin of the factor ϕ_{ij}.

If R represents a $\pi/2$ rotation, we have $Rd_P^\dagger R^\dagger = -d_P^\dagger$ and $Ra_{P\sigma\pm}^\dagger R^\dagger = \pm \mathrm{i} a_{P\sigma\pm}^\dagger$. Likewise from the Hermitian conjugates of these equations we have $Rd_P R^\dagger = -d_P$ and $Ra_{P\sigma\pm} R^\dagger = \mp \mathrm{i} a_{P\sigma\pm}^\dagger$. Note the reversal of sign due to the factor of i. We note that in the multi-site terms, $a_{P\sigma+}$ always appears with $a_{P\sigma-}$. If both terms are undaggered, such as in the g_P term, then under rotation there is no net sign change. (The g_P term however gains a factor of ϕ_{ij} from the unpaired $d_P^\dagger$.) However, terms like $a_{P\sigma+}^\dagger a_{P\sigma-}$ do have a sign change under rotation, as both terms produce a factor of +i. Thus, the rotational symmetry of the full Hamiltonian dictates that each of these terms has a factor of ϕ_{ij}.

The significance of this, as noted in [102], is that while the Hamiltonian can support a superfluid with d-wave excitations, there can be no nodal quasiparticles. Elaborating briefly: In a BCS-like theory of interacting fermions, one can form quasi-

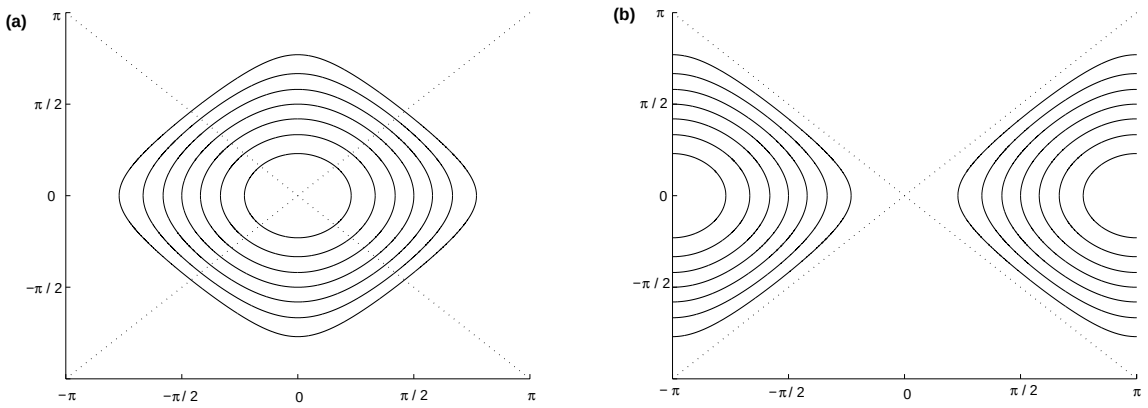

Figure 6.3: Fermi surfaces in **k**-space, in units of inverse lattice spacing. **(a):** Some example Fermi surfaces for less than half filling. **(b):** The same Fermi surfaces shifted due to additional factors of -1, as described in the text. On both figures, the dotted lines represent the points along which the gap is zero. Note that for any of the unshifted Fermi surfaces in **(a)**, there are four nodal points where the lines of gap zeros intersect the Fermi surface. For the shifted Fermi surfaces in **(b)**, the gap is never zero on the Fermi surface, and thus no nodal points occur.

particles with an energy $E(\mathbf{k}) = \sqrt{(\epsilon_{\mathbf{k}} - \mu)^2 + \Delta_g(\mathbf{k})^2}$, where $\epsilon_{\mathbf{k}}$ gives the kinetic energy of the particles in the absence of interaction, μ is the chemical potential, and Δ_g is a gap arising from the interaction between particles.[105] Ordinarily, $\epsilon_{\mathbf{k}}$ possesses an s-wave symmetry, and for some surface in **k**-space (the Fermi surface) $\epsilon_{\mathbf{k}} - \mu = 0$. In particular, below half filling the Fermi surface will enclose $\mathbf{k} = 0$. If $\Delta_g(\mathbf{k})$ has d-wave symmetry then it will be zero along the lines $k_x = k_y$ and $k_x = -k_y$, which necessarily intersect the s-wave Fermi surface. (See Figure 6.3 (a)) Thus, there are four nodal points where $E(\mathbf{k}) = 0$, because the gap goes to zero at those points on the Fermi surface. This is what we would see if only the g_P term contained the factor ϕ_{ij}, since this would correspond to a d-wave interaction between particles with an s-wave Fermi surface.

However, in the case that actually occurs we do not have nodal quasiparticles. This is most readily seen by mapping the Hamiltonian (equation 6.4) into a more customary form for the consideration of BCS theory. First, if we restrict ourselves to

the case of low hole doping (as in reference [101]), the excitations from half-filling are sufficiently sparse that we can neglect the t_{daP} terms. Furthermore, the t_{aP} terms essentially represent the hopping of single fermions from one site to another, other than the fact that they change "flavor" (from + to −). Because the creation operator $a^\dagger_{Pi\sigma\pm}$ is defined for each site i, we can just swap the definitions of $a^\dagger_{Pi\sigma+}$ and $a^\dagger_{Pi\sigma-}$ on every other site (in a checkerboard pattern). In other words, the definition of $a^\dagger_{Pi\sigma+}$ on any particular site matches the definition of $a^\dagger_{Pi\sigma-}$ on those sites that are adjacent to it. Thus the effective Hamiltonian becomes:

$$\begin{aligned} H_P^{eff} = &\sum_i \left[(\Delta_P - 2\mu)\, d^\dagger_{Pi} d_{Pi} - \mu \sum_{\sigma,s} a^\dagger_{Pi\sigma s} a_{Pi\sigma s} \right] \\ &+ \sum_{\langle i,j\rangle,\sigma,s} \mathcal{P} \left[t_{aP} \phi_{ij} a^\dagger_{Pi\sigma s} a_{Pj\sigma s} + \text{H. c.} \right] \mathcal{P} \\ &+ \sum_{\langle i,j\rangle,\sigma,s} \mathcal{P} \left[g_P \phi_{ij} d^\dagger_{Pi} \left(a_{Pi\uparrow s} a_{Pj\downarrow s} - a_{Pi\downarrow s} a_{Pj\uparrow s} \right) + \text{H. c.} \right] \mathcal{P} \end{aligned} \tag{6.5}$$

The kinetic energy $\epsilon_{\mathbf{k}}$ for the non-interacting particles is given by the t_{aP} term, and thus the Fermi surface $\epsilon_{\mathbf{k}} - \mu = 0$ is the same as in the traditional case except for the effect of the factor ϕ_{ij} on the t_{aP} term. We can see the effect of this factor by noting that it is eliminated if we make a further redefinition to $a^\dagger_{Pi\sigma\pm}$, namely changing its sign for every other site along a particular direction. That is, we map $a^\dagger_{Pi\sigma\pm}$ to $-a^\dagger_{Pi\sigma\pm}$ on every other column of the lattice. This has the effect of shifting the Fermi surface by π/a in $\mathbf{k}$-space (where a is the lattice spacing). To see this, consider how this transformation acts on the $\mathbf{k}$-space expansion of $a^\dagger_{Pi\sigma\pm}$:

$$a^\dagger_{Pi\sigma\pm} = \frac{1}{\sqrt{N}} \sum_{\mathbf{k}} \mathrm{e}^{\mathrm{i}\mathbf{k}\cdot\mathbf{R_i}} a^\dagger_{P\mathbf{k}\sigma\pm} \rightarrow \frac{1}{\sqrt{N}} \sum_{\mathbf{k}} \mathrm{e}^{\mathrm{i}[(k_x+\pi/a)x_i + k_y y_i]} a^\dagger_{P\mathbf{k}\sigma\pm} \tag{6.6}$$

where $\mathbf{k} = (k_x, k_y)$ and $\mathbf{R}_i = (x_i, y_i)$.

While the g_P terms of the effective Hamiltonian give rise to a gap $\Delta_g(\mathbf{k})$ with d-wave symmetry, the lines where $\Delta_g(\mathbf{k}) = 0$ will not intersect the shifted Fermi

surface (See Figure 6.3 (b)). Thus, $E(\mathbf{k})$ is everywhere non-zero and there are no nodal quasiparticles.

6.4 Chapter Summary

In this chapter, we considered the case where an optical superlattice allows only weak interactions between plaquettes. We derived an effective low-energy Hamiltonian from degenerate perturbation theory. Because the plaquettes themselves have d-wave excitations, the resulting Hamiltonian can support d-wave superfluidity (as shown in detail for the non-generalized Hubbard model case in [100, 101]). However, we find it cannot support the nodal quasiparticles typical of high-T_c superconductivity, due to certain symmetry factors that must occur due to the symmetries of the plaquette excitations themselves.

CHAPTER VII

Dissertation Summary and Suggestions for Further Study

In this dissertation, we have studied the intersection of two important experimental techniques of ultracold atomic physics, namely the optical lattice and the use of Feshbach resonance. With optical lattices, many diverse interaction configurations have been achieved; those studied here represent only some of the most basic. Nevertheless, even the simple square lattice is enough to achieve Hamiltonians such as the Hubbard model, which support rich physics and are of great importance to the study of condensed matter. The addition of Feshbach resonance allows the interatomic interactions to be tuned over a wide range of values. Thus the combination of these techniques presents a highly controllable, clean testbed for studying condensed matter phenomena, as well as the possibility of new physics.

We have focused on the case of fermions in an optical lattice near Feshbach resonance, and have summarized in detail the argument (from [3, 24]) that such a system is described by a Hamiltonian of the form of the generalized Hubbard model (GHM). In particular, we have emphasized that the GHM arises in a very different way in this system than in condensed matter, and that the GHM occurs in two such different contexts can be understood as a consequence of symmetry. (Specifically, we describe how the GHM is the most general Hamiltonian allowed for a system with certain

symmetries and a few other key features).

The bulk of this dissertation has focused on two questions, the first of which is how to determine the parameters of the GHM. In this effort we studied the two-body problem, before moving on to give a proposed experiment which could be used to measure the model's parameters using a double well superlattice.[77]. Having introduced the superlattice, we used it in consideration of the second main question addressed by this dissertation: How to create a d-wave superfluid state in an optical lattice. This is of relevance to the study of High-T_c superconductivity, where the excitation gap has been found to have d-wave symmetry. In particular, we first studied the possible states of a deep plaquette superlattice (that is, one which suppressed all inter-plaquette interactions) over a wide range of parameters.[82] From here we discussed the case of a more shallow plaquette superlattice, such that weak interplaquette interactions were allowed. Having calculated the Hamiltonian of such a system from perturbation theory, and also from symmetry considerations, we note that while a d-wave superfluid is achievable (see for instance, the proposal in Ref. [100]), there is as yet no simple procedure for producing the sort of nodal quasiparticles characteristic of high-T_c.

Several directions present themselves for further study. First, we can hope to see an experimental confirmation that this system is indeed described by the Generalized Hubbard Model, and an empirical determination of its parameters, as proposed in Chapter 4. Once the values of the GHM parameters for this system are known, the system might be studied by the same advanced numerical techniques employed in condensed matter physics, such as DMRG or dynamic cluster methods. Concurrent with this, we can hope to see more efforts to directly detect various exotic phases in experiments on these systems. Finally, we can hope to see a means of creating

a d-wave superfluid state with nodal quasiparticles, analogous to the high-T_c superconducting state.

In any case, we can expect strong interactions between ultracold atomic physics and condensed matter for many years to come, to the benefit of both fields.

APPENDICES

APPENDIX A

Mapping the Effective Hamiltonian to the Generalized Hubbard Model

In Chapter 2, we showed that the effective Hamiltonian for fermions in an optical lattice near a Feshbach resonance is:

$$H = \sum_i \Delta(B) d_i^\dagger d_i + \sum_{\langle i,j \rangle} \sum_\sigma \left(t_a a_{i\sigma}^\dagger b_i b_j^\dagger a_{j\sigma} + t_{da} d_i^\dagger d_j a_{j\sigma}^\dagger a_{i\sigma} + \text{H. c.} \right) + \sum_{\langle i,j \rangle} \left[g \left(d_i^\dagger b_j^\dagger + b_i^\dagger d_j^\dagger \right) \left(a_{i\uparrow} a_{j\downarrow} - a_{i\downarrow} a_{j\uparrow} \right) + \text{H. c.} \right] \tag{A.1}$$

where we have taken the t_d term to be negligible. Here $d_i^\dagger$ creates a dressed molecule state, $a_{i\sigma}^\dagger$ creates an atom of spin σ, and $b_i^\dagger$ creates a slave boson. The slave bosons are used to enforce the constraint of no double occupancy, by requiring $b_i^\dagger b_i + a_{i\uparrow}^\dagger a_{i\uparrow} + a_{i\downarrow}^\dagger a_{i\downarrow} + d_i^\dagger d_i = I$.

The dressed molecule is not equivalent to a pair of atoms in the lowest band, but rather is a complex superposition over many bands. Nevertheless, we can *mathematically* map the dressed molecule to the doubly occupied state: $d_i^\dagger |0\rangle \rightarrow a_{i\downarrow}^\dagger a_{i\uparrow}^\dagger |0\rangle$ Note that after applying the mapping the creation of a molecule no longer commutes with the creation of an atom on the same site. For this reason, where our Hamiltonian contains products of operators acting on the same site as each other, these must be placed in normal order (that is, with all creation operators to the left of the annihilation operators) before applying the mapping $d_i^\dagger \rightarrow a_{i\downarrow}^\dagger a_{i\uparrow}^\dagger$.

Applying this mapping to the appropriately ordered operators gives:

$$d_i^\dagger d_i \rightarrow a_{i\downarrow}^\dagger a_{i\uparrow}^\dagger a_{i\uparrow} a_{i\downarrow} = \hat{n}_{i\uparrow}\hat{n}_{i\downarrow}$$

$$d_i^\dagger a_{i\sigma} a_{j\sigma}^\dagger d_j \rightarrow a_{i\downarrow}^\dagger a_{i\uparrow}^\dagger a_{i\sigma} a_{j\sigma}^\dagger a_{j\uparrow} a_{j\downarrow} = a_{i\bar{\sigma}}^\dagger \hat{n}_{i\sigma}\hat{n}_{j\sigma} a_{j\bar{\sigma}}$$

$$\begin{aligned}\left(d_i^\dagger b_j^\dagger + b_i^\dagger d_j^\dagger\right)\left(a_{i\uparrow}a_{j\downarrow} - a_{i\downarrow}a_{j\uparrow}\right) \rightarrow\ & a_{i\downarrow}^\dagger a_{i\uparrow}^\dagger a_{i\uparrow} b_j^\dagger a_{j\downarrow} + b_i^\dagger a_{i\uparrow} a_{j\downarrow}^\dagger a_{j\uparrow}^\dagger a_{j\downarrow} \\ & - a_{i\downarrow}^\dagger a_{i\uparrow}^\dagger a_{i\downarrow} b_j^\dagger a_{j\uparrow} - b_i^\dagger a_{i\downarrow} a_{j\downarrow}^\dagger a_{j\uparrow}^\dagger a_{j\uparrow} \\ & = a_{i\downarrow}^\dagger \hat{n}_{i\uparrow} b_j^\dagger a_{j\downarrow} + a_{j\uparrow}^\dagger \hat{n}_{j\downarrow} b_i^\dagger a_{i\uparrow} + a_{i\uparrow}^\dagger \hat{n}_{i\downarrow} b_j^\dagger a_{j\uparrow} + a_{j\downarrow}^\dagger \hat{n}_{j\uparrow} b_i^\dagger a_{i\downarrow} \\ & = \sum_\sigma \left(a_{i\sigma}^\dagger \hat{n}_{i\bar{\sigma}} b_j^\dagger a_{j\sigma} + a_{j\sigma}^\dagger \hat{n}_{j\bar{\sigma}} b_i^\dagger a_{i\sigma}\right)\end{aligned}$$

At this point, we no longer need to require $b_i^\dagger b_i + a_{i\uparrow}^\dagger a_{i\uparrow} + a_{i\downarrow}^\dagger a_{i\downarrow} + d_i^\dagger d_i = I$, as double occupancy is no longer forbidden. The only remaining role of the slave bosons is to enforce that terms such as $a_{i\sigma}^\dagger b_i$ cannot create an atom of spin σ if the site is already occupied by an atom of spin $\bar{\sigma}$, and similarly the Hermitian conjugate of this term cannot annihilate an atom from a doubly occupied site. We can continue to enforce this restriction while eliminating slave bosons, by applying the mapping $a_{i\sigma}^\dagger b_i \rightarrow a_{i\sigma}^\dagger \left(1 - \hat{n}_{i\bar{\sigma}}\right)$. Under this mapping, we have:

$$a_{i\sigma}^\dagger b_i b_j^\dagger a_{j\sigma} \rightarrow a_{i\sigma}^\dagger \left(1 - \hat{n}_{i\bar{\sigma}}\right)\left(1 - \hat{n}_{j\bar{\sigma}}\right) a_{j\sigma}$$

$$\sum_\sigma \left(a_{i\sigma}^\dagger \hat{n}_{i\bar{\sigma}} b_j^\dagger a_{j\sigma} + a_{j\sigma}^\dagger \hat{n}_{j\bar{\sigma}} b_i^\dagger a_{i\sigma}\right) \rightarrow \sum_\sigma \left(a_{i\sigma}^\dagger \hat{n}_{i\bar{\sigma}} \left(1 - \hat{n}_{j\bar{\sigma}}\right) a_{j\sigma} + a_{j\sigma}^\dagger \hat{n}_{j\bar{\sigma}} \left(1 - \hat{n}_{i\bar{\sigma}}\right) a_{i\sigma}\right)$$

Having applied all of these transformations, the Hamiltonian given in equation (A.1) becomes:

$$\begin{aligned}H = & \sum_{\langle i,j\rangle,\sigma} \left[t_a \left(1 - n_{i\bar{\sigma}}\right)\left(1 - n_{j\bar{\sigma}}\right) + g n_{i\bar{\sigma}} \left(1 - n_{j\bar{\sigma}}\right) + g n_{j\bar{\sigma}} \left(1 - n_{i\bar{\sigma}}\right) + t_{da} n_{i\bar{\sigma}} n_{j\bar{\sigma}}\right] a_{i\sigma}^\dagger a_{j\sigma} \\ & + \text{H.c.} + \sum_i \Delta n_{i\uparrow} n_{i\downarrow} - \mu \left(n_{i\uparrow} + n_{i\downarrow}\right) \\ = & \sum_{\langle i,j\rangle,\sigma} \left[t_a + g_1 \left(n_{i\bar{\sigma}} + n_{j\bar{\sigma}}\right) + g_2 n_{i\bar{\sigma}} n_{j\bar{\sigma}}\right] a_{i\sigma}^\dagger a_{j\sigma} + \text{H.c.} + \sum_i \Delta n_{i\uparrow} n_{i\downarrow} - \mu \left(n_{i\uparrow} + n_{i\downarrow}\right)\end{aligned} \tag{A.2}$$

where $g_1 = g - t_a$, and $g_2 = t_{da} - 2g + t_a$. This is the generalized Hubbard model.

BIBLIOGRAPHY

BIBLIOGRAPHY

[1] K. M. O'Hara, M. E. Gehm, S. R. Granade, S. Bali, and J. E. Thomas, Phys. Rev. Lett. **85**, 2092 (2000).

[2] J. L. Bohn, J. J. P. Burke, and C. H. Greene, Phys. Rev. A **59**, 3660 (1999).

[3] L.-M. Duan, Phys. Rev. Lett. **95**, 243202 (2005).

[4] J. Hubbard, Proc. R. Soc. London Ser. A **276**, 238 (1963).

[5] P. A. M. Dirac, Proc. R. Soc. London Ser. A **123**, 714 (1929).

[6] F. Bloch, Z. Phys. **52**, 555 (1928).

[7] M. Greiner, O. Mandel, T. Esslinger, T. W. Hänsch, and I. Bloch, Nature **415**, 39 (2002).

[8] C. Orzel, A. K. Tuchman, M. L. Fenselau, M. Yasuda, and M. A. Kasevich, Science **291**, 2386 (2001).

[9] D. Jaksch, C. Bruder, J. I. Cirac, C. W. Gardiner, and P. Zoller, Phys. Rev. Lett. p. 3108 (1998).

[10] D. Jaksch and P. Zoller, Annals of Physics **315**, 52 (2005).

[11] C. Regal, M. Greiner, and D. Jin, Phys. Rev. Lett. **92**, 040403 (2004).

[12] M. W. Zwierlein, C. A. Stan, C. H. Schunck, S. M. F. Raupach, A. J. Kerman, and W. Ketterle, **92**, 120403 (2004).

[13] C. Chin, M. Bartenstein, A. Altmeyer, S. Riedl, S. Jochim, J. H. Denschlag, and R. Grimm, Science **305**, 1128 (2004).

[14] R. Duine and H. Stoof, Phys. Rep. **396**, 115 (2004).

[15] Q. Chen, J. Stajic, S. Tan, and K. Levin, Phys. Rep. **412**, 1 (2005).

[16] R. B. Diener and T.-L. Ho, Phys. Rev. Lett. **96**, 010402 (2006), Phys. Rev. A **73**, 017601 (2006).

[17] D. B. M. Dickerscheid, U. A. Khawaja, D. van Oosten, and H. T. C. Stoof, Phys. Rev. A **71**, 043604 (2005), Phys. Rev. Lett. **94**, 230404 (2005).

[18] L. D. Carr and M. J. Holland, Phys. Rev. A **72**, 031604 (2005).

[19] F. Zhao, Phys. Rev. B **72**, 220501 (R) (2005).

[20] F. Zhou and C. Wu, New J. Phys. **8**, 166 (2006).

[21] M. Köhl, H. Moritz, T. Stöferle, K. Günter, and T. Esslinger, Phys. Rev. Lett. **94**, 080403 (2005).

[22] T. Stöferle, H. Moritz, K. Günter, M. Köhl, and T. Esslinger, Phys. Rev. Lett. **96**, 030401 (2006).

[23] K. Xu, Y. Liu, J. Abo-Shaeer, T. Mukaiyama, J. Chin, D. Miller, W. Ketterle, K. M. Jones, and E. Tiesinga, Phys. Rev. A **72**, 043604 (2005).

[24] L.-M. Duan, Europhys. Lett. **81**, 20001 (2008).

[25] G. H. Wannier, Phys. Rev. **52**, 191 (1937).

[26] M. Airoldi and A. Parola, Phys. Rev. B **51**, 16327 (1995).

[27] J. Hirsh, Physica C **158**, 326 (1989).

[28] J. Hirsh, Physica B **199200**, 366 (1994).

[29] J. Amadon and J. Hirsch, Phys. Rev. B **54**, 6364 (1996).

[30] B. B. lka, Phys. Rev. B **57**, 10303 (1998).

[31] L. Didukh and V. Hankevych, Physica Status Solidi B **211**, 703 (1998).

[32] L. Didukh, V. Hankevych, and Y. Skorenkyy, Physica B: Physics of Condensed Matter **284**, 1537 (2000).

[33] J. E. Hirsch and F. Marsiglio, Phys. Rev. B **41**, 2049 (1990).

[34] F. M. andJ. E. Hirsch, Phys. Rev. B **41**, 6435 (1990).

[35] A. Aligia, E. Gagliano, L. Arrachea, and K. Hallberg, Eur. Phys. Journ. B **5**, 371 (1998).

[36] L. Arrachea and A. A. Aligia, Phys. Rev. B **61**, 9686 (2000).

[37] R. Strack and D. Vollhardt, Phys. Rev. Lett. **70**, 2637 (1993).

[38] A. A. Ovchinnikov, J. Phys.: Condens. Matter **6**, 11057 (1994).

[39] A. A. Aligia, L. Arrachea, and E. R. Gagliano, Phys. Rev. B **51**, 13774 (1995).

[40] D. J. Scalapino, in *Handbook of High Temperature Superconductivity*, edited by J. R. Schrieffer (Springer, 2006), chap. 13.

[41] J. H. de Boer and E. J. W. Verwey, Proc. Phys. Soc. London **49**, 59 (1937).

[42] R. Peierls, Proc. Phys. Soc. London, Ser. A **49**, 72 (1937).

[43] N. F. Mott, Proc. Phys. Soc. London, Ser. A **49**, 72 (1937).

[44] N. F. Mott, Proc. Phys. Soc. London, Ser. A **62**, 416 (1949).

[45] N. F. Mott, Can. J. Phys. **34**, 1356 (1956).

[46] N. F. Mott, Philos. Mag. **6**, 287 (1961).

[47] N. W. Ashcroft and N. D. Mermin, *Solid State Physics* (Brooks Cole, New York, 1976).

[48] L.-M. Duan, Europhys. Lett. **67**, 721 (2004).

[49] M. Imada, A. Fujimori, and Y. Tokura, Rev. Mod. Phys. **70**, 1039 (1998).

[50] R. Micnas, J. Ranninger, and S. Robaszkiewicz, Rev. Mod. Phys. **62**, 113 (1990).

[51] U. Fano, Phys. Rev. **124**, 1866 (1961).

[52] H. Feshbach, Ann. Phys. **19**, 287 (1962).

[53] E. Merzbacher, *Quantum Mechanics (3rd ed.)* (John Wiley and Sons, New York, 1998).

[54] S. Jochim, *Bose-Einstein Condensation of Molecules (doctoral dissertation)* (University of Innsbruck, 2004).

[55] G. Breit and I. I. Rabi, Phys. Rev. **38**, 2082 (1931).

[56] P. S. Julienne, E. Tiesinga, and T. Koehler, Journal of Modern Optics **51**, 1787 (2004).

[57] M. Greiner, C. A. Regal, and D. S. Jin, Nature **426**, 537 (2003).

[58] R. B. Diener and T.-L. Ho, cond-mat/0405174.

[59] M. H. Szymanska, K. Goral, T. Kohler, and K. Burnett, Phys. Rev. A **72**, 013610 (2005).

[60] M. Holland, S. Kokkelmans, M. Chiofalo, and R. Walser, Phys. Rev. Lett. **87**, 120406 (2001).

[61] W. Yi and L.-M. Duan, Phys. Rev. A **73**, 063607 (2006).

[62] Y. Ohashi and A. Griffin, Phys. Rev. Lett. **89**, 130402 (2002).

[63] G. Grynberg and C. Robilliard, Phys. Rep. **355**, 335 (2001).

[64] P. Berman, Quantum Optics (lecture notes) (2007).

[65] S. Chu, L. Hollberg, J. Bjorkholm, A. Cable, and A. Ashkin, Phys. Rev. Lett. **55**, 48 (1985).

[66] P. Lett, R. Watts, C. Westbrook, W. Phillips, P. Gould, and H. Metcalf, Phys. Rev. Lett. **61**, 169 (1988).

[67] T. W. Hänsch and A. L. Schawlow, Opt. Commun. **13**, 68 (1975).

[68] J. Dalibard and C. Cohen-Tannoudji, J. Opt. Soc. Am. B **6**, 2023 (1989).

[69] P. Ungar, D. Weiss, E. Riis, and S. Chu, J. Opt. Soc. Am. B **6**, 2058 (1989).

[70] S. Trotzky, P. Cheinet, S. Fölling, M. Feld, U. Schnorrberger, A. M. Rey, A. Polkovnikov, E. A. Demler, M. D. Lukin, and I. Bloch, Science **319**, 295 (2008).

[71] S. Fölling, S. Trotzky, P. Cheinet, M. Feld, R. Saers, A. Widera, T. Müller, and I. Bloch, Nature **448**, 1029 (2007).

[72] S. Jochim, M. Bartenstein, G. Hendl, J. H. Denschlag, , R. Grimm, A. Mosk, and M.Weidemüller, Phys. Rev. Lett. **89**, 273202 (2002).

[73] T. Loftus, C. A. Regal, C. Ticknor, J. L. Bohn, and D. S. Jin, Phys. Rev. Lett. **88**, 173201 (2002).

[74] G. Kotliar and A. Ruckenstein, Phys. Rev. Lett. **57**, 1362 (1986).

[75] F. Lechermann, A. Georges, G. Kotliar, and O. Parcollet, Phys. Rev. B **76**, 155102 (2007).

[76] M. Anderlini, P. J. Lee, B. L. Brown, J. Sebby-Strabley, W. D. Phillips, and J. V. Porto, Nature **448**, 452 (2007).

[77] T. Goodman and L.-M. Duan (2008), arXiv:0808.2072, accepted for publication in Phys. Rev. A.

[78] J. R. Schrieffer, Solid State Commun. **92**, 129 (1994).

[79] D. J. Scalapino, Phys. Rep. **250**, 330 (1995).

[80] D. van Harlingen, Rev. Mod. Phys. **67**, 515 (1995).

[81] C. C. Tsuei and Kirtley, Rev. Mod. Phys. **72**, 969 (2000).

[82] T. Goodman and L.-M. Duan, Phys. Rev. A **74**, 052711 (2006).

[83] S. R. White and D. J. Scalapino, Phys. Rev. B **55**, 06504 (1997).

[84] L.-M. Duan, E. Demler, and M. D. Lukin, Phys. Rev. Lett. **91**, 090402 (2003).

[85] C. J. Morningstar and M. Weinstein, Phys. Rev. D **54**, 4131 (1996).

[86] E. Altman and A. Auerbach, Phys. Rev. B **65**, 104508 (2002).

[87] J. Sebby-Strabley, M. Anderlini, P. S. Jessen, and J. V. Porto, `cond-mat/0602103`.

[88] S. Trebst, U. Schollwoeck, M. Troyer, and P. Zoller, `cond-mat/0506809`.

[89] W. Hofstetter, J. I. Cirac, P. Zoller, E. Demler, and M. D. Lukin, Phys. Rev. Lett. **89**, 220407 (2002).

[90] P. W. Anderson, Science **235**, 1196 (1987).

[91] J. Zaanen, G. A. Sawatzky, and J. W. Allen, Phys. Rev. Lett. **55**, 418 (1985).

[92] P. W. Anderson and J. R. Schrieffer, Phys. Today **44**, 55 (1991).

[93] T. Maier, M. Jarrell, T. Schulthess, P. Kent, and J. White, Phys. Rev. Lett. **95**, 237001 (2005).

[94] G.Hager, G. Wellein, E. Jeckelmann, and H. Fehske, Phys. Rev. B **71**, 75108 (2005).

[95] J. E. Hirsch and H. Q. Lin, Phys. Rev. B **37**, 5070 (1988).

[96] E. Y. Loh, J. E. Gubernatis, R. T. Scalettar, S. R. White, D. J. Scalapino, and R. L. Sugar, Phys. Rev. B **41**, 9301 (1990).

[97] S. R. White, D. J. Scalapino, R. L. Sugar, E. Y. Loh, J. E. Gubernatis, and R. T. Scalettar, Phys. Rev. B **40**, 506 (1989).

[98] S. R. White, D. J. Scalapino, R. L. Sugar, N. E. Bickers, and R. T. Scalettar, Phys. Rev. B **39**, 839 (1989).

[99] D. J. Scalapino and S. Trugman, Philos. Mag. B **74**, 607 (1996).

[100] A. M. Rey, R. Sensarma, S. Foelling, M. Greiner, E. Demler, and M. D. Lukin (2008), arXiv:0806.0166.

[101] W.-F. Tsai and S. A. Kivelson, Phys. Rev. B **73**, 214510 (2006).

[102] W.-F. Tsai and S. A. Kivelson, Phys. Rev. B **76**, 139902(E) (2007).

[103] H. Yao, W.-F. Tsai, and S. A. Kivelson, Phys. Rev. B **76**, 161104(R) (2007).

[104] W.-F. Tsai, H. Yao, A. Laeuchli, and S. A. Kivelson, Phys. Rev. B **77**, 214502 (2008).

[105] J. Bardeen, L. N. Cooper, and J. R. Schrieffer, Phys. Rev. **108**, 1175 (1957).